EFFICIENT MACHINE LEARNING USING PARTITIONED RESTRICTED BOLTZMANN MACHINES

by

Hasari Tosun

A dissertation submitted in partial fulfillment
of the requirements for the degree

of

Doctor of Philosophy

in

Computer Science

MONTANA STATE UNIVERSITY
Bozeman, Montana

May, 2016

DEDICATION

To Suzan, my dear wife

ACKNOWLEDGEMENTS

I would like to thank my advisor, Dr. John Sheppard for his staunch support throughout my research at Montana State University. At the times when I was about to give it up, he always encouraged and pushed me to excel. Without his guidance, this research would not have been possible.

I would also like to thank my committee members, John Paxton, Rocky Ross, and Clem Izurieta for their helpful comments and advice, and to thank the members of the Numerical Intelligent Systems Laboratory at Montana State University for their comments and advice during the development of this work. Thanks too to Ben Mitchell at John Hopkins University for his collaboration.

Finally, I would like to thank my wife for supporting me during the development of this work. Suzan released me of other duties as I worked on my research. My children, Sundus, Eyub and Yakob, are too little to understand what the PhD is. Their constant question was "when will your school be done?" You were patient with me. Now that my work is complete, I will share it with you in time.

TABLE OF CONTENTS

TABLE OF CONTENTS – CONTINUED

TABLE OF CONTENTS – CONTINUED

LIST OF TABLES

Table Page

LIST OF FIGURES

Figure Page

LIST OF FIGURES – CONTINUED

Figure Page

LIST OF ALGORITHMS

Algorithm Page

ABSTRACT

Restricted Boltzmann Machines (RBM) are energy-based models that are used as generative learning models as well as crucial components of Deep Belief Networks (DBN). The most successful training method to date for RBMs is Contrastive Divergence. However, Contrastive Divergence is inefficient when the number of features is very high and the mixing rate of the Gibbs chain is slow.

We develop a new training method that partitions a single RBM into multiple overlapping atomic RBMs. Each partition (RBM) is trained on a section of the input vector. Because it is partitioned into smaller RBMs, all available data can be used for training, and individual RBMs can be trained in parallel. Moreover, as the number of dimensions increases, the number of partitions can be increased to reduce runtime computational resource requirements significantly. All other recently developed methods for training RBMs suffer from some serious disadvantage under bounded computational resources; one is forced to either use a subsample of the whole data, run fewer iterations (early stop criterion), or both. Our *Partitioned-RBM* method provides an innovative scheme to overcome this shortcoming.

By analyzing the role of spatial locality in Deep Belief Networks (DBN), we show that spatially local information becomes diffused as the network becomes deeper. We demonstrate that deep learning based on partitioning of Restricted Boltzmann Machines (RBMs) is capable of retaining spatially local information. As a result, in addition to computational improvement, reconstruction and classification accuracy of the model is also improved using our *Partitioned-RBM* training method.

CHAPTER 1

INTRODUCTION

In this chapter, we present the motivation for developing Partitioned Restricted Boltzmann Machines (Partitioned-RBM), specifically in applications where the computational resources are bounded. After a brief introduction to the characteristics of current datasets and the limitation of RBMs, we introduce Partitioned-RBM as an alternative training method that addresses computational requirements. Then, we summarize our major contributions and conclude with an overview of each section of this dissertation.

1.1 Motivation

As the volume of data is increasing exponentially, the corresponding need for efficient learning algorithms is also increasing. In addition to the traditional Internet, in the Internet of Thing (IoT) where a variety of smart devices are connected to each other and to the Internet, the volume of data generated is immense. There are some basic characteristics of recent data: 1) it is collected from many sources, 2) it is very high dimensional, 3) it is complex, having many latent variables with complex distributions, and 4) it is spatio-temporal. Representing such data efficiently and developing computationally efficient algorithms is a challenging task. Most of the training algorithms for learning are based on gradient descent with data likelihood objective functions that are intractable to compute [1].

An example of data generated by users and sensors is images. Image pixel resolution is increasing continuously. An image taken by a cheaper camera with 2048×1536

pixels resolution has 3.1 million total pixels. Thus, without any preprocessing, the dimension of the image is 3.1 million. If one were to construct a neural network, the input layer would need to have 3.1 million neurons. If the network had a single hidden layer, also with 3.1 million neurons, then propagating information from one layer to next would involve 9×10^{12} calculations. This is even more prohibitive when deep neural networks with multiple hidden layers are used. As of 2010, Google indexed approximately 10 billion images [2]. Current machine learning methods can not handle such datasets when the number of images are on the order of billions.

An immediate solution to overcome the time complexity of training algorithms is to distribute learning on many nodes for processing. However, in current Deep Neural Network (DBN) algorithms, to accomplish an optimization task on multiple machines, a central node is needed for communicating intermediate results. As a result, the communication becomes a bottleneck.

In addition to training and inference time complexity, representation is an issue: what is the best model to represent and process features effectively? The performance of machine learning methods is dependent on the choice of data representation. Recent studies show a representation that maximizes sparsity has properties of the receptive fields of simple cells in the mammalian primary visual cortex; receptive fields are spatially localized, oriented, and selective to structure at different spatial scales [3]. In a sparse representation, most of the extracted features will be sensitive to variations in data; thus, sparseness is a key component of good representation [4]. Moreover, there is a need for distributed representations where a concept is represented by many neurons and a neuron is involved in many concepts. Energy-based models such as Markov Random Fields, Boltzmann Machines, and Autoencoders have gained significant success. However, these algorithms, although tractable, are slow if data dimensionality is very high.

We implemented a partitioned Restricted Boltzmann Machine (RBM) and trained an individual RBM separately [5]. We realized that partitioned RBMs are not only more accurate in terms of their generative power, they are also fast. Our results shows that they are also very accurate in terms of their discriminative power, namely in a classification task. As a result, a learning method with many partitioned small RBMs is more accurate and efficient. Training Partitioned-RBMs involves several partition steps. In each step, the RBM is partitioned into multiple RBMs. We demonstrate that Partitioned-RBMs have better representation and computational performance as compared to monolithic RBMs.

1.2 Contributions

In this section, we briefly list the major contributions of this dissertation. A more comprehensive summary is given in Chapter 8.

- We develop a novel partitioned learning method in Chapter 4 . Partitioned-RBMs enable data-independent parallelization and since each sub partition has fewer nodes and weights to be updated, our method has better computational performance. We find that Partitioned-RBMs possess natural sparsity characteristics because each Partitioned-RBMs are trained on localized regions of the dataset.

- We show in Chapter 5 that Partitioned-RBMs can be used efficiently as discriminative models with better performance in terms of computational requirements.

- We demonstrate in Chapter 6 that Partitioned-RBMs can be used effectively as part of Deep Belief Networks while preserving spatially local features.

- In Chapter 7, we apply Partitioned-RBMs to time series classification datasets, and show that Partitioned-RBMs perform well in classifying time series with high dimensions.

1.3 Organization

This section describes the organization of the remaining chapters of the dissertation and gives a brief overview of the focus of each chapter.

In Chapter 2, we review the background work common to this line of research. We describe concepts related to energy-based models. Most energy-based models rely on the Boltzmann distribution, the partition function, and free energy. Thus, we describe these concepts and derive energy functions for the Boltzmann distribution. We then describe Constrastive Divergence (CD) algorithm in detail. This discussion is followed by an introduction on deep learning and Deep Belief Networks (DBN). Finally, we introduce tools for evaluating spatially local features. These tools will be used in analyzing data and derived features in the subsequent.

In Chapter 3, we review the literature of Deep Belief Networks, Boltzmann Restricted Machines and related approaches.

In Chapter 4, we discuss partitioning theory and develop a generic partitioned based training procedure. We describe how data and model is partitioned. We then develop Partitioned Restricted Boltzmann Machine (PRBM). Applying to an image dataset, we analyze performance characteristics of Partitioned-RBMs.

In Chapter 5, we develop a discriminative version of Partitioned-RBM. We apply our model to an image classification task and show classification accuracy and computational performance of the model.

In Chapter 6, we assess the characteristics of Partitioned-RBMs in the context of deep learning. Specifically, we carry out analysis on how Partitioned-RBMs used in DBNs can exploit spatially local features with performance improvements.

In Chapter 7, we apply Partitioned-RBMs to temporal datasets. We demonstrate that Partitioned-RBMs can classify time series effectively.

In Chapter 8, we draw conclusions and summarize the contributions resulting from this work. We list future work and conclude with a list of published papers resulting from this research.

1.4 Notation

All notation used throughout this thesis is described in this section.

a, b, c, w	lowercase italic symbols for scalars
$\mathbf{a}, \mathbf{b}, \mathbf{c}, \mathbf{x}$	lowercase bold symbols for vectors
$\mathbf{W}$	uppercase bold symbols for matrices
$\mathbf{x}^\top$	by default, all vectors a column vectors $\mathbf{x}^\top$ denotes row vector
x_i	ith element of vector $\mathbf{x}$
$\mathbf{x}_i$	ith row vector of matrix $\mathbf{X}$
$\mathbf{x}_{ij}$	the ith row and jth column of matrix $\mathbf{X}$
$X(w)$, or X	denotes random variables

CHAPTER 2

BACKGROUND

Today, most of the data generated by humans and devices is unlabeled and of very high dimension. Methods in deep learning attempt to manage the data flood and curse of dimensionality by discovering structure and abstractions in the data. Because of similarities in how physical systems organize, most energy-based neural networks have become popular. In this chapter, we present the theoretical foundation for energy-based models. We derive the necessary energy-based mathematical formulas and present existing related learning methods. We also describe various methods and tools for analysis of spatial and temporal features.

2.1 Boltzmann Distribution

In this section, we describe the *Boltzmann Distribution*, as the foundation of *statistical mechanics*. In statistical mechanics, a certain quantity of matter under thermodynamic study or analysis is called a *system*. When the thermodynamic system was viewed as black box, the Austrian physicist Ludwig Boltzmann(1844-1906) thought of a system in terms of atoms and molecules and described entropy (a measure of the number of specific ways in which a thermodynamic system may be arranged) in terms of possible disposition of atoms [6]. Boltzmann characterized thermodynamic systems with possible arrangements of atoms and molecules. In other words, he examined the second law of thermodynamics in terms of its possible atomic arrangements. This line of thinking helped to create the field of statistical mechanics.

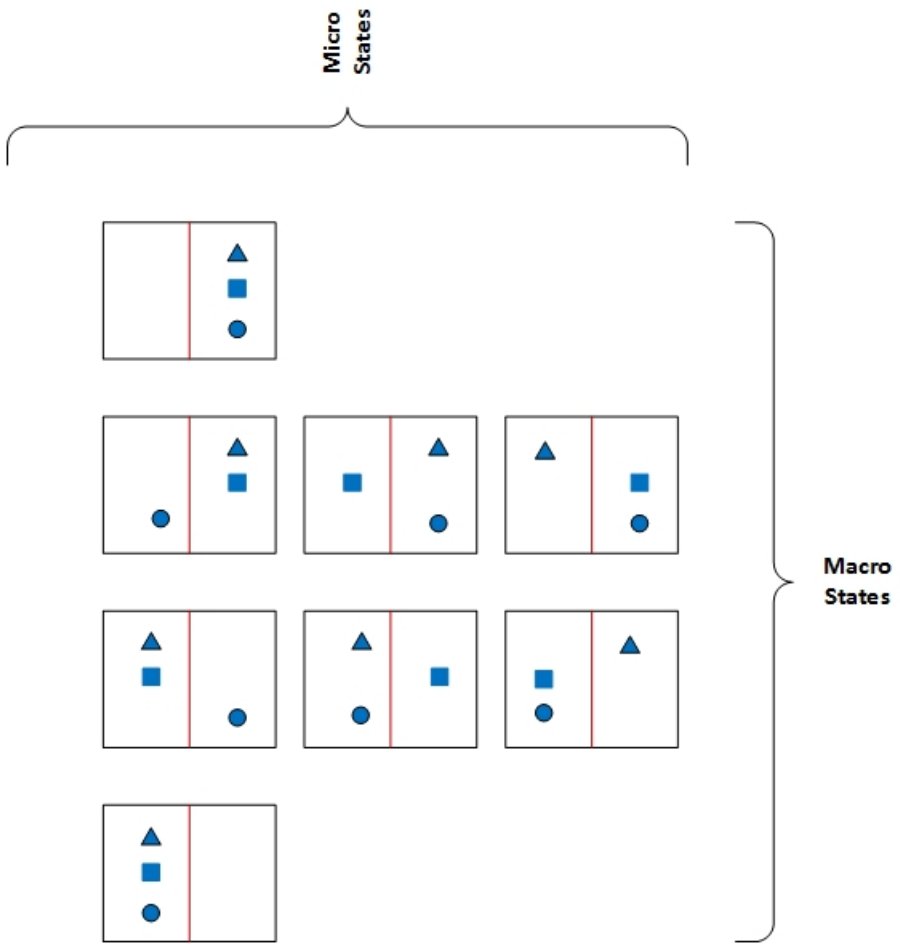

Figure 2.1: Micro states of two-partitions system with three distinguishable particles

Definition 2.1.1. *(Microstate) A microstate in statistical mechanics is identified by "a detailed particle-level description of the system." For example, microstates for a system with equal-volume parts and three distinguishable particles has* $2^3 = 8$ *different microstates, as illustrated in Figure 2.1.*

Definition 2.1.2. *(Macrostate) A macrostate in statistical mechanics consists of a set of microstates that can be described with a relatively small set of variables. Specifically, a macrostate is a thermodynamic or equilibrium state that can be defined in terms of variables energy* (E)*, volume* (V)*, and particle number* (n)*. For example,*

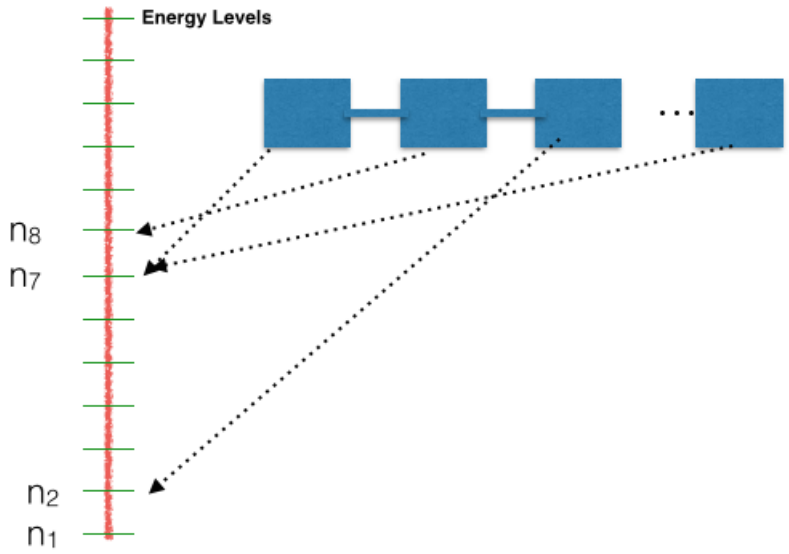

Figure 2.2: Energy levels or occupation numbers of N particles

Figure 2.1, shows four macrostates one of which is a two-sided system where two particles are in the left partition and one particle is on the right. This macrostate has three microstates.

Boltzmann defined special macrostates by the number of particles n_i that occupy a particular energy level i. These macro states are also called "occupation numbers." A set of occupation numbers, $n_1, n_2..., n_j$ defines a particular macrostate of the system. Suppose we have n copies of a system in a heat bath as show in Figure 2.2 where n is very large. Drawing from n, we want to know how many boxes occupy state i or energy level i. Since there are an infinite number of states, most of these states will have zero assignments, and all boxes have the same average energy. Moreover, assume that the total energy is $E_{total} = n \times \bar{E}$, where $\bar{E}$ is the average energy. Then, the number of ways that occupational numbers can be realized is

$$\Omega = \frac{n!}{\prod_{i=1}^{n} n_i}.$$

The probability that any given box will be in state i is given by $P(i) = \frac{n_i}{n}$. Thus, we have following constraints:

$$\sum_{i=1}^{n} P(i) = 1 \tag{2.1}$$

$$\sum_{i=1}^{n} n_i E_i = n\bar{E} \tag{2.2}$$

where the average energy can be written in terms of probability as $\bar{E} = \sum_{i=1}^{n} P(i)E_i$. Instead of maximizing Ω, it is easier to maximize the $\log(\Omega)$. Thus, $\log(\Omega) = \log(n!) - \sum_{i=1}^{n} \log(n_i!)$. Using Stirling's approximation, $\log(n!) \cong n\log(n) - n$, we get

$$\log(\Omega) \cong -n \sum_{i=1}^{n} P(i)\log(P(i)) \tag{2.3}$$

Note that, $-\sum_{i=1}^{n} P(i)\log(P(i))$ is the entropy of a single system. To optimize (finding minimum or maximum) Equation 2.3 subject to the constraints defined in Equation 2.1 and Equation 2.2, we apply Lagrange Multipliers as $-\sum_{i=1}^{n} P(i)\log(P(i)) - \alpha\sum_{i=1}^{n} P(i) - \beta\sum_{i=1}^{n} n_i E_i = 0$, where α and β are the Lagrange multipliers. Differentiating the function with respect to $P(i)$, the probability is obtained as:

$$P(i) = e^{-(1+\alpha)} e^{-\beta E_i}. \tag{2.4}$$

The term β is defined in terms of temperature as $\frac{1}{k_b T}$ where k_b is the Boltzmann constant and T is temperature. Historically, $e^{-(1+\alpha)} = \frac{1}{Z}$ where Z is the *partition function*. The partition function is the sum over all the microstates of the system. In probability theory, it is used as normalization constant. Using the constraint in

Equation 2.1, we rewrite the partition function as:

$$Z(\beta) = \sum_{i=1}^{n} e^{-\beta E_i} \tag{2.5}$$

Thus, the probability can be written as:

$$P(i) = \frac{1}{Z} e^{-\beta E_i} \tag{2.6}$$

This equation is the Boltzmann Distribution. Z ensures that the $\sum_{i=1}^{n} p(i) = 1$. The partition function contains a great deal of information. For example, average energy, $\bar{E}$, can be written as $\bar{E} = -\frac{\partial \log Z}{\partial \beta}$. The following are important definitions and equations related to the partition function.

Definition 2.1.3. *(Free Energy) Free energy is "useful" work obtainable from a thermodynamic system at a constant temperature. It is also called Helmholtz Free energy:*

$$A = -\frac{\log(Z)}{\beta}$$

Definition 2.1.4. *(Average energy of the system)*

$$\bar{E} = -\frac{\partial \log(Z)}{\partial \beta}$$

Definition 2.1.5. *(Entropy of the system)*

$$T \times S = E - A$$

$$S = \log(Z) - \beta \frac{\partial \log(Z)}{\partial \beta}$$

2.2 Restricted Boltzmann Machine

One of the well known approaches for feature representation is the Restricted Boltzmann Machine (RBM). An RBM is a type of Hopfield net and a restricted version of the general Boltzmann Machines (BM). A BM is a network of visible and hidden stochastic binary units where the network is fully connected. On the other hand, an RBM network is a bi-partite graph where only hidden and visible nodes are coupled. There are no dependencies among visible nodes or among hidden nodes. The RBM model was first proposed by Smolensky [7] in 1986. Hinton *et al.* developed an algorithm to train a BM in 1985 as a parallel network for constraint satisfaction [8].

As discussed in Section 2.1, in statistical mechanics, the Boltzmann distribution is the probability of a random variable that realizes a particular energy level (Equation 2.6) [6]. In machine learning, β is usually set to 1, except in the context of algorithms such as simulated annealing. In simulated annealing the temperature T controls the evolution of the states of the system. The partition function, Z, is generally intractable to compute. However, when Z is computable, all other properties of the system such as entropy, temperature, etc. can be calculated.

The RBM is a generative model with visible and hidden nodes as shown in Figure 2.3. The model represents a Boltzmann energy distribution [6], where the probability distribution of the RBM with visible ($\mathbf{x}$) and hidden nodes ($\mathbf{h}$) is given in following equation:

$$P(\mathbf{x}, \mathbf{h}) = \frac{\exp(-E(\mathbf{x}, \mathbf{h}))}{Z}$$

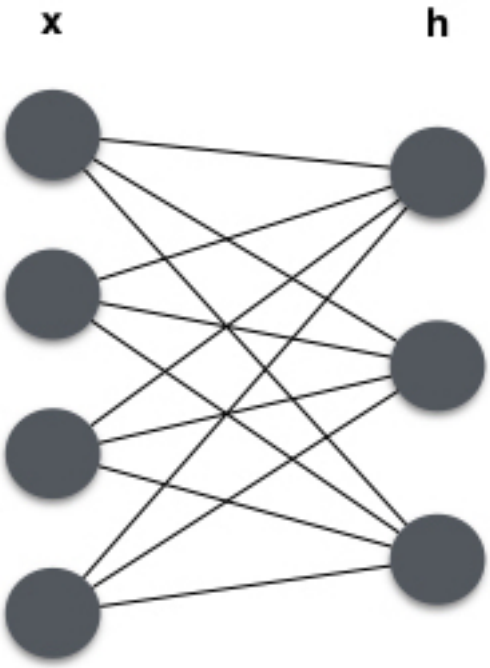

Figure 2.3: Restricted Boltzmann Machine

The conditional probability can be written in terms of the energy function as follows:

$$P(\mathbf{h}|\mathbf{x}) = \frac{\exp(-E(\mathbf{x}, \mathbf{h}))}{\sum_{\mathbf{h}} \exp(-E(\mathbf{x}, \mathbf{h}))}$$

The partition function defines configurations over all possible $\mathbf{x}$ and $\mathbf{h}$ vectors

$$Z = \sum_{\mathbf{x},\mathbf{h}} \exp(-E(\mathbf{x}, \mathbf{h})) \tag{2.7}$$

The probability of data $P(\mathbf{x})$ is obtained by marginalizing over the hidden vector $\mathbf{h}$.

$$P(\mathbf{x}) = \sum_{\mathbf{h}} P(\mathbf{x}, \mathbf{h}) = \sum_{\mathbf{h}} \frac{\exp(-E(\mathbf{x}, \mathbf{h}))}{Z} \tag{2.8}$$

The energy function of an RBM is then given as

$$E(\mathbf{x}, \mathbf{h}) = -\mathbf{h}^\top \mathbf{W}\mathbf{x} - \mathbf{b}^\top \mathbf{x} - \mathbf{c}^\top \mathbf{h}$$

Here, $\mathbf{b}$ and $\mathbf{c}$ are bias vectors on visible and hidden layers respectively.

We can rewrite the energy function as a sum over both hidden and visible nodes as:

$$E(\mathbf{x}, \mathbf{h}) = -\sum_{j}^{n}\sum_{k}^{m} h_j w_{jk} x_k - \sum_{k}^{m} b_k x_k - \sum_{j}^{n} c_j h_j$$

where n is number of hidden nodes and m number of visible (input) nodes. $P(\mathbf{x})$ defined in equation 2.8 can be written as the sum over all configurations of size n :

$$\begin{aligned}
P(\mathbf{x}) &= \sum_{\mathbf{h}\in\{0,1\}^n} \exp(\mathbf{h}^\top \mathbf{W}\mathbf{x} + \mathbf{b}^\top \mathbf{x} + \mathbf{c}^\top \mathbf{h})/Z \\
&= \underbrace{\sum_{h_1\in\{0,1\}} \sum_{h_2\in\{0,1\}} \cdots \sum_{h_n\in\{0,1\}}}_{\mathbf{h}\in\{0,1\}^n} \exp(\mathbf{h}^\top \mathbf{W}\mathbf{x} + \mathbf{b}^\top \mathbf{x} + \mathbf{c}^\top \mathbf{h})/Z \\
&= \sum_{h_1\in\{0,1\}} \sum_{h_2\in\{0,1\}} \cdots \sum_{h_n\in\{0,1\}} \exp(\sum_{j=1}^{n}(h_j \mathbf{w}_j \mathbf{x} + b^\top \mathbf{x} + c_j h_j)/Z \\
&= \sum_{h_1\in\{0,1\}} \sum_{h_2\in\{0,1\}} \cdots \sum_{h_n\in\{0,1\}} \prod_{j=1}^{n} \exp(h_j \mathbf{w}_j \mathbf{x} + b^\top \mathbf{x} + c_j h_j)/Z \\
&= \prod_{j=1}^{n} \sum_{h_j\in\{0,1\}} \exp(h_j \mathbf{w}_j \mathbf{x} + b^\top \mathbf{x} + c_j h_j)/Z
\end{aligned} \tag{2.9}$$

Since $\mathbf{b}^\top \mathbf{x}$ is not dependent on $\mathbf{h}$ and it can be taken out of sum and product:

$$P(\mathbf{x}) = \exp(\mathbf{b}^\top \mathbf{x}) \prod_{j=1}^{n} \sum_{h_j\in\{0,1\}} \exp(h_j \mathbf{w}_j \mathbf{x} + c_j h_j)/Z$$

Replacing $h = 0$ and $h = 1$, we obtain

$$P(\mathbf{x}) = \exp(\mathbf{b}^\top \mathbf{x}) \prod_{j=1}^{n} (1 + \exp(\mathbf{w}_j \mathbf{x} + c_j))/Z$$

Using the fact $\exp(\log(\mathbf{x})) = \mathbf{x}$, $P(\mathbf{x})$ can be written as:

$$P(\mathbf{x}) = \exp(\mathbf{b}^\top \mathbf{x} + \sum_{j=1}^{n} \log(1 + \exp(\mathbf{w}_j \mathbf{x} + c_j)))/Z$$

Finally, $f(x) = \log(1+\exp(\mathbf{x}))$ is the *softplus* function. Writing the above function in term of *softplus*, we obtain the following equation:

$$P(x) = \exp(\mathbf{b}^\top \mathbf{x} + \sum_{j=1}^{n} \text{softplus}(\mathbf{w}_j \mathbf{x} + c_j))/Z$$

Inspired from statistical mechanics, the exponential term $F(\mathbf{x}) = \mathbf{b}^\top \mathbf{x} + \sum_{j=1}^{n} \log(1 + \exp(\mathbf{w}_j \mathbf{x} + c_j))$ is called free energy. Thus,

$$P(\mathbf{x}) = \exp(-F(\mathbf{x}))/Z \tag{2.10}$$

2.2.1 Inference in RBM: Conditional Probability

Calculating $P(\mathbf{x}, \mathbf{h})$ is not tractable due to the partition function, Z. However, the conditional probability, $P(\mathbf{h}|\mathbf{x}) = P(\mathbf{x}, \mathbf{h}) / \sum_{h'} P(\mathbf{x}, \mathbf{h}')$, has rather a simple form. To differentiate from $\mathbf{h}$, we use $\mathbf{h}'$ to represents all hidden vectors (configurations) of size n. Using equation 2.2, we obtain

$$P(\mathbf{h}|\mathbf{x}) = \frac{\exp(\mathbf{h}^\top \mathbf{W}\mathbf{x} + \mathbf{b}^\top \mathbf{x} + \mathbf{c}^\top \mathbf{h})/Z}{\sum_{h' \in \{0,1\}^n} \exp(\mathbf{h}'^\top \mathbf{W}\mathbf{x} + \mathbf{b}^\top \mathbf{x} + \mathbf{c}^\top \mathbf{h}')/Z}$$

The Z and $\mathbf{b}^\top \mathbf{x}$ values cancel out. If we write this equation as an explicit sum over all indices, we obtain

$$P(\mathbf{h}|\mathbf{x}) = \frac{\exp(\sum_{j=1}^{n} h_j \mathbf{w}_j \mathbf{x} + c_j h_j)}{\underbrace{\sum_{h'_1 \in \{0,1\}} \sum_{h'_2 \in \{0,1\}} \cdots \sum_{h'_n \in \{0,1\}}}_{\mathbf{h}' \in \{0,1\}^n} \exp(\sum_{j=1}^{n} h'_j \mathbf{w}_j \mathbf{x} + c_j h'_j)}$$

Using $c^{\left[\sum_{n=s}^{t} f(n)\right]} = \prod_{n=s}^{t} c^{f(n)}$ rule, we rewrite it as:

$$P(\mathbf{h}|\mathbf{x}) = \frac{\prod_{j=1}^{n} \exp(h_j \mathbf{w}_j \mathbf{x} + c_j h_j)}{\sum_{h'_1 \in \{0,1\}} \sum_{h'_2 \in \{0,1\}} \cdots \sum_{h'_n \in \{0,1\}} \prod_{j=1}^{n} \exp(h'_j \mathbf{w}_j \mathbf{x} + c_j h'_j)}$$

Further we can rewrite the denominator as a product:

$$P(\mathbf{h}|\mathbf{x}) = \frac{\prod_{j=1}^{n} \exp(h_j \mathbf{w}_j \mathbf{x} + c_j h_j)}{\prod_{j=1}^{n} \sum_{h'_j \in \{0,1\}} \exp(h'_j \mathbf{W}_j \mathbf{x} + c_j h'_j)}$$

The denominator can be simplified further using $j = 0$ and $j = 1$:

$$P(\mathbf{h}|\mathbf{x}) = \frac{\prod_{j=1}^{n} \exp(h_j \mathbf{w}_j \mathbf{x} + c_j h_j)}{\prod_{j=1}^{n} (1 + \exp(\mathbf{w}_j \mathbf{x} + c_j))}$$

Using the same product, we obtain

$$P(\mathbf{h}|\mathbf{x}) = \prod_{j=1}^{n} \frac{\exp(h_j \mathbf{w}_j \mathbf{x} + c_j h_j)}{(1 + \exp(\mathbf{w}_j \mathbf{x} + c_j))}$$

It turns out the term inside the product is a probability distribution. Thus, it must be $P(h_j|\mathbf{x})$ because of the Markov property. As result, the equation can be written as follows.

$$P(\mathbf{h}|\mathbf{x}) = \prod_{j=1}^{n} P(h_j|\mathbf{x})$$

Algorithm 2.1 GRADIENT-DESCENT($J(\theta)$, α)

1: **Input**: $J(\theta)$: cost function, α: learning rate.
2: **Model Parameters**: θ: model parameter,
3: **repeat**{
4: $\quad \theta_i \leftarrow \theta_i - \alpha \times \frac{\partial J(\theta)}{\partial \theta_i}$
5: }

Now, we can calculate $P(h_j = 1|\mathbf{x})$ as follows:

$$P(h_j = 1|\mathbf{x}) = \frac{\exp(\mathbf{w}_j\mathbf{x} + c_j)}{(1 + \exp(\mathbf{w}_j\mathbf{x} + c_j))}$$

If we multiply both numerator and denominator by $\exp(-\mathbf{w}_j\mathbf{x} - c_j)$, the conditional probability is simplified as:

$$P(h_j = 1|\mathbf{x}) = \frac{1}{(1 + \exp(-\mathbf{w}_j\mathbf{x} - c_j))}$$

The result is a sigmoid function where $\sigma(x) = \frac{1}{1+e^{-x}}$:

$$P(h_j = 1|\mathbf{x}) = \sigma(\mathbf{w}_j\mathbf{x} + c_j) \tag{2.11}$$

2.2.2 Training RBM: Stochastic Gradient Descent

To train an RBM so that it assigns high probability to data, a negative log-likelihood method is used. In a typical gradient descent, there is a cost objective function $J(\theta)$ we would like to optimize. Here θ is a set of model parameters, so, the generic algorithm for gradient descent is given as Algorithm 2.1.

Note that all parameters θ_i should be updated simultaneously. Moreover, this simple algorithm is used for both Logistic Regression and Linear Regression. The difference is the respective cost function used in the algorithm. Generally, each pa-

Algorithm 2.2 STOCHASTIC-GRADIENT-DESCENT($J(\theta)$, α)

```
1: Input: J(θ): cost function, α: learning rate.
2: Model Parameters: θ: model parameter,
3: shuffle dataset
4: repeat{
5:    for each data sample{
6:       θ_i ← θ_i − α × ∂J(θ)/∂θ_i
7:    }
8: }
```

rameter update involves the complete batch of the dataset at once. Parameters are updated until convergence occurs. However, a stochastic gradient descent updates the model parameters after each data instance. Thus, it optimizes the model to fit the current data instance. Algorithm 2.2 depicts a generic stochastic gradient descent. Because the model parameters are updated after each data instance, data is shuffled beforehand.

For RBMs, we use negative log-likelihood to optimize the energy function. Using equation 2.2 the log-likelihood is calculated as follows.

$$\frac{-\partial \log(P(\mathbf{x}))}{\partial \theta} = \frac{\partial}{\partial \theta}\left(-\log \sum_{h} \frac{\exp(-E(\mathbf{x}, \mathbf{h}))}{Z}\right)$$

where θ represents the model parameters (W, b, and c). To derive the gradient, first the log is expanded and Z is replaced with equation 2.7. Then, partial differentiation

is carried out.

$$\begin{aligned}
\frac{-\partial \log(P(\mathbf{x}))}{\partial\theta} &= \frac{\partial}{\partial\theta}\left(-\log\sum_{h}\frac{\exp(-E(\mathbf{x},\mathbf{h}))}{Z}\right) \\
&= -\frac{1}{\partial\theta}\left(\sum_{h}\exp(-E(\mathbf{x},\mathbf{h})\right) + \frac{1}{\partial\theta}\left(\sum_{h,x}\exp(-E(\mathbf{x},\mathbf{h})\right) \\
&= \frac{1}{\sum_h \exp(-E(\mathbf{x},\mathbf{h}))}\sum_{h}\exp(-E(\mathbf{x},\mathbf{h})\frac{\partial E(\mathbf{x},\mathbf{h})}{\partial\theta} \\
&- \frac{1}{\sum_{h,x} \exp(-E(\mathbf{x},\mathbf{h}))}\sum_{h,x}\exp(-E(\mathbf{x},\mathbf{h}))\frac{\partial E(\mathbf{x},\mathbf{h})}{\partial\theta} \\
&= \sum_{h} P(\mathbf{h}|\mathbf{x})\frac{\partial E(\mathbf{x},\mathbf{h})}{\partial\theta} - \sum_{h,x} P(\mathbf{x},\mathbf{h})\frac{\partial E(\mathbf{x},\mathbf{h})}{\partial\theta}.
\end{aligned} \tag{2.12}$$

The first term is the expectation over $\mathbf{h}$, and the negative term is the expectation over both $\mathbf{h}$ and $\mathbf{x}$. Thus, the stochastic gradient becomes

$$\frac{-\partial \log(P(\mathbf{x}))}{\partial\theta} = \underbrace{E_h\left[\frac{\partial E(\mathbf{x},\mathbf{h})}{\partial\theta}|x\right]}_{\text{positive phase}} - \underbrace{E_{h,x}\left[\frac{\partial E(\mathbf{x},\mathbf{h})}{\partial\theta}\right]}_{\text{negative phase}} \tag{2.13}$$

The gradient contains two terms that are referred as the *positive* and the *negative* phase respectively. The first positive phase increases the probability of the training data by decreasing free energy, while the negative phase decreases the probability of a sample generated by the model. Computing the expectation over the first term is tractable; however, computing the second term is not. Thus, Hinton introduced the Contrastive Divergence(CD) algorithm that uses Gibbs sampling to estimate the second term [9].

2.2.3 Contrastive Divergence

In this section, we describe the Contrastive Divergence (CD) algorithm, the seminal algorithm for training Restricted Boltzmann Machines. CD provides a reasonable approximation to the likelihood gradient. The CD-1 algorithm (i.e, Contrastive Divergence with one step) is usually sufficient for many applications [1, 10].

To calculate updates in CD, we need to do the derivation of equation 2.13 with respect to weight vector $\mathbf{W}$.

$$\begin{aligned}\frac{E(\mathbf{x},\mathbf{h})}{\partial w_{jk}} &= \frac{\partial}{\partial w_{jk}}\left(-\sum_j\sum_k h_j w_{jk} x_k - \sum_k b_k x_k - \sum_j c_j h_j\right) \\ &= -\frac{\partial}{\partial w_{jk}}\left(\sum_j\sum_k h_j w_{jk} x_k\right) \\ &= -h_j x_k\end{aligned} \tag{2.14}$$

We can find the expectation of the positive term in equation 2.13 with respect to jk as follows:

$$\begin{aligned}E_{\mathbf{h}}\left[\frac{\partial E(\mathbf{x},\mathbf{h})}{\partial w_{jk}}|\mathbf{x}\right] &= E_{\mathbf{h}}\left[-h_j x_k|\mathbf{x}\right] \\ &= \sum_{h_j\in\{0,1\}} -h_j x_k P(h_j|\mathbf{x}) \\ &= -p(h_j=1|\mathbf{x})x_k\end{aligned} \tag{2.15}$$

Since the negative term in equation 2.13 is not tractable to compute in CD, an approximation $\tilde{\mathbf{x}}$ is obtained using Gibbs sampling. Thus, the resulting gradient for CD becomes $-P(h_j=1|\tilde{\mathbf{x}})\tilde{x_k}$, similar to equation 2.15 for the positive phase. The

W parameter update is carried out as follows:

$$\begin{aligned} w_{jk} &\leftarrow w_{j,k} - \alpha \left(\frac{E(x,h)}{\partial w_{jk}} \right) \\ &\leftarrow w_{jk} + \alpha(p(h_j = 1|\mathbf{x})x_k - p(h_j = 1|\tilde{\mathbf{x}})\tilde{x_k}) \end{aligned} \tag{2.16}$$

where $\alpha \in (0, 1)$ is a learning rate. Using the same technique, updates for all parameters take the form:

$$\begin{aligned} w_{jk} &\leftarrow w_{jk} + \alpha(P(h_j = 1|\mathbf{x})x_k - P(h_j = 1|\tilde{\mathbf{x}})\tilde{x_k}) \\ b_j &\leftarrow b_j + \alpha(x_j - \tilde{x_j}) \\ c_j &\leftarrow c_j + \alpha(P(h_j = 1|x) - P(h_j = 1|\tilde{x})) \end{aligned} \tag{2.17}$$

As shown in Figure 2.4, the hidden node activations in each step depend only on values of visible nodes in the previous step. Similarly, the visible node activations depend only on the values of hidden nodes in the previous step. Thus, this chain of sampling back and forth from the model has the Markov property. As a result, the sampling process is a Markov chain, as follows: First, $P(\mathbf{h}|\mathbf{x})$ is calculated using the sigmoid function and $\mathbf{h}^0$ is sampled from P($\mathbf{h}|\mathbf{x}$). Then, $P(\mathbf{x}|\mathbf{h^0})$ is computed. The new visible vector, $\mathbf{x}^1$ is sampled from $P(\mathbf{x}|\mathbf{h^0})$. Finally, $\mathbf{h}^1$ is calculated the same way by sampling from $P(\mathbf{h^1}|\mathbf{x^1})$. The process can be repeated k-times. An alternative description of Contrastive Divergence algorithm is given by Bengio [10].

Finally, Algorithm 2.3 shows the pseudocode for training RBMs using the one step Contrastive Divergence method. The algorithm accepts a sample data instance and model parameters; weight vector ($\mathbf{W}$), visible layer bias vector ($\mathbf{b}$), hidden layer bias vector($\mathbf{c}$), learning rate (α). It updates model parameters as follows.

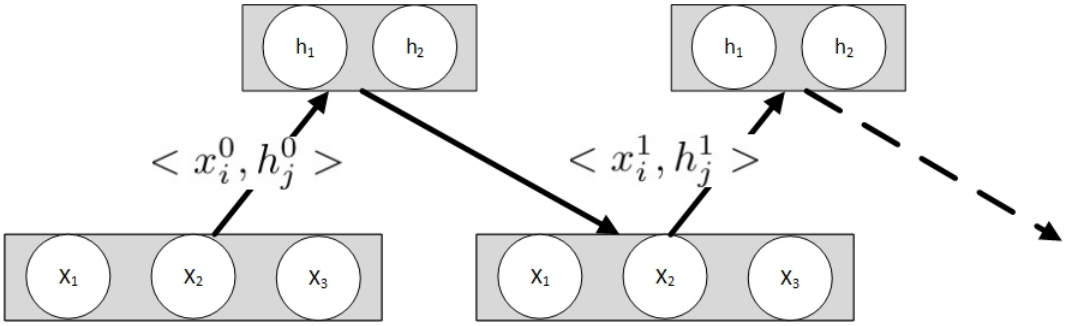

Figure 2.4: CD Markov Chain

Algorithm 2.3 CD-1($\mathbf{x}_i$, α)

1: **Input**: $\mathbf{x}_i$: data sample, α: learning rate.
2: **Model Parameters**: $\mathbf{W}$: weight vector, $\mathbf{b}$: bias vector on visible nodes, $\mathbf{c}$: bias vector on hidden nodes
Notation: $\mathbf{x} \sim P$ means $\mathbf{x}$ is sampled from P
Positive Phase:
3: $\mathbf{x^0} \leftarrow \mathbf{x_i}$
4: $\mathbf{h^0} \leftarrow \sigma(\mathbf{c} + \mathbf{W}\mathbf{x})$
Negative Phase:
5: $\tilde{\mathbf{h}}\mathbf{^0} \sim \mathbf{P}(\mathbf{h}|\mathbf{x^0})$
6: $\tilde{\mathbf{x}} \sim \mathbf{P}(\mathbf{x}|\tilde{\mathbf{h}}\mathbf{^0})$
7: $\mathbf{h^1} \leftarrow \sigma(\mathbf{c} + \mathbf{W}\tilde{\mathbf{x}})$
Update parameters:
8: $\mathbf{b} \leftarrow \mathbf{b} + \alpha(\mathbf{x^0} - \tilde{\mathbf{x}})$
9: $\mathbf{c} \leftarrow \mathbf{c} + \alpha(\mathbf{h^0} - \mathbf{h^1})$
10: $\mathbf{W} \leftarrow \mathbf{W} + \alpha(\mathbf{h^0}\mathbf{x^0} - \mathbf{h^1}\tilde{\mathbf{x}})$

First, in the positive phase (lines 3-4), the probability of the hidden node is calculated for all hidden nodes, given the visible vector. In the negative phase (lines 5-7), the probability of each hidden node is determined by sampling from the model. First a sample of points for the hidden nodes is drawn based on the current estimate of the distribution $\mathbf{P}(\mathbf{h}|\mathbf{x^0})$ (line 5). Using these sampled points $\mathbf{h^0}$, the current estimate of $\mathbf{P}(\mathbf{x}|\mathbf{h})$ is used to sample points for the visible nodes $\mathbf{x}$ (line 6). Finally, on line 7, the probabilities of the hidden nodes are updated based on the sampled vector for the visible nodes. The parameters of the network are updated on lines 8-10.

Contrastive Divergence need not be limited to one forward and backward pass in this matter, and Algorithm 2.3 can be extended by creating a loop around lines 3–7. Then for $k > 1$, the positive and negative phases are repeated k times before the parameters are updated.

2.3 Autoencoders

An Autoencoder is a feed-forward neural net that predicts its own input [11]. It often introduces one or more hidden layers that have lower dimensionality than the inputs so that it creates a more efficient code for the representation [3]. As a generative model, the autoencoder encodes the input $\mathbf{x}$ into some representation $c(\mathbf{x})$; the input can be reconstructed from the resulting code.

Training is done by using reconstruction error. The training process involves updating model parameters (weights and biases) by minimize this reconstruction error [10].

Bengio claimed that if the autoencoder is trained with one linear hidden layer by minimizing squared error, then the resulting code corresponds to principal components of the data. However, if the hidden layer is non-linear, the autoencoder has a different representation than PCA. It has the ability to capture multi-modal aspects of the input distribution. Often, the following formula is used to minimize negative log-likelihood of the reconstruction, given the encoding $c(\mathbf{x})$:

$$reconstruction\ error = \log P(\mathbf{x}|c(\mathbf{x}))$$

For binary $\mathbf{x} \in [0,1]^d$, the the loss function can be written as:

$$\log P(\mathbf{x}|c(\mathbf{x})) = \sum_{i}^{n} x_i \log f_i(c(\mathbf{x})) + (1 - x_i) \log(1 - f_i(c(\mathbf{x})))$$

where n is number features and $f(\cdot)$ is the decoder. Thus, the network will generate the input as $f(c(\mathbf{x}))$. $c(\mathbf{x})$ is a lossy compression. Both encoder and decoder functions are sigmoid function:

$$\mathbf{y} = c(\mathbf{x} = \sigma(\mathbf{W}\mathbf{x} + \mathbf{c})$$

where $\mathbf{W}$ is the weight matrix and $\mathbf{c}$ is the bias vector in the hidden nodes. The decoder can be written as:

$$\mathbf{z} = f(y) = \sigma(\mathbf{W}^T\mathbf{y} + \mathbf{b})$$

where $\mathbf{c}$ is bias vector on input nodes and $\mathbf{z}$ is the reconstructed input vector.

2.4 Deep Learning

The performance of machine learning algorithms depends heavily on set of features used in the model. Thus, a feature detector is the first component of a learning process. Using extracted features, the learning algorithm forms a hypothesis that functions as a learned model. A feature is one or more attributes of the dataset (or some transformation of the attributes) considered important in describing the data. For example, in the handwritten digit recognition task, using raw pixel values may not be sufficient. Many learning methods either rely on derived features such as the gradient of histograms, while others project raw pixels onto a higher dimensions. Feature engineering is an expansive process and often requires domain specific

knowledge. In an attempt to achieve a more generic algorithm, it is desirable that the algorithm does not depend on this feature extraction process. In other words, ideally the algorithm should identify the explanatory factors automatically.

According to Bengio *et al.* [4] a good representation, in the case of a probabilistic model, is the one that captures the posterior distribution of the underlying explanatory factors for the observed input. Deep learning methods learn representations by composition of multiple non-linear transformations in order to obtain more abstract representations.

As stated by Bengio *et al.* [4] a good representation is expressive and distributive; a reasonable representation can capture many possible input configurations. The second most important aspect of representation is abstraction. Abstract concepts are formed in terms of less abstract features and abstract concepts are generally invariant to local changes of the input. Finally, the third aspect of good representation is that it must disentangle the factors of variation. Because different explanatory factors of the data tend to change independently in the input distribution, disentangling these factors may lead to better representations.

In 2006, Hinton *et al.* experimented with a deep learning architecture [11] and demonstrated that a network with multiple layers can represent features superior to many traditional methods. Since then, deep learning has become one of the most active research areas in machine learning. The core idea is to learn a hierarchy of features one level at a time in an unsupervised fashion. Each level is composed with previously learned transformations. Figure 2.5 illustrates a *stack* of RBMs where input to each layer is the output of the previous layer. A typical learning process involves unsupervised learning of one layer at a time in a greedy fashion. This learning method is called "greedy layerwise unsupervised training."

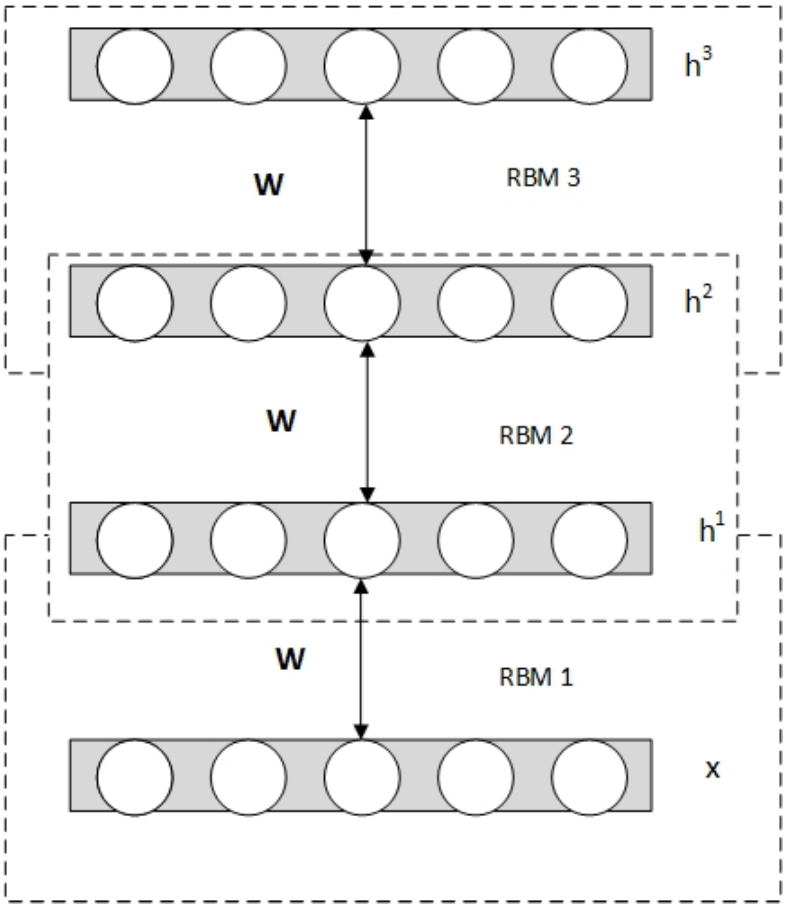

Figure 2.5: Three-layer Deep Belief Network

Figure 2.6 shows the layerwise training process where weights and biases for previous layers are frozen. The RBM of the last layer is training by transforming raw features through the previous two RBMs. Thus, the last layer is trained independent of other layers. In addition to RBMs, autoencoders can be used as component of deep neural networks.

When the stack of a deep network is trained with the greedy layerwise unsupervised pre-training process, the resulting deep features can be used as input to a standard supervised learning method or as initialization for a deep supervised neural

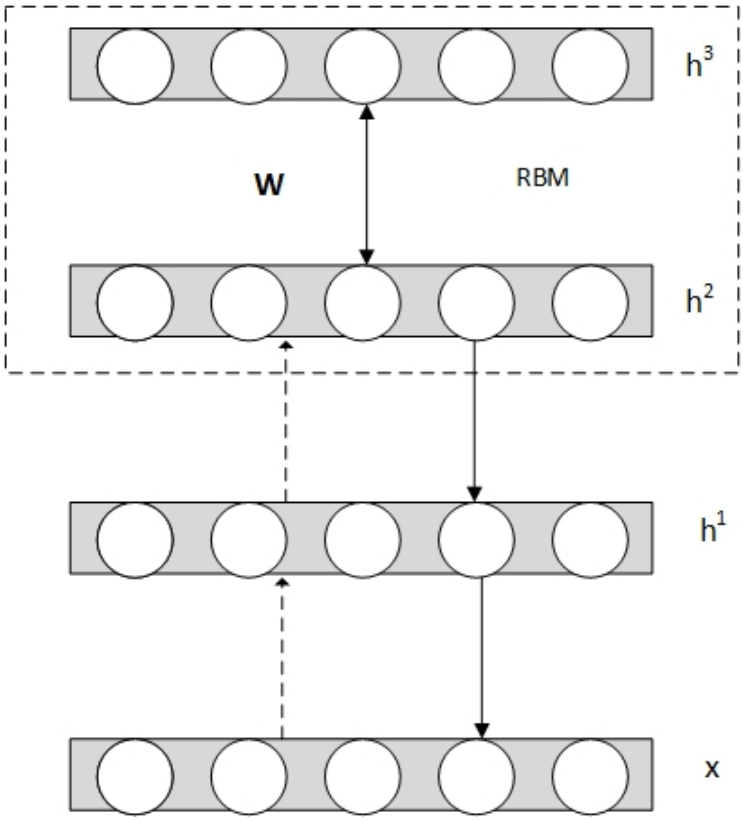

Figure 2.6: Three-layer Deep Belief Network: Training - Last Layer

network. In the latter case, the first N layers are trained in an unsupervised fashion. The result of the stack serves as input to a supervised deep neural network.

2.5 Spatial and Temporal Feature Analysis

In this section, we introduce a few spatial and temporal techniques for qualitative and quantitative analysis of spatial and temporal features. These techniques are widely used in geostatistics and time series classification. However, here we selective use spatial techniques that will inform us the existence of spatially local features in a given dataset. Furthermore, we discuss Temporal Time Warping, a scoring function, in the context of time series classification task.

2.5.1 Variograms

Coined after D. G. Krige, a South African mining engineer, in geostatistics, Kriging (or Gaussian process regression) is a regression technique that uses a Gaussian process. It is widely used in the domain of spatial analysis and prominently applied to the field of oil exploration. The technique is used for making predictions from observed spatial data. It predicts a value of a spatial feature at a given point by interpolating values of surrounding data points, weighted according to the spatial covariance of the neighboring values [12, 13]. Basic Kriging uses variograms in a spatial setting.

To introduce Kriging and variograms, let $Z(s)$ be a random process (or a Gaussian process) that produces n data samples $Z(s_1), Z(s_2), ..., Z(s_n)$. Using these data points, an inference is made on the process to predict a known functional $g(Z(\cdot))$. As described by Cressie, a point prediction assumes that $g(Z(\cdot)) = Z(s_0)$ for the known location s_0 [12]. Thus, *spatial prediction* refers to predicting $g(Z(\cdot))$ from data collected in n known locations, $s_1, ..., s_n$. For ordinary Kriging, one attempts to minimize squared-error. The process $Z(\cdot)$ is assumed to have the following property:

$$2\gamma(h) = var(Z(s+h) - Z(s)), h \in \mathbb{R}^d \tag{2.18}$$

where h is a separation (i.e., distance) vector, and $\gamma(\cdot)$ is known as the (experimental) semivariance [14]. The following relationship holds between variograms, variance, and covariance :

$$\gamma(h) = cov(0) - cov(h)$$

where

$$cov(h) = E\{Z(s+h) \cdot Z(s)\} - E\{Z(s)\}^2$$

and

$$cov(0) = var(Z(s))$$

Semivariance measures differences in observed values over a set of distance bands or lags. For such a function to be defined properly, some fairly strong assumptions about the data must be made (including but not limited to it being sampled from a static, isotropic spatial distribution).

In order to compute variograms, one has to find the squared differences between all pairs of values in the dataset first. Then, these differences are allocated to lag classes (bins) based on the distance separating the pair (often the direction is also considered). The result is a set of semivariance values for distance lags, $h = 0, ..., H$ where H is less than the greatest distance between pairs. When plotting bin values per lag, the resulting graph is called a variogram plot. In a way, the bins are inter-feature (i.e. sampling location) distances, and the height of each column is the mean of the variance of the (sample value) differences between all feature pairs that are that distance apart. If we can model the inter-feature variance with distance using a variogram, the values at unknown distances can be predicted or estimated by an interpolation process.

2.5.2 Autocorrelation and Correlograms

In order to estimate linear predictors, the following assumption is also made:

$$cov(Z(s_1), Z(s_2)) = C(s1 - s2), \forall s_1, s_2$$

where $C(\cdot)$ is called *covariogram* or stationary covariance function [12]. This function is called *autocovariance* function by time-series analysts. When $C(0) > 0$,

$$\rho(h) = C(h)/C(0) \tag{2.19}$$

is called *correlogram*. In the time-series field, this measure is called autocorrelation. Autocorrelation is used to diagnose non-stationarity in time series. Thus, if $Z(\cdot)$ is stationary, then the following holds:

$$2\gamma(h) = 2(C(0) - C(h)) \tag{2.20}$$

We can make a similar histogram using correlations (or any other pair-wise statistical measure) between feature-pairs of a given distance. A serial correlation coefficient is given below for lag h:

$$\rho(h) = \frac{\sum_{t=1}^{n-h}(x_t - \bar{x})(x_{t+k} - \bar{x})}{\sum_{t=1}^{n}(x_t - \bar{x})} \tag{2.21}$$

For a random series, the $\rho(h)$ values for all h time steps will be approximately 0. They will be distributed according to $N(0, 1/n)$ [14]. If there is a short term correlation, the $\rho(h)$ will start at 1.0 and decrease gradually to 0 as the distances increase. If the overall process shows a steady increase over time, the correlogram will not be zero. This determines that the time series is not stationary.

In spatial statistics, the concept is adapted to spatial data, but it is not easy to translate this directly to spatial statistics. Often, on a $2D$ grid, joint counts of events

are calculated and the probability of a particular pattern is estimated. This yields formulas that are similar to the correlogram in time-series.

For a more in depth treatment of variograms, correlograms, and spatial statistics in general, the reader is directed to books on the subject [12] and [14].

2.5.3 Distributed Stochastic Neighbor Embedding

To embed data in a 2-dimensional space for visualization, *t-Distributed Stochastic Neighbor Embedding* (t-SNE) has been shown to be an effective technique [15]. Moreover, t-SNE is also a dimensionality reduction technique that is particularly good for visualizing high dimensional data.

The t-SNE method is similar to Multidimensional Scaling (MDS) and Locally Linear Embedding (LLE) techniques. MDS computes the low dimensional embedding that preserves pairwise distances between data points [16]. On the other hand, LLE builds a map of similarities in the data by finding a set of the nearest neighbors of each point. It then computes a weight for each data point as a linear combination of distances to its neighbor [17]. Both MDS and LLE use eigenvector-based optimization techniques to find the low-dimenstional embedding of the points.

The t-SNE method builds a map in which distances between points reflect similarities in the data. It embeds high-dimensional data in lower dimensional space by minimizing the discrepancy between pairwise statistical relationships in the high and low dimensional spaces. For a dataset of n points, let $i, j \in [1, n]$ be indices, and let $x_i \in \mathbf{X}$ and $y_i \in \mathbf{Y}$ refer to the ith datapoint of the original dataset and the low-dimensional equivalent respectively. Given a candidate embedding, t-SNE first calculates all pairwise Euclidean distances between data points in each space. The pairwise Euclidean distance between x_i and x_j is used to calculate a conditional

probability, $P_{j|i}$, which is the probability that x_i would pick x_j as its neighbor. This probability is based on a Gaussian centered at x_i. Similarly, pairwise conditional probabilities $q_{j|i}$ are calculated for each pair (y_i, y_j) in the low-dimensional embedding. As an objective function, t-SNE tries to minimize the discrepancies between the conditional probabilities for corresponding pairs in the high dimensional and low dimensional spaces by using *Kullback-Leibler* divergence (KL-divergence). This is an intractable global optimization problem, so often gradient descent is used to find a local optimum.

One drawback of t-SNE is that for large, high-dimensional datasets, even the local search can be quite slow. In such cases, PCA is sometimes used as a pre-processing step to speed up the computation and to suppress high-frequency noise. A typical example might retain the top 30 eigenvectors and project the original data into the eigenbasis. t-SNE would then be applied to this 30-dimensional dataset to reduce it to a 2-dimensional set for visualization.

The resulting $2D$ plots make the structure (or lack thereof) readily apparent. Since the optimization is done on pair-wise vector distances, feature ordering (i.e. spatially local structure) in the high-dimensional data does not change the qualitative properties of the low-dimensional data significantly. Moreover, since the mapping is non-linear and non-parametric, it is relatively insensitive to whether information is encoded using sparse or distributed representations. As a result, t-SNE allows us to examine the presence of structure without having to worry about the form of that structure impacting our analysis. Figure 2.7 shows a $2D$ embedding of *MNIST* dataset using t-SNE.

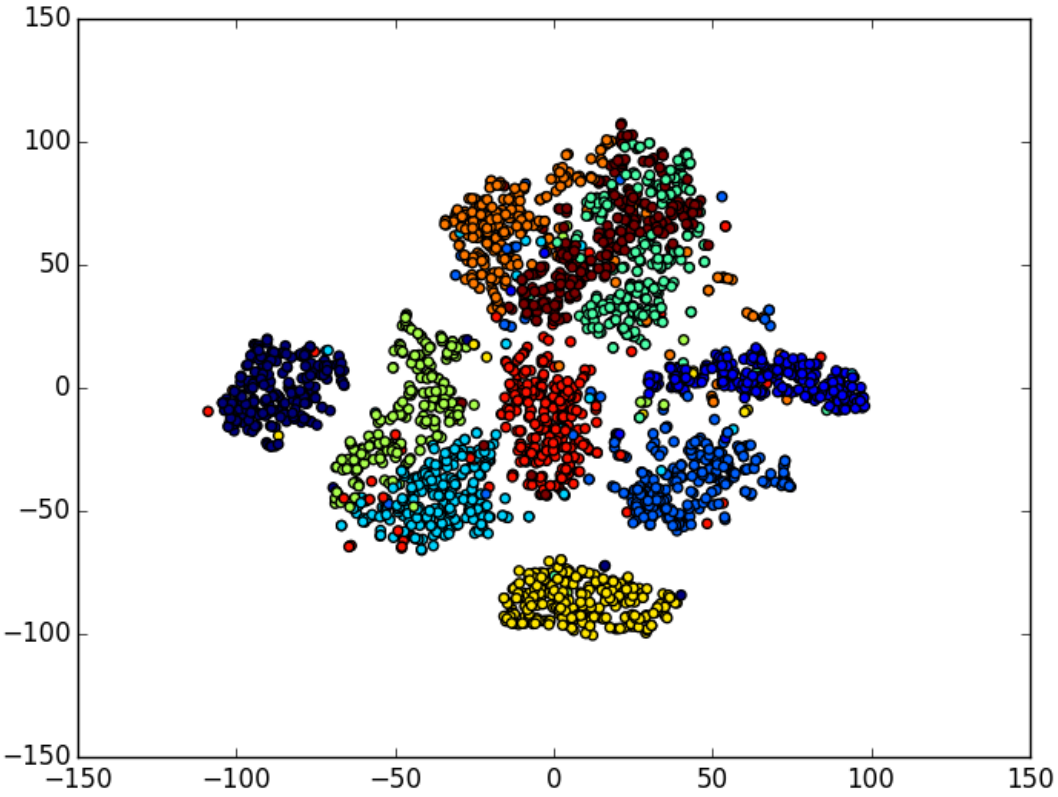

Figure 2.7: t-SNE Embedding of the MNIST Dataset

2.5.4 Dynamic Time Warping

Time series classification often involve computing a similarity or distance score that measures the similarity between two temporal sequences. Dynamic Time Warping (DTW) is an approach applied to two time series so that the distance measure between them is minimized. Specifically, DTW uses dynamic programming to find an optimal alignment with respect to a given distance function. It was developed by *Sakoe* and *Chiba* for speech recognition [18]; however, it has many applications, including but not limited to gene sequence comparison, time series classification, speaker recognition, partial shape matching, and other time series data such as video and audio.

Consider two time series s and t with length n and m respectively. The key idea in DTW is that sequences s and t can be arranged to form a $n \times m$ grid where each point (i, j) is the alignment between element s_i and t_j. The warping path, W, is constructed to align elements of s and t such that it minimizes the distance between them. Since W forms a sequence of grid points ($W = w_1, w_2, \ldots w_k$), each w value corresponds to a grid point (i, j) .

The warping path is subject to the following constraints:

- **Boundary conditions**: the warping path starts at $(0, 0)$ and ends at (n, m).
- **Continuity**: the warping path only traces adjacent points in the grid.
- **Monotonicity**: the points must be ordered monotonically with respect to time.

Thus, the DTW is a minimization over potential warping paths. Although there are an exponential number of paths, we calculate the minimum-cost path using dynamic programming as follows:

$$\gamma(i, j) = \delta(i, j) + \min\{\gamma(i-1, j), \gamma(i-1, j-1), \gamma(i, j-1)\} \tag{2.22}$$

where $\gamma(i, j)$ is the cumulative distance and $\delta(i, j)$ is the cost function between two points.

Several distance functions can be used. Following are the two most common distance functions:

$$\begin{aligned} \delta(i, j) &= \|s_i - t_i\| \\ \delta(i, j) &= \|s_i - t_i\|^2 \end{aligned} \tag{2.23}$$

The pseduocode for dymamic time warping is given in Algorithm 2.4. Essentially, the cumulative matrix cost is initialized on line 4-7. The cumulative cost function for

Algorithm 2.4 DTW(**s**, **t**)

```
1: s: time series 1, t: time series 2
2: n ← s.size
3: m ← t.size
4: γ: matrix of size s and t
5: γ[: 0] ← ∞
6: γ[0 :] ← ∞
7: γ[0 : 0] ← 0
8: for i ← 1 until n {
9:    for j ← 1 until m {
10:     cost = δ(s_i, t_j)
11:     γ(i, j) = cost + min{γ(i − 1, j), γ(i − 1, j − 1), γ(i, j − 1)}
12:   }
13: }
14: return γ(n, m)
```

each point is calculated on line 11. Since this algorithm iterate over both time series, the time complexity of the algorithm is $O(n^2)$.

CHAPTER 3

RELATED WORK

In this chapter we present a review of literature related to sampling methods, Restricted Boltzmann Machines, deep learning, autoencoders, spatial statistics and time series classification.

3.1 Sampling Methods

Welling and Teh introduced a Bayesian learning method based on Stochastic Gradient Langevian dynamics (SGLD) [19]. They claim that in order for Bayesian methods to be practical in large scale machine learning, stochastic methods need to be adapted because a typical Markov Chain Monte Carlo (MCMC) algorithm requires computations over the whole dataset. Thus, the authors proposed a method that combines Robbins-Monro type algorithms that stochastically optimize a likelihood function with Langevin dynamics. Langevin dynamics is stochastic graident that inject a noise into the parameter update so that the trajectory of the parameters will converge to the full posterior distribution rather than just the maximum a posterior mode. In order to sample from the posterior, the authors introduced a mini-batch technique where parameters are updated after a single mini-batch. In other words, the stochastic gradient is a sum over the current mini-batch of size n. Thus, this algorithm requires $O(n)$ computations to generate one sample. Unlike the long burn-in time that MCMC uses, this technique enable one to use a large dataset. They discovered that if the injected noise is distributed normally with an ϵ variance $N(0, \epsilon_t)$ where e_t changes per iteration, the dynamics becomes Langevin. Welling and Teh observed that the

stochastic gradient noise dominates initially, and the algorithm behaves as an efficient stochastic ascent algorithm. However, for large t, as $\epsilon \to 0$, the injected noise will dominate the stochastic gradient and the MH rejection probability will approach 0.

Key findings of this research are, 1) SGLD can generate samples from a posterior at $O(n)$ complexity where $n \ll N$, and 2) under certain conditions, the posterior can be approximated by a normal distribution. However, one disadvantage of this method is that, with an increasing number of iterations, the mixing rate of algorithm decreases. To address this issue, they proposed to keep the step size to a constant once it has decreased to a critical threshold. Nonetheless, SGLD takes large steps in the direction of small variance and smalls steps in directions of large variance. This results in the slow mixing rate.

Anh and Welling followed the same line research to address the slow mixing rate using Fisher Scoring [20]. The question asked was "Can we approximately sample from a Bayesian posterior distribution if we are only allowed to touch a small mini-batch of data-items for every sample we generate?" Based on Bayesian asymptotic theory, as N becomes large, the posterior distribution becomes Gaussian. This is called the Bayesian Central Limit Theorem [21]. The theorem states that, under certain regularity conditions, $p(\theta|x_1, ..., x_N) \simeq N(\theta_0, I_N^{-1})$ where I_N is the Fisher information. Moreover, the Fisher information is the average covariance of gradients calculated from a mini-batch. Thus, the authors replaced Langevin dynamics with Fisher information. Unlike SGLD, this method was designed such that it samples from a Gaussian approximation of the posterior distribution for large step sizes, thus, increasing the mixing rate. Perhaps the most importing aspect of the above is tradein a small bias in the estimate of posterior against computational gains: this method allows us to use more samples and as a result, it reduces sampling variance. In our

partitioned method, we apply the same concept; more partitioning allows us to use more samples, which in turn results in more accurate generative models.

3.2 Restricted Boltzmann Machines

After first proposed by Smolensky [7] in 1986, the Restricted Boltzmann Machine did not gain popularity for almost 17 years. Although training of the RBM was tractable, it was initially inefficient. Slow computers and the limiation to using small datasets also contributed the slow adoption of RBMs. With better computational resources and bigger datasets, and Hinton's *et al.* development of Contrastive Divergence [9], RBMs are now used as basic components of deep learning algorithms [11, 22, 23] and successfully applied to classification tasks [24–26]. Moreover, RBMs have been applied to many other learning tasks including Collaborative Filtering [27].

As RBMs became popular, research on training them efficiently increased. Gibbs sampling is a Markov chain Monte Carlo (MCMC) sampling algorithm [28] for obtaining a sequence of samples from a posterior distribution. It is an iterative process that samples from a distribution closer to the posterior distribution. The graph of states over which the sampling algorithm produces samples is called a "Markov Chain." As we described in the Section 2.2.3, the Contrastive Divergence algorithm performs Gibbs sampling for k-steps to compute weight updates. However, for each data sample, it creates a new Markov Chain. In other words, the state of the Markov chain is not preserved for subsequent updates. Tieleman modified the Contrastive Divergence method by making Markov chains persistent [1]. In other words, the Markov chain is not reset for each training example. This has been shown to outperform Contrastive Divergence with one step, *CD-1*, with respect to classification accuracy. Even so,

many applications have demonstrated minimal (if any) improvement in performance using persistent Markov chains. Brekal *et al.* introduced an algorithm to parallelize training RBMs using parallel Markov chains [29]. They run several Markov chains in parallel and treat this set of chains as a composite chain; the gradient is approximated by weighted averages of samples from all chains.

When RBMs are trained in an unsupervised fashion, there is no guarantee that the hidden layer representing learned features will be useful for a classification task. Thus, there is considerable research on RBMs in supervised or semi-supervised learning when labeled data is available [24–26, 30–32]. One of the most significant current research achievements with RBMs by Larochelle *et al.* is to apply them as a standalone classifier [25]. In combination with a generative objective function, Larochelle *et al.* developed a discriminative objective function to train RBMs as classifiers. It was demonstrated that when a hybrid objective function is used, the classification accuracy can be increased significantly. Interestingly, as demonstrated and discussed in detail in Chapter 5, the results could not be replicated due to an overflow when computing the gradient of the discriminative objective function.

Schmah *et al.* took a different approach in applying RBMs to classification tasks: instead of using a monolithic RBM to represent all classes, the authors trained one RBM per class label [33]. However, a major drawback of this approach is that it cannot model latent similarities between classes. Nonetheless, an interesting result of their study is the demonstration that generative training can improve discriminative performance, even if all data are labeled. Studying two methods of training, one almost entirely generative and one discriminative, the authors found that a generatively trained RBM yielded better discriminative performance for one of the two tasks studied.

3.3 Deep Learning

As described in Section 2.4, according to Bengio *et al.*, good representation is the basis for deep learning [4]. Deep learning develops good representation by compositions of multiple non-linear transformations in order to obtain more abstract representations. Bengio *et al.* gives most important aspects of good representations: 1) They must be expressive and distributive. That is, a reasonable representation should capture many possible input configurations. 2) They must be abstract representations. Since abstract concepts are formed in terms of lower level features, abstract concepts must be invariant to the input. 3) They must disentangle the factors of variation. For instance, images of faces may contain factors of variation such as pose (translation, scaling, rotation), identity (male, female), and other attributes. Disentangling these factors results in finding abstract features that minimize dependence and are more invariant to most of these variations.

There were other attempts to derive a theory to explain the success of deep learning. Erhan and Bengio [34] suggest that unsupervised pre-training acts as a regularizer, and we have suggested in previous work [35] that it also takes advantage of spatially local statistical information in the training data.

Historically, deep networks were difficult to train because of a credit assignment problem; standard error-backpropagation suffers from gradient diffusion if applied to a deep network, resulting in generally poor performance [36]. Most deep learning techniques now get around this problem by performing some form of "unsupervised pre-training," which often involves learning the weights to minimize reconstruction error for (unlabeled) training data, one layer at a time in a bottom up fashion. This is

then followed by a supervised learning algorithm that, it is hoped, has been initialized in a good part of the search space.

When Restricted Boltzmann Machines are used to form a DBN, the network is trained layer-wise while minimizing reconstruction error. This is a form of unsupervised pre-training. Once all layers have been trained, the resultant network can then be used in different ways, including adding a new output layer and running a standard gradient descent algorithm to learn a supervised task such as classification. The aim of stacking RBMs in this way is to learn features in order to obtain a high level representation.

While techniques similar to modern deep learning algorithms have been proposed previously (see Fukushima [37], for example), it has only been the past few years that have seen deep learning come into its own. Hinton *et al.* were the first to experiment with deep learning architectures after developing an efficient algorithm for training RBMs [38]. Their results suggested that networks with multiple layers can represent features that are distributive and abstract.

Following this seminal discovery, deep learning has become one of the most active research areas. Several studies on deep learning were quickly published following Hinton's discovery in 2006: In the same year, Ranzato *et al.* developed a deep sparse encoder [39]. In 2007, Bengio *et al.* explored variants of DBN and extended it to continuous input values [22]. Two years later, Lee *et al.* developed a sparse variant of the deep belief network [40]. The core idea in these early studies is to learn a hierarchy of features one level at a time and in unsupervised fashion. A typical learning involves unsupervised learning of one layer at a time in greedy fashion.

Typically, autoencoders and RBMs are used as components for deep learning [10, 11, 22, 23, 41, 42]. In other words, RBMs and autoencoders are used to form a

deep neural network model. It was shown that layerwise stacking of RBMs and auto encoders yielded better representation [43, 44].

With large initial weights, Hinton and Salakhutdinov discovered that autoencoders typically find poor local minima [11]. On the other hand, with small initial weights, the gradients in the early layers are tiny, thus, making it infeasible to train autoencoders with many hidden layers. Hinton and Salakhutdinov describe a method for effectively initializing the weights that allows deep autoencoder networks to learn low-dimensional codes. This is accomplished by pretraining on a stack of RBMs. After pretraining, the RBMs "unrolled" to create a deep autoencoder. The autoencoder is then fine-tuned using backpropagation of the error derivatives. It is also possible that an autoencoder with more hidden nodes than visible/input nodes to learn the identity [10]. It was shown by Ranzato *et al.* that when sparsity is introduced in hidden layers, autoencoders creates more efficient representations [39]. These types of autoencoders are known as sparse autoencoders.

To make learned representations of autoencoders robust to partial corruption of the input pattern, Vincent *et al.* explicitly introduced partial corruption of the input that is fed to the network [45]. The stochastic corruption process randomly corrupts some inputs to be 0. Hence, the denoising autoencoder is trying to predict the corrupted (i.e. missing) values from the uncorrupted (i.e., non-missing) values for randomly selected subsets of missing patterns. These denoising autoencoders are shown have better learned representations [45]. Denoising autoencoders can be defined in terms of information theory, and Vincent theorized that minimizing the expected reconstruction error amounts to maximizing a lower bound on mutual information. Xie *et al.* argue that training denoising autoencoders with noise patterns that fit to specific situations can also improve the performance of unsupervised feature learning [46].

Convolutional Neural Networks (CNN), developed by LeCun [47,48] are also considered as deep architectures. CNNs exploit spatially-local features by combining neurons of adjacent layers. In other words, the input of a hidden unit may come from a subset of units in the previous layer. Moreover, in CNNs, each hidden node filter is replicated across the entire visual fields. The replicated units share the same weight and bias vectors. This enables the model to detect features regardless their position. CNNs demonstrated good performance for a number of traditionally difficult tasks, many in the domain of computer vision. Some examples are handwritten character recognition and object recognition.

Similar to Convolutional Neural Networks, Lee *et al.* developed a Convolutional Deep Belief Network (CDBN) model composed of redundant RBMs where each RBM has $V \times V$ visible nodes and K group of $H \times H$ binary hidden units [49]. $V \times V$ represents the image dimensions. Each group K is associated with a set of shared weights. In addition to a hidden layer (detection layer), the network also has a pooling layer of K groups of units with $P \times P$ binary units each. The authors demonstrated that a DBN based on this model is translation-invariant, and it efficiently learns hierarchical representations from unlabeled images. These findings are consistent with other studies on Convolutional Neural Networks.

The Deep Boltzmann Machine (DBM) is another type of deep learning architecture [43]. Like DBNs, the pretraining for DBMs is also greedy layer-wise, but in DBMs, the training process involves creating two redundant RBMs (doubling the inputs and doubling the hidden variables) and then using these two modules in estimating the probabilities themselves. When these two modules are composed to form a single network, the influence of the various nodes are halved. Salakhutdinov *et al.* demonstrated that deep Boltzmann machines learn good generative models and perform well on visual object recognition tasks.

3.4 Dropout

Dropout is a method to prevent neural networks from overfitting and improving the performance of neural networks by preventing co-adaptation of feature detectors by injecting noise in a model. A learning model with a large number of parameters (e.g., neural networks) can easily overfit the training data. Thus, when a learning model is trained on a small dataset, it naturally performs poorly on testing data in that it can overfit the training data. When training a large feedforward neural network, Hinton *et al.* introduced a dropout process, where for each training case each hidden node is randomly omitted from the network with a probability [50]. This technique assures that a hidden unit cannot rely on other hidden units being present. Hinton *et al.* argued that the overfitting is greatly reduced by randomly omitting half of the feature detectors in a feedforward neural networks.

Applying the same dropout concept to deep neural networks, Dahl *et al.*, carried out dropout in all hidden layers during supervised training [51]. When calculating hidden node activations, the authors multiplied the net input from the layer below by a factor of $\frac{1}{1-r}$, where r is the dropout probability for units in the layer below. This deep neural network with dropout performed well on a large speech recognition task.

In the same line of research, Srivastava *et al.* developed a dropout Restricted Boltzmann Machine model and compare it to standard Restricted Boltzmann Machines. Applying to many speech, vision and text datasets, the authors demonstrated that the dropout RBMs are better than standard RBMs [52]. However, the authors noted that a large dropout rate may slow down training.

3.5 Partitioned Model Learning

While many learning techniques (such as Deep Belief Networks) treat all the elements of an input vector as whole, some take an approach that partitions the data vectors into shorter sub-vectors, and performs analysis on the sub-vectors before re-combining the analyzed data to form a representation of the full data vector. Convolutional Networks are the most well known of these, though there are several others, including [37,53] and [54]. Fukushima developed one of the earliest deep architecture which he calls Self-organizing Neural Network Model [37]. The architecture strongly resembles Convolutional networks. With the same line of research, Behnke and Rojas proposed a hierarchical neural architecture with goal of transforming a given image into a sequence of representation with increasing level of abstraction [53].

In the context of Deep Belief Networks (DBN), the DistBelief model and data parallelization framework was developed by Dean *et al.* [55]. Here, the DBN model is partitioned into parts. The overlapping parts then exchange messages. Moreover, models are replicated in different computation nodes and trained on different subsets of data to provide data parallelization. Although this algorithm is related to our work, it is primarily a distributed stochastic gradient descent algorithm. In contrast to this method, we partition a single RBM into multiple small RBMs and combine the small RBMs to learn the final model.

Work by Schulz *et al.* is perhaps the first attempt to exploit partitioning in RBM [56]. The authors observed that the connectivity of RBM is problematic when they monitored learned features. Specifically, they observed that, typically, RBMs learned localized features. They observed that in early stages, feature detectors are global (represent global features). However, most of the detectors had uniform weights

as a result of very late stages of the learning process. Thus, the most training is wasted. Similar to Dean *et al.* described above, they partition the network in fixed regions. Unlike Dean *et al.*, they also add lateral connections in the hidden layer (connections between hidden nodes) to improve representational power of the model. In short, Schulz *et al.* try to reduce the number of parameters to make learning feasible at cost of relationships between long-range features. Although they attempt partially to compensate for the effect of not modeling long-range interactions with lateral connections, this method is not well-suited for data where long-range features (e.g., relative configurations of an object in an image) are correlated significantly.

In promising research done by Strasser *et al.*, Factored Evolutionary Algorithms (FEA) are related to our partitioned training method [57]. Perhaps the most important aspect of this research is that they convert problems into Factor Graphs and utilize stochastic or evolutionary algorithms to optimizes a set of parameters by overlapping partitioned subpopulations. Each subpopulation optimizes a subset of parameters. In addition to a subpopulation optimizing over a subset of parameters, the authors defined a competition technique where the algorithm finds the subpopulations with state assignments that have the best fitness for each dimension. In order for overlapping subpopulations to share their current knowledge, the authors defined a sharing method. Similarly, an RBM in its pure form can be regarded as a Factor Graph; for a given visible vector, a hidden node is independent of other hidden nodes. Thus, each hidden node connecting to the visible nodes is a factor. One can think of the each partition in our Partitioned-RBM as a factor Graph. Similar to FEA, Partitioned-RBM optimizes only a subset of parameters using small partitioned RBMs. However, our sharing algorithm is implicit. As we create fewer partitions, we optimize over overlapping set of parameters; therefore, there is no need for an explicit sharing technique.

3.6 Temporal Classification

DTW was first developed by Sakoe and Chiba for speech recognition [18]. In addition, Sankof demonstrated that DTW can be applied to gene sequence comparison [58]. In gene sequencing, for given finite sequences s and t, one needs to determine the minimum number of substitutions, insertions, and deletions required to change s into t.

Later, Bemdt and Clifford applied DTW to time series analysis for applications in knowledge discovery [59]. The authors demonstrated that DTW can be used as an efficient tool for discovering patterns in large time series datasets. Moreover, the authors proposed that DTW can be used for both categorical and continuous data by adding a temporal dimension (creating time series data).

In recent years, indexing large time series became an important task. Euclidean distance was used in algorithms (e.g., k-Nearest Neighbor) to index the time series data. Keogh and Ratanamahatana discovered that DTW is a more robust measure for indexing time series [60]. It was proven that an indexing method based on DTW not only guarantees no false dismissals, it can also index large datasets efficiently.

Ding *et al.* carried out a comprehensive study to compare various distance measures in querying and mining time series data [61]. Considering two key aspects of time series data—representation methods and similarity measures—they compared all measures for effectiveness and efficiency. Using 1-Nearest Neighbor (1-NN), the authors experimented with various comparison measures including DTW and Euclidean distance. Moreover, they demonstrated that for time series classification, as the size of the training set increases, the accuracy of various measures converge to that

of Euclidean distance. But on small data sets, DTW is significantly more accurate than Euclidean distance.

Following the same experiments carried out by Ding *et al.* described above, Wang *et al.* also experimented with various methods for querying and mining time series data [62]. In order to provide a comprehensive evaluation, they performed the experiments on 38 time series data sets, from the UCR Time Series repository [63]. Their findings on time series classification were also consistent with that of Ding.

Hu *et al.*, developed a method for classifying of time series; however, they were only concerned with the task of correctly extracting individual subsequences, such as gait cycles, heartbeats, gestures, and behaviors. Since classification of a subsequence is generally much more difficult than the task of actually classifying the whole time series, they introduced an alignment-free algorithm for classification where it does not require sequences to be closely related and be aligned perfectly. They maintained that DTW does not work in subsequence classificaiton task [64].

Contradicting Hu *et al.*, Rakthanmanon *et al.* maintained that DTW is the best measure when applied to searching and mining trillions of time series subsequences. They emphasized that normalizing subsequences is help classification accuracy of k-NN [65]. In some real datasets, such as in a video sequence, features can be at different scale and/or different offset. Algorithms that are not invariant to such changes (i.e., k-NN) perform poorly, because small changes in some features can have a dominating contribution to the distance function. The authors demonstrated that k-NN had significantly higher classification accuracy on Z-normalized data as compared with un-normalized data.

CHAPTER 4

PARTITIONED LEARNING

In this chapter, we first develop a generic learning method via partitioning the model into sub components. Each component is in turn trained on a subsection of the input vector. This training process is the main contribution of this work. We then apply this technique to Restricted Boltzmann Machines (RBMs). In the remaining chapters, we demonstrate that this method not only improves runtime complexity of training algorithms, it also significantly improves performance of the learning methods in terms of classification accuracy and representation power.

4.1 Data Partitioning Theory

In order to train a partitioned model, we first need to describe how we partition the input vectors. There are many ways to partition the data; however, any particular partitioning method may have statistical effects on the learning model. Mitchell *et al.* introduced the following notation to describe different partitioning schemes [66].

Given data vectors in $\mathbb{R}^n$, we define a partitioning function π as

$$\pi : \mathbb{R}^n \rightarrow \{\mathbf{u}_0, \ldots, \mathbf{u}_k\}, \mathbf{u}_i \in \mathbb{R}^s,$$

which takes a single input vector in $\mathbb{R}^n$ and produces a set of k output vectors in $\mathbb{R}^s$, where $s < n$. This partitioning scheme creates subsets that can be either disjoint or

1	2	3	4
5	6	7	8
9	10	11	12
13	14	15	16

Figure 4.1: 4×4-pixels image data

overlapping partitions, we expand the above data partitioning function as follows

$$\pi(\mathbf{x}, k, \rho) : \mathbb{R}^n \rightarrow \{\mathbf{u}_0, \ldots, \mathbf{u}_k\}, \mathbf{u}_i \in \mathbb{R}^s$$

where $\mathbf{x}$ is one data instance, k is the number of partitions, and ρ is the percent overlap between partitions.

As a simple example, consider Figure 4.1 where data represents a 4×4-pixel image. Pixels are numbered from 1 to 16. Data instance $\mathbf{x}$ is

$$\{1, 2, 3, 4, 5, 6, 7, 8, 9, 10, 11, 12, 13, 14, 15, 16\}$$

A naïve partitioning function can split this vector in subinstances as:

$$[\{1, 2, 3, 4\}, \{5, 6, 7, 8\}, \{9, 10, 11, 12\}, \{13, 14, 15, 16\}]$$

where $n = 16$, $s = 4$, and $k = 4$. On the other hand if we consider a function that simply splits the vector of length 16 into two equal length halves, we obtain following partitions:

$$[\{1, 2, 3, 4, 5, 6, 7, 8\}, \{9, 10, 11, 12, 13, 14, 15, 16\}]$$

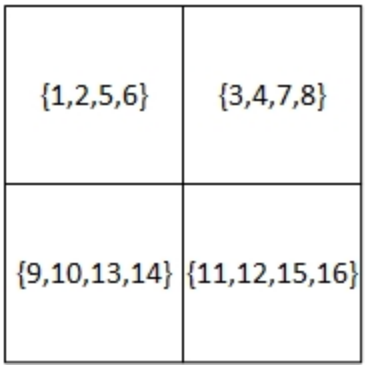

Figure 4.2: Quadtree partitioning

where in this case, $n = 16$, $s = 8$, and $k = 2$. But this naïve partitioning does not preserve any spatially local information. A more advanced partitioning function that preserves spatially local features is a quadtree [67]. A quadtree is a tree data structure in which each internal node has four children. Quadtrees are used for partitioning two-dimensional data by recursively subdividing it into four regions along the two axes. If we apply quadtree partitioning with $k = 4$, we obtain the following partitions:

$$[\{1, 2, 5, 6\}, \{3, 4, 7, 8\}, \{9, 10, 13, 14\}, \{11, 12, 15, 16\}]$$

Figure 4.2 depicts quadtree partitioning.

Notice that quadtree partitioning preserves spatially local features. If we join partitions to create fewer partitions, we still preserve the local features. For example, if we choose $k = 2$, the following partitions are obtained:

$$[\{1, 2, 3, 4, 5, 6, 7, 8\}, \{9, 10, 11, 12, 13, 14, 15, 16\}]$$

Thus, quadtree partitioning has better chance of preserving spatially local features compared with the naïve partitioning technique. The partitioned-based learning

method that we describe in next section can exploit spatially local characteristics of the data.

4.2 Partitioned Learning Algorithm

In this section, we describe a generic learning algorithm that not only partitions the input vector, it also partitions model parameters. In other words, it converts a monolithic model into submodels where each submodel is trained on a corresponding partition of the input vector. However, learning proceeds in a few stages where in each stage, the model and the input vector are split into fewer partitions. In other words, as the stages proceed, smaller partitions are combined into larger partitions. First, we have to show how the model parameters are partitioned. The following example describes the process.

As an example Figure 4.3 shows an RBM with 4 visible nodes and 2 hidden nodes. Ignoring biases, model parameters are stored in a weight matrix constructed based on links between hidden nodes and visible nodes. Thus, the model parameters for this network are:

$$W = \begin{array}{c} \\ h_1 \\ h_2 \end{array} \begin{array}{c} \begin{array}{cccc} x_1 & x_2 & x_3 & x_4 \end{array} \\ \begin{pmatrix} w_{11} & w_{12} & w_{13} & w_{14} \\ w_{21} & w_{22} & w_{23} & w_{24} \end{pmatrix} \end{array}$$

If we split the model into two partitions, as shown in Figure 4.4, we obtain two submodels. Each submodel contains a subset of the parameters and some parameters are ignored. When trained independently, two sub models work on the same parameter matrix; however, the algorithm only updates a region of the matrix corresponding to the given submodel. Thus, in the first stage of learning with two splits, one can

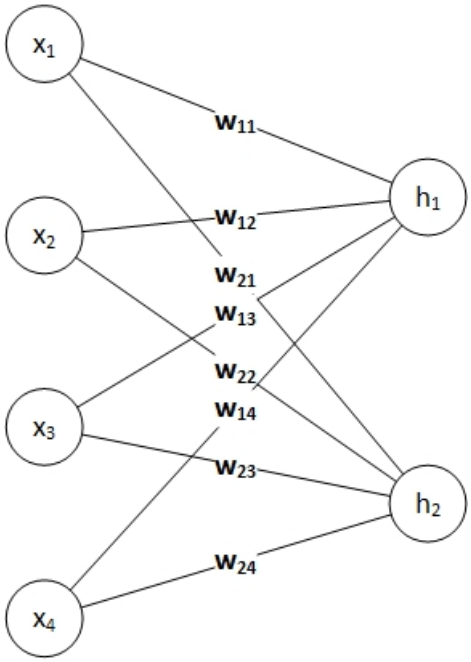

Figure 4.3: A sample RBM with no splits

train two models in parallel. Only the following parameters are updated in the first stage (shown in bold and underlined):

$$W = \begin{array}{c} \\ h_1 \\ h_2 \end{array} \begin{array}{c} \begin{array}{cccc} x_1 & x_2 & x_3 & x_4 \end{array} \\ \begin{pmatrix} \underline{\mathbf{w}_{11}} & \underline{\mathbf{w}_{12}} & w_{13} & w_{14} \\ w_{21} & w_{22} & \underline{\mathbf{w}_{23}} & \underline{\mathbf{w}_{24}} \end{pmatrix} \end{array}$$

Thus, the first partitioned RBM works on $\{\mathbf{w}_{11}, \mathbf{w}_{12}\}$, and the second RBM works on $\{\mathbf{w}_{23}, \mathbf{w}_{24}\}$. The parameters that represent weights between the two partitions are not updated in the first stage. In other words, we initially ignore long-range connections. For example, if there is a correlation between features in partitions 1 and 10, this correlation is not exploited in the first stage. However, in the second stage, when we have only one model with no split, the full parameter matrix is updated.

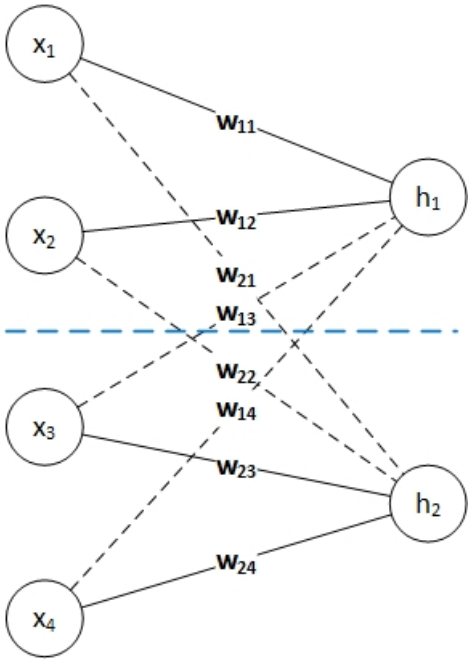

Figure 4.4: A sample RBM with two splits

Definition 4.2.1. *(Long-range connection) A long-range connection is a link between two nodes that takes more than one stage to appear in the same partition.*

Algorithm 4.1 shows the main steps for training a learning model via partitioning. First, this technique is a meta algorithm that divides the parameters into a set of partitions and runs the training algorithm on each partition. Moreover, it uses a set of stages where, in each successive stage, it uses fewer partitions so that the algorithm covers the full parameter matrix. Thus, for each stage (Line 2) it carries out the partitioning process. On lines 2-5, it partitions the parameter set and data instances. On lines 6-8, it executes the training algorithm on each partition. Typically, the last stage will have one partition. In other words, this algorithm will update all parameters when the last stage contains a single partition. However, this algorithm provides the following advantage: in early stages, while there are many partitions, one can afford to use all data samples. For the last stage, most of the parameters are

Algorithm 4.1 PARTITIONED-LEARNING(D, π, *stages*, ρ)

```
1: Input: D:Data instances, π: Partitioning function. ρ: percent overlap. stages:
   list of stages. Each stage determines number of splits
   W:model parameters
2: for each s in stages{
3:   k ← s.partitions   //number of partitions
4:   W^p ← π(W, k, ρ) //Partitioned Model Parameters
5:   D^p ← π(D, k, ρ)   //Partitioned Dataset
6:    for each i in k {
7:     TRAIN(W_i^p, D_i^p)
8:    }
9: }
```

already optimized, so using fewer samples improves the performance of the algorithm overall.

Another motivation behind our approach is that when there are small partitions, they can be trained with more training epochs. As we reduce the number of splits, training requires fewer epochs because, again, several model parameters are already optimized within various partitions. Therefore, less time is required to train the final model with fewer splits.

Another key advantage of this training method is that, when applied to Neural networks, it acts as a natural dropout technique. Dropout is a method to prevent neural networks from overfitting and improving neural networks by preventing co-adaptation of feature detectors by injecting noise in a model, such as hidden nodes in RBMs [50–52]. Although dropout prevents overfitting, adding so much noise during training slows down learning. The partitioning based training method we described does not have this disadvantage.

4.3 Partitioned Restricted Boltzmann Machines

We propose a training method for RBMs that partitions the network into several overlapping subnetworks as described in Section 4.2. With our method, training involves several partition steps. In each step, the RBM is partitioned into multiple RBMs as shown in Figure 4.5. We call these small RBMs "Atomic RBMs." In this figure, the partitions do not overlap; we discuss the version with overlap later in this section. These atomic RBMs are trained in parallel with a corresponding partition of training data using CD-1, which describe in Section 2.2.3. In other words, the feature vector is also partitioned, and each individual RBM is trained on a section of that feature vector.

Since each stage of a Partitioned RBM is trained using a set of sub-vectors partitioned from the training instances, in effect, each "sub-RBM" is trained on instances that contain only the features that correspond to the input nodes assigned to that RBM. Once all partitions have been trained, a new partitioning with fewer splits is created, which forms the basis for the next stage. As described previously, at each successive stage, we create fewer partitions. For example, in Figure 4.5, we initially generate four RBMs. In the second step, we generate two, and final training occurs on the full RBM. It should be noted that the training process in all steps is over the same weight matrix. In other words, during training, each RBM partition updates a subsection of the weight vector defined between all visible nodes and hidden nodes.

As described in Section 4.2, when RBMs are small they can be trained with more training epochs. However, in later stages when there are fewer partition or a single partition, training requires fewer epochs because model parameters are already

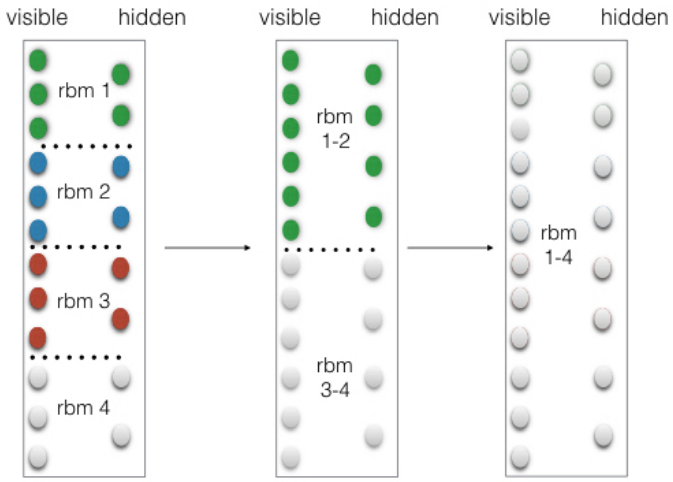

Figure 4.5: Example partitioning approach for an RBM

optimized within the various partitions. Therefore, less time is required to train successive RBMs with fewer splits.

The pseudo-code for our training procedure is given in Algorithm 4.2. The algorithm accepts a list of configurations as input. Each configuration defines training properties of a layer for training; it describes the number of partitions in each layer, the learning rate, the number of training samples for each layer, and the number of iterations for each layer. On lines 2-3, it creates the weight matrix, the bias vector for the visible nodes, and the bias vector for the hidden nodes. Then, for each configuration, it selects the training samples and calls the $PARTITIONED{-}RBM{-}UPDATE$ procedure (lines 5-8).

The $PARTITIONED{-}RBM{-}UPDATE$ procedure creates a list of Atomic RBMs based on the configuration on line 1. For instance, if the configuration has 10 split points it will create a list of 10 RBMs. Each RBM will operate on a portion of $\mathbf{W}$, $\mathbf{b}$, and $\mathbf{c}$. Then for each training instance, it splits the training instance into the number of partitions (line 3). If $configuration.overlap$ is greater than 0, each split will share $configuration.overlap$ percent elements of the neighboring partition.

Algorithm 4.2 PARTITIONED-RBM($\mathcal{L}$, **nvisible**, **nhidden**)

1: **Input**: $\mathcal{L}$ a list of configurations that describe splits and training instances for each network layer training. Each configuration contains the number of splits, the number of training samples, the learning rate, the overlapping rate. *nvisible*: the number of visible nodes. *nhidden*: the number of hidden nodes.
2: $\mathbf{W} \leftarrow$ Create and initialize weight matrix for $nvisible \times hidden$ nodes
3: $\mathbf{b} \leftarrow$ Create and initialize bias vector for visible layer
4: $\mathbf{c} \leftarrow$ Create and initialize bias vector for hidden layer
5: **for each** $\mathbf{l}$ in $\mathcal{L}$:
6: $\quad \mathcal{X} \leftarrow$Training instances
7: $\quad$ **PARTITIONED-RBM-UPDATE**($\mathbf{l}$, $\mathcal{X}$, $\mathbf{W}$, $\mathbf{b}$, $\mathbf{c}$)
8: **end for**

Algorithm 4.3 PARTITIONED-RBM-UPDATE($\mathbf{l}$, $\mathcal{X}$, $\mathbf{W}$, $\mathbf{b}$, $\mathbf{c}$)

1: $rbmList \leftarrow$ **PARTITIONED-RBM-INIT**$(\mathbf{l}, \mathbf{W}, \mathbf{b}, \mathbf{c})$
2: **for each** x_i in $\mathcal{X}$:
3: $\quad splits \leftarrow$split x_i data instance into number of l.splits partitions
4: $\quad$ **for each** rbm_i in $rbmList$:
5: $\quad\quad rbm_i$.CD-1$(splits(i), l.learningRate)$
6: $\quad$ **end for**
7: **end for**

Finally, it calls CD-1 algorithm to train an atomic RBM for the given data split and learning rate.

The $PARTITIONED{-}RBM{-}INIT$ procedure creates a list of atomic RBMs for a given configuration. On lines 2-3, it determines the number of visible and hidden nodes for each partition. Then for each partition and RBM it creates, it calculates the base pointer for determining on what part of $\mathbf{W}$, $\mathbf{b}$, and $\mathbf{c}$ this particular Partitioned RBM operates (lines 6-7). Finally, on line 8, it creates an atomic RBM with this configuration.

Based on the intuition that neighboring RBMs may share some features (nodes), for overlapping partitions, we define similar partitions as described above. However,

Algorithm 4.4 PARTITIONED-RBM-INIT(**l**, **W**, **b**, **c**)

1: **Input**: **l**: split configuration, **W**: weight matrix, **b**: visible layer bias vector, **c**: hidden layer bias vector
2: $nvsible \leftarrow l.visible/l.splits$
3: $nhidden \leftarrow l.hidden/l.splits$
4: $rbms$: Atomic RBM list
5: **for** i in $configuration.splits$:
6: $vbase \leftarrow$base index in visible vector
7: $hbase \leftarrow$base index in hidden vector
8: $rbm_i \leftarrow$ new RBM of $\{\mathbf{W}, \mathbf{b}, \mathbf{c}, vbase, hbase, nvisible, nhidden\}$
9: **end for**
10: **return rbms**

in this model, each partition has some percent of its nodes overlap with its neighboring partitions. As shown in the example in Figure 4.6, the RBMs are sharing two hidden and two visible nodes. Since nodes are shared, partitioned RBMs cannot be trained concurrently without some kind of synchronization.

Performance gains come from all training stages sharing the same weight matrix. As each RBM covers its own part of the globally shared weights and biases, this method enables data-independent parallelization of earlier stages. The later stages, while allowing less parallelization, begin their training with weights that have been pre-trained in the earlier stages. This has several advantages. First, when RBMs have fewer nodes and weights to be updated, they can be trained more quickly; for each Gibbs step, CD-1 involves $O(S \times H \times V)$ probability calculations per iteration where S, H and V are number of samples, hidden nodes, and visible nodes respectively. Thus, we estimate that the total number of Markov chain calculations for a regular RBM is approximately

$$ChainOps \simeq O(I \cdot S \cdot H \cdot V) \tag{4.1}$$

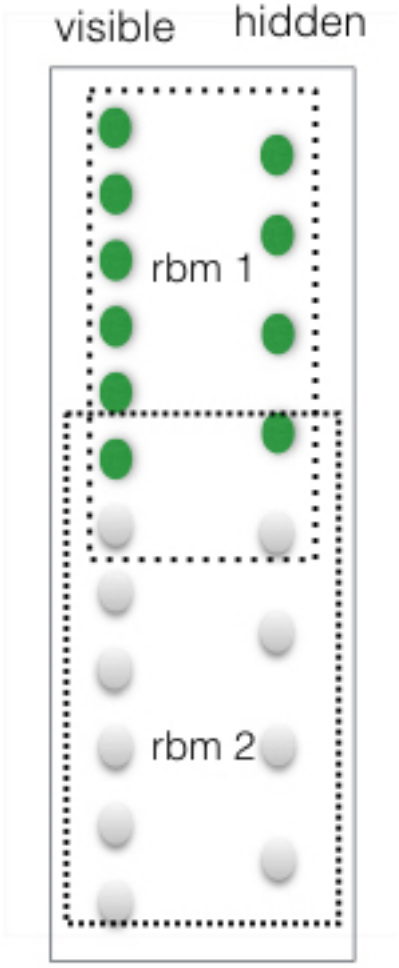

Figure 4.6: RBM With Overlapping Partitions

where I is the number of iterations for the complete training. Fewer chain operations translate into less CPU time. Since Partitioned-RBM is split in each stage and runs in parallel, the number of samples for a stage can be configured to improve runtime performance. We can then estimate that the total number of Markov chain calculations for a Partitioned-RBM is

$$ChainOps \simeq O\left(I \cdot H \cdot V \cdot \sum_{\substack{n \in \{n_0, n_1, \ldots, 1\} \\ s \in \{s_0, s_1, \ldots,\}}} \frac{s_i}{n_i^2}\right) \tag{4.2}$$

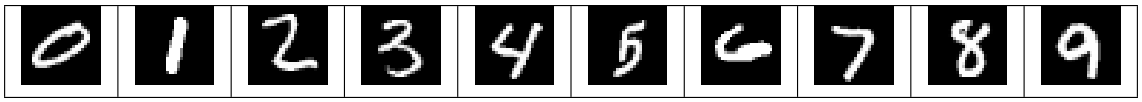

Figure 4.7: Sample MNIST Images

where n_i represents number of splits in stage i, and s_i represents number of samples used at each stage for training. If we keep I, H, and V constant, we can vary the number of samples used in each stage and/or the number of partitions to improve runtime performance. We show that such a scheme works without degradation of the classification accuracy of the model.

4.4 Experimental Setup

The MNIST dataset is used for our experiments due to its wider association with RBMs. The MNIST database (Mixed National Institute of Standards and Technology database) is a database of handwritten digits, constructed from National Institute of Standards and Technology's(NIST) SD-3 and SD-1 databases. MNIST has 60,000 training instances; we repeatedly split this dataset for our cross-validation experiments. Each image is 28×28 pixels, and encodes a single handwritten digit (0 to 9). The raw digit images are scaled to fit in a 20×20 region (original aspect ratio maintained), and are then centered in the final 28×28 image, resulting in a white border around every image. This dataset was introduced in [47], and can be obtained from [68]. Some sample images are presented in Figure 4.7.

We measure performance of our method using reconstruction error, which is defined to be the average pixel differences between the original and reconstructed images. Unless stated otherwise, we use CD-1 for all training steps. The unpartitioned RBM

has 500 hidden nodes and $28 \times 28 = 784$ visible nodes. CD-1 training for one sample is carried out as follows:

- For all hidden nodes, find the probability of hidden node h_i as $\sigma(c_i + \sum_j W_{ij} x_j)$ and sample h_{i1} from a binomial distribution given h_i.
- For all visible nodes, find the probability of visible node x_j as $\sigma(b_j + \sum_i W_{ij} h_{i1})$ and sample x_{j1} from a binomial distribution given x_j.
- For all hidden nodes, find the probability of hidden node h_{i2} as $\sigma(c_i + \sum_j W_{ij} x_{j1})$.
- Calculate the gradient:
  - $\mathbf{W} = \mathbf{W} + \epsilon(h_{i1} x_j - h_{2i} x_{j1})$ where ϵ is the learning rate.
  - $\mathbf{b} = \mathbf{b} + \epsilon(x_j - x_{j1})$
  - $\mathbf{c} = \mathbf{c} + \epsilon(h_{i1} - h_{i2})$

where $\sigma(x) = \frac{1}{1+e^{-x}}$. Since operations at each step of CD involves *visible_nodes* $\times$ *hidden_nodes* updates, we estimate that the total number of Markov chain calculations using Equation 4.1. Fewer chain operations translate into less CPU time.

To get the reconstructed image from the DBN, we propagate the image to the hidden layer (in case of DBN, all the way to the last hidden layer of Deep Belief Network), then reconstruct it by reverse propagation to the visible layer. The resulting vector is binarized and compared with the original vector to calculate a reconstruction error, E. If x is the original vector, x' is the reconstruction, and both are of length n, then E is defined as:

$$E(\mathbf{x}, \mathbf{x}') = \frac{1}{n} \sum_{i=1}^{n} I(x_i \neq x_i') \tag{4.3}$$

For reconstruction error, we first obtain the binary representation of the original image and the reconstructed image. Thirty is chosen as the threshold for converting pixel values [0-255] to binary 0 or 1. Thus, pixel values greater than or equal to 30 are set to 1 while values less than 30 are set to 0. Then, the reconstruction error is calculated as in Equation 4.3.

4.5 Results

Table 4.1 shows the results of our first experiment. *Single RBM* represents a fully connected RBM that is used as a baseline for comparison. The learning rate is set to 0.01 for all RBMs (Single RBM performed best with the learning rate 0.01). The size of training sample for each RBM is shown in samples column. Unless stated otherwise, for the following experiments, we ran the training algorithm on samples for one iteration only—at most, each sample is used only once. Each RBM-X represents a step with X partitions. Samples chosen for RBM-X are always from the first N samples of the total images. RBM-1 represents the final model. For these experiments, partitions are trained sequentially. Thus, if we train them concurrently, the total *ChainOperations* will be lower. As compared to Single RBM, RBM-1 has significantly lower reconstruction error. The total *ChainOperations* for partitioned RBMs is also less than Single RBM. In the table, using a t-test, significant results with 99% confidence are shown in bold. Partitioned-RBM after training on 20 partitions, significantly outperformed the Single RBM. Furthermore, the total number of chain operations for Partitioned-RBM is substantially less than for Single RBM.

Since we want fast convergence for the first step, in the following experiment we varied the learning rate to enable this. Results are shown in Table 4.2. The

Table 4.1: Training Characteristics

Configuration	**Number of RBMs**	**Samples**	**Learning Rate**	**Reconstruction Error (%)**	**Chain Operations (10^9)**
Single RBM	1	60000	0.01	3.85	23.52
RBM-28	28	60000	0.01	4.76	0.84
RBM-20	20	50000	0.01	4.03	0.98
RBM-15	15	40000	0.01	**3.19**	1.05
RBM-10	10	30000	0.01	**2.67**	1.18
RBM-5	5	25000	0.01	**2.29**	1.96
RBM-2	2	20000	0.01	**2.33**	3.92
RBM-1	1	20000	0.01	**2.36**	7.84
Total					**17.77**

Table 4.2: Training Characteristics wrt Learning Rate

Configuration	**Number of RBMs**	**Samples**	**Learning Rate**	**Reconstruction Error (%)**	**Chain Operations (10^9)**
RBM-28	28	60000	0.03	**3.23**	0.84
RBM-20	20	50000	0.03	**2.93**	0.98
RBM-15	15	40000	0.03	**2.66**	1.05
RBM-10	10	30000	0.025	**2.30**	1.18
RBM-5	5	25000	0.020	**2.08**	1.96
RBM-2	2	20000	0.010	**2.10**	3.92
RBM-1	1	20000	0.010	**2.10**	7.84
Total					**17.77**

Partitioned-RBM with 99% confidence intervals outperforms the Single RBM in all steps including the first stage, RBM-28 (with 28 partitions). Moreover, reconstruction errors are even lower compared to our previous experiment.

Using the same configuration above, we varied the learning rate (denoted lr in the results) for the Single RBM and RBM-1. Learning rates for other RBM-X are fixed as in the configuration given in Table 4.2. Reconstruction errors for different learning rates are given in Table 4.3. Results demonstrate with 99% confidence that Partitioned-RBM is less sensitive to different learning rates as compared to the Single RBM.

We also wanted to determine if overlapping partitions would affect the results. We ran our experiment with 5% overlap, which means that each RBM shares 5% of

Table 4.3: Training Characteristics wrt Learning Rate

	$lr = 0.03$	$lr = 0.01$	$lr = 0.005$	$lr = 0.0005$	$lr = 0.00005$
Single RBM	4.43	3.85	4.22	9.40	23.15
RBM-1	**3.45**	**2.10**	**1.95**	**1.83**	**1.92**

Table 4.4: Overlapping Partitions

Configuration	**Number of RBMs**	**Samples**	**Learning Rate**	**Reconstruction Error (%)**	**Chain Operations(10^9)**
RBM-28	28	60000	0.03	**3.11**	0.90
RBM-20	20	50000	0.03	**2.76**	1.10
RBM-15	15	40000	0.03	**2.50**	1.18
RBM-10	10	30000	0.025	**2.19**	1.35
RBM-5	5	25000	0.020	**1.95**	2.27
RBM-2	2	20000	0.010	**1.92**	4.30
RBM-1	1	20000	0.010	**2.08**	7.84
Total					**18.94**

its neighbor's nodes (5% from the left neighbor and 5% from the right neighbor). We ran overlapping partitions sequentially. As shown in Table 4.4, reconstruction errors are even lower with only a modest increase in overhead in terms of *ChainOperations*.

Using the same configurations in Table 4.4, we compared overlapping with non-overlapping Partitioned-RBM algorithms. Applying the t-test, results show that the overlapping algorithm outperforms the non-overlapping algorithm with 99% confidence in almost every stage. However, in the last stage, the results were not significantly different, as shown in Table 4.5. We hypothesize that since overlapping partitions have more connections in each partition, they will require more training samples.

Finally, 10-fold cross validation results are given in Table 4.6. Rather than using the provided training and test data sets. we pooled all of the data and split samples into 10 equal size subsamples. One subsample was used as the validation data for testing and the remaining 9 subsamples were used for training. We repeated this process 10 times. It should be noted that the numbers of samples for partitioned RBMs are not equal (Table 4.6) because we wanted to keep the total time complexity

Table 4.5: Non-overlapping vs. Overlapping Partitions

Configuration	Overlapping Reconstruction Error(%)	NonOverlapping Reconstruction Error(%)	Overlapping Chain Operations(10^9)	NonOverlapping Chain Operations(10^9)
RBM-28	**3.11**	3.23	0.90	0.84
RBM-20	**2.76**	2.93	1.10	0.98
RBM-15	**2.50**	2.66	1.18	1.05
RBM-10	**2.19**	2.30	1.35	1.18
RBM-5	**1.95**	2.08	2.27	1.96
RBM-2	**1.92**	2.10	4.30	3.92
RBM-1	2.08	2.10	7.84	7.84
Total			**18.94**	**17.77**

Configuration	No Overlap:Average Reconstruction Error (%)	Overlap: Average Reconstruction Error(%)	Chain Operations per fold (10^9) No-Overlap/Overlap
Single RBM	4.06		21.12
RBM-28	**3.32**	**3.32**	0.76/0.81
RBM-20	**3.07**	**2.92**	0.88/1.00
RBM-15	**2.68**	**2.62**	0.94/1.06
RBM-10	**2.35**	**2.29**	1.06/1.21
RBM-5	**2.12**	**2.09**	1.76/2.04
RBM-2	**2.15**	**2.08**	3.53/3.88
RBM-1	**2.18**	**2.14**	7.06/7.06
Total			**16.00/17.06**

Table 4.6: 10-Fold Cross Validation Results

of Partitioned-RBM to be no worse than the Single RBM. Partitioned-RBM outperforms Single RBM with 99% confidence. Moreover, overlapping RBMs have lower average reconstruction error as compared to non-overlapping ones.

To compare the original images visually with the some of our reconstructed images, we present some examples in Figure 4.8.

Learning behavior with respect to the number of training samples is given in Figure 4.9. We compare RBM-10 with RBM Single. After each training cycle where we add 10,000 more images, we tested the algorithms on 10,000 images. RBM-10 outperforms RBM Single with 99% confidence on all training steps.

As we described at the begining of the Section 4.5, so far we ran these experiments for one iteration only. To see how our learning method behaves with additional

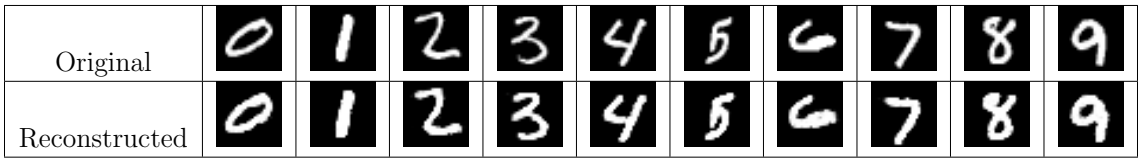

Figure 4.8: Original vs. Reconstructed Images

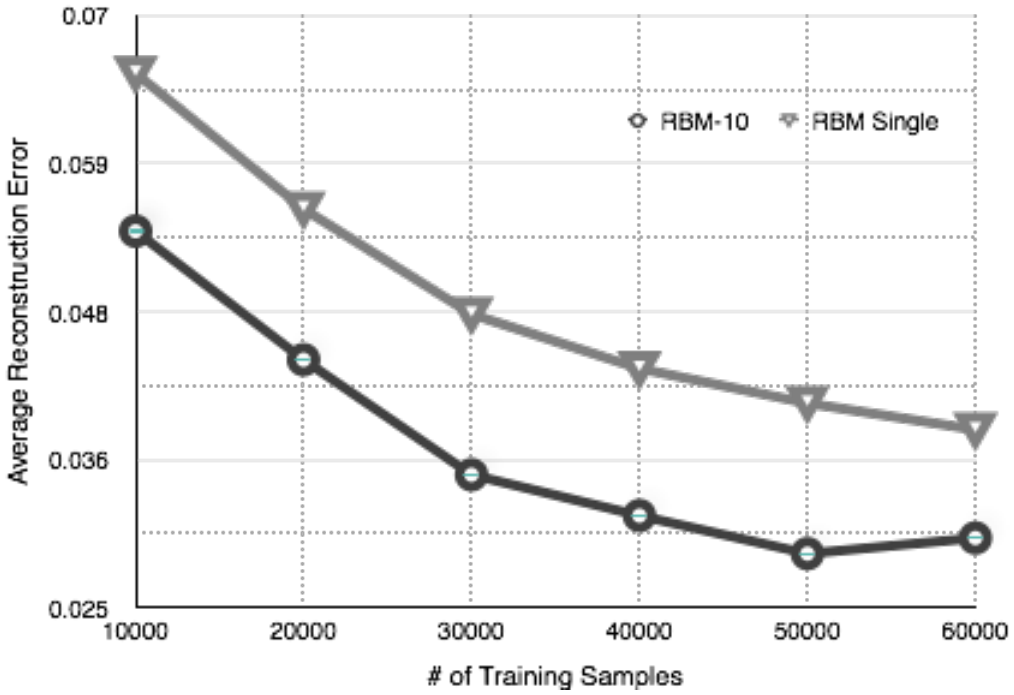

Figure 4.9: Reconstruction Error vs. Training Samples

iterations, we ran Partitioned-RBM and Single RBM for 15 iterations. Results are shown in Table 4.7. Starting with RBM-10, Partitioned-RBM significantly outperforms Single RBM with 99% confidence. For Partitioned-RBM, on average, the error is approximately 5 pixels out of 28×28 pixels, whereas it is 10 pixels for the Single RBM.

The *Special Database 19* dataset from the National Institute of Standards and Technology (NIST) is the official training dataset for handprinted document and character recognition from 3600 writers, including 810K character images and 402K

Table 4.7: Training Iterations

Configuration	**Number of RBMs**	**Samples**	**Learning Rate**	**Reconstruction Error (%)**
Single RBM	1	60000	0.050	1.29
RBM-28	28	60000	0.030	1.75
RBM-20	20	30000	0.030	1.45
RBM-15	15	20000	0.030	1.35
RBM-10	10	20000	0.025	**1.08**
RBM-5	5	20000	0.020	**0.94**
RBM-2	2	20000	0.010	**0.75**
RBM-1	1	30000	0.050	**0.67**

Table 4.8: Training Characteristics with NIST dataset

Configuration	**Number of RBMs**	**Training Samples**	**Learning Rate**	**Reconstruction Error (%)**	**Chain Operations** (10^9)
Single RBM	1	62000	0.010	4.82	507.90
RBM-28	28	62000	0.030	**3.74**	19.92
RBM-20	20	50000	0.030	**3.65**	24.09
RBM-15	15	40000	0.030	**3.70**	25.19
RBM-10	10	30000	0.025	**3.69**	28.70
RBM-5	5	25000	0.020	**3.63**	47.78
RBM-2	2	20000	0.010	**3.67**	90.14
RBM-1	1	20000	0.010	**3.74**	163.8
Total					**399.62**

handwritten digits. Unlike the MNIST dataset, images are 128 by 128 pixels. We selected 62K images for training and testing. The dataset consists of 62 types of images for lowercase and uppercase letters, and numbers. Thus, in our dataset each type has 1,000 images. We used 10% for testing and 90% for training. Hold-out test results are shown in Table 4.8. Based on the t-test results, Partitioned-RBM significantly outperforms Single RBM, again with substantially fewer chain operations.

Finally, Partitioned-RBMed reconstruction error for each character is given in Table 4.9. The average reconstruction error is lowest for I, i, and 1 and it is highest for W,Q and B.

4.6 Conclusion

We showed that our Partitioned-RBM training algorithm with small RBM partitions outperforms training full RBMs using CD-1. In addition to having superior results in terms of reconstruction error, Partitioned-RBM is also faster as compared to the single, full RBM. The reason that Partitioned-RBM is faster is due to having fewer connections in each training step. However, the reasons for the superior generative characteristics in terms of reconstruction error is due to the fact that it is not trained fully in the last stage so that weights or feature detectors become uniform. Thus, it behaves as a dropout. Moreover, we hypothesize that it can also be explained as, in each training step, fewer nodes are involved and a small partition RBM settles in a low energy configuration more rapidly. As we move to other stages with less partitions, fewer training instances are needed to modify the energy configuration to obtain lower energy in the full network.

Uppercase	Error	Lowercase	Error	Number	Error
A	3.93	a	3.55	0	2.95
B	**6.24**	b	4.14	1	*1.95*
C	2.8	c	2.68	2	3.55
D	5.22	d	4.49	3	4.01
E	3.34	e	2.79	4	3.67
F	3.61	f	4.14	5	4.07
G	5.68	g	5.15	6	3.35
H	4.25	h	3.35	7	3.2
I	*1.47*	i	*1.93*	8	4.49
J	4.47	j	3.2	9	3.97
K	4.89	k	4.15		
L	3.08	l	1.97		
M	4.26	m	4.69		
N	3.64	n	2.83		
O	2.58	o	2.69		
P	4.62	p	3.78		
Q	**6.62**	q	4.5		
R	3.53	r	2.37		
S	3.24	s	2.98		
T	3.08	t	3.48		
U	3.56	u	3.09		
V	3.18	v	2.87		
W	**6.92**	w	4.17		
X	4.38	x	3.19		
Y	3.75	y	3.37		
Z	5.04	z	3.57		

Table 4.9: Reconstruction Error per Character

CHAPTER 5

PARTITIONED DISCRIMINATIVE NETWORKS

Recently, researchers have shown an increased interest in considering Restricted Boltzmann Machines (RBMs) as a standalone classifiers; however, many researchers have only aimed at obtaining higher recall and precision of the learning model. So far, there has been little discussion about runtime performance. In this chapter, we introduce a partitioned based RBM for classification tasks. The objective of this chapter is to evaluate the classification accuracy of Partitioned-RBMs under bounded resources.

5.1 Discriminative Restricted Boltzmann Machines

Larochelle *et al.* carried out a comprehensive study of RBMs in classification tasks and successfully applied RBMs as a standalone learning technique, which they call *classRBM* [70]. In addition to a generative training objective function for the CD algorithm, the authors developed a discriminative training objective function as well. Furthermore, combining these two objective functions, they created a hybrid objective function that was then used for the gradient calculations. The authors reported that the hybrid method produced excellent results; however, we could not replicate their results because the discriminative training objective function calculations resulted in an overflow for reasonably large networks. The following objective function is a

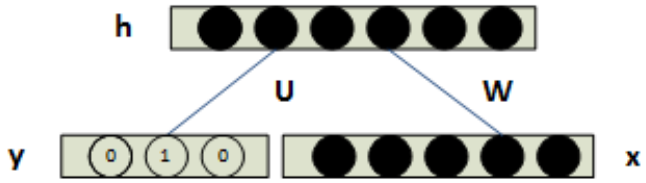

Figure 5.1: Class RBM Network

conditional distribution that forms the basis for discriminative learning:

$$p(\mathbf{y}|\mathbf{x}) = \frac{\exp(d_y + \sum_j^N s(c_j + U_{jy} + \sum_i W_{ji}x_i))}{\sum_{y^* \in \{1,\ldots,C\}} \exp(d_y + \sum_j^N s(c_j + U_{jy^*} + \sum_i W_{ji}x_i))} \tag{5.1}$$

where $\mathbf{c}$ is the weight vector for the bias on the hidden nodes, and $\mathbf{U}$ is the weight vector between hidden nodes and class nodes. Finally, $s(x) = \log(1 + \exp(\mathbf{x}))$ is the $softplus$ function. An example network is shown in Figure 5.1. Here, $\mathbf{x}$, $\mathbf{h}$, and $\mathbf{y}$ represent vectors of visible, hidden, and class label nodes (output nodes), respectively. Class nodes are all set to 0 except for the node corresponding to the target class label, which is set to 1.0. For instance, when there are 10 classes and a specific data instance has the third label, the corresponding output vector, $\mathbf{y}$, is $[0.0, 0.0, 1.0, 0.0, 0.0, 0.0, 0.0, 0.0, 0.0, 0.0]$.

Unfortunately, the conditional distribution in Equation 5.1 can only be computed exactly and efficiently when there is a reasonably small number of classes. Otherwise, the denominator will result in an exponential number of terms, as we have to sum over all classes. A more serious weakness with this method, however, is that in practice it suffers from computational overflow.

For each y_i value, ignoring $\mathbf{c}$ biases and $\mathbf{U}$, the value in the $softplus$ function is a vector of $\mathbf{W}_{H,V}\mathbf{x}_{V,1}$, where V and H are number of visible and hidden nodes respectively. If the $\mathbf{W}$ matrix is initialized with values randomly chosen between

$\frac{-1.0}{\max\{V,H\}}$ and $\frac{+1.0}{\max\{V,H\}}$ and for $H = 1500$ and $V = 784$, the resulting matrix values will be distributed uniformly between -0.00067 and 0.00067. Thus, the value for $\exp(*)$ in $softplus$ function ranges from 0.9993 to 1.0007. The $\log(1 + *)$ expression results in values around 0.69. Then, ignoring d_y, the $\sum(*)$ expression has value of $H \times 0.69$. Finally, it results in $\exp(H \times 0.69)$. Thus, with $H = 1500$, we have exp(1035). For modern CPUs, exp(710.0) results in overflow (infinity). Therefore, the maximum number of hidden nodes one can use is around 710.0/0.69, that is 1028 nodes.

It should be noted that we ignored many variables in this formula to simplify the analysis. Thus, even for 1028 nodes, it is not guaranteed that the overflow will not happen. Overflow can be encountered when one uses fewer than 1000 nodes. In addition to the overflow, the time complexity of an RBM increases with addition of the discriminative gradient.

Because we could not use $classRBM$ for some reasonably sized experiments, here we propose a model where we train partitions as described in Chapter 4 without using class labels except for the last stage. As shown in Figure 5.2, class nodes are added to the visible vector of the final stage with one node per class. Thus, we train the final stage in a supervised fashion.

5.2 Discriminative Partitioned Restricted Boltzmann Machines

For discriminative RBMs, we propose Partitioned Restricted Boltzmann Machine (PRBM) model where we train partitions as described in Chapter 4 without using class labels except for the last layer. As shown in Figure 5.2, class nodes are added,

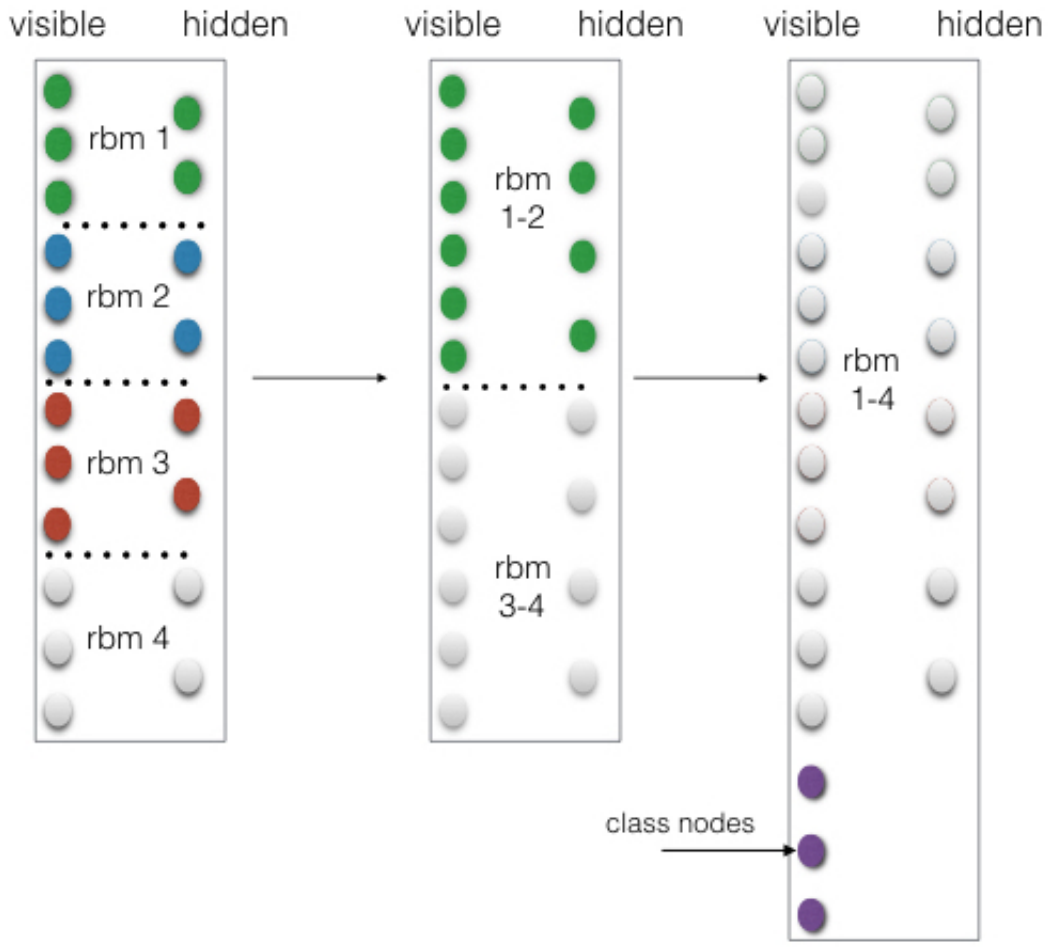

Figure 5.2: Discriminative Partitioned RBM

one node per class, to the visible vector of the final layer. Class nodes are trained by setting the node that represents the label to 1.0 and the rest to 0.

To classify a new data sample, the input vector will be constructed with all class nodes set to 0. Then, the input vector will be propagated to the hidden layer using Equation 2.11. We repeat this equation here for convenience:

$$P(h_j = 1|\mathbf{x}) = \sigma(\mathbf{w}_j\mathbf{x} + c_j)$$

A new visible vector will be sampled from the model based on the activation of hidden nodes. Since the visible vector contains class nodes as well, the class nodes' values will be used to predict the class label. The class node with the highest activation value will determine the class label.

Because PRBM is partitioned into smaller RBMs, all available data can be used for training, and individual RBMs can be trained in parallel. Moreover, as the number of dimensions increases, the number of partitions can be increased to reduce runtime computational resource requirements significantly. All other recently developed methods using RBMs for classification suffer from some serious disadvantage under bounded computational resources; one is forced either to use a subsample of the whole data, run fewer iterations (early stop criterion), or both. Our Partitioned-RBM method provides an innovative scheme to overcome these shortcomings.

As proposed in Chapter 4, the training process for Partitioned-RBM splits a single RBM into multiple partitions. Each partition is then trained on a subsection of the data instances. In our experiments, we demonstrated that this training process improves the performance in terms of both generative power and speed. Moreover, we will show in Chapter 6, applying spatial statistical analysis tools, we found that traditional RBMs do not preserve spatially local structure whereas Partitioned-RBMs are preserve and make use of local structure [69].

We believe that far too little attention has been paid to runtime performance and far too much attention has been paid to obtaining higher classification accuracy rates. To the best of our knowledge, using RBMs with bounded computational resources, namely CPU time, has not been considered previously. Hence, the goal of this chapter is to find out if there exists a method for improving the runtime performance of RBMs without significantly degrading classification accuracy. When we developed the Partitioned-RBM to obtain better reconstruction accuracy, we noticed

that runtime performance is also superior to regular RBMs [5]. Thus, our previous results suggest that Partitioned-RBMs can perform significantly better under bounded computational resources.

Another key aspect of our Partitioned-RBM is that the training process introduces an intrinsic sparsity by design. At each training stage, only the weights inside individual partitions are optimized; the weights connecting the visible layer of one partition to the hidden layer of another partition are untouched. Thus, the Partitioned-RBM weights are inherently sparse. This is important because Larochelle *et al.* showed that a sparse version of the hybrid RBM significantly outperforms all other techniques in terms of classification error rates; the results were even better than Deep Belief Network results reported in the literature [25]. Larochelle *et al.* introduced sparsity by subtracting a small constant δ value, a hyper-parameter, from biases after each parameter update. In our case, the training of smaller partitions and gradually piecing them together accomplishes a similar result.

Algorithm 5.1 is a slightly modified version of the CD-1 training technique for classification tasks. On line 2-6, we calculate hidden node activations. When the training is done for the classification (when there are class nodes), we add the contribution of the class input nodes by multiplying with the **U** matrix. In other words, the squashing function that calculates hidden node activations, in addition to $\mathbf{Wx}$, has the $\mathbf{Uy}$ component. On line 7, new values for $\mathbf{h}$ are sampled from the hidden activations. Using sampled h values, the new values for $\mathbf{x}$ and $\mathbf{y}$ are calculated on lines 8-11. Using new predicted values of $\mathbf{x}$ and $\mathbf{y}$, new hidden activation probabilities are obtained on lines 12-16. Depending on whether the network is trained for classification or not, the contribution of $\mathbf{Uy}$ is added to the probability calculations

Algorithm 5.1 PARTITIONED-DISC-RBM

1: $\mathbf{W}$: weight matrix from hidden nodes to visible nodes, $\mathbf{U}$: weight matrix from hidden nodes to output nodes. $\mathbf{b}$: bias on visible nodes, $\mathbf{c}$: bias on hidden nodes, $\mathbf{d}$: bias on class nodes. ϵ: is the learning rate. $\mathbf{x} \sim p$ means $\mathbf{x}$ is sampled from p. $\sigma(x) = \frac{1}{1+e^{-x}}$
2: **if** classification **then**
3: $\quad h_i \leftarrow \sigma(c_i + \sum_j W_{ij} x_j + \sum_j U_{ij} y_j)$
4: **else**
5: $\quad h_i \leftarrow \sigma(c_i + \sum_j W_{ij} x_j)$
6: **end if**
7: $h_{i1} \sim p(h_i)$ {sample h_{i1} from a binomial distribution given h_i}
8: $x_j \leftarrow \sigma(b_j + \sum_i W_{ij} h_{i1})$
9: $x_{j1} \sim p(x_j)$
10: $y_j \leftarrow \sigma(d_j + \sum_i U_{ij} h_{i1})$
11: $y_{j1} \sim p(y_j)$
12: **if** classification **then**
13: $\quad h_{i2} \leftarrow \sigma(c_i + \sum_j W_{ij} x_{j1} + \sum_j U_{ij} y_{j1})$
14: **else**
15: $\quad h_{i2} \leftarrow \sigma(c_i + \sum_j W_{ij} x_{j1})$
16: **end if**
Update parameters:
17: $\mathbf{W} \leftarrow \mathbf{W} + \epsilon(h_{i1} x_j - h_{2i} x_{j1})$
18: $\mathbf{b} \leftarrow \mathbf{b} + \epsilon(x_j - x_{j1})$
19: $\mathbf{c} \leftarrow \mathbf{c} + \epsilon(h_{i1} - h_{i2})$
20: **if** classification **then**
21: $\quad \mathbf{U} \leftarrow \mathbf{U} + \epsilon(h_{i1} y_j - h_{2i} y_{j1})$
22: $\quad \mathbf{d} \leftarrow \mathbf{d} + \epsilon(y_{i1} - y_{i2})$
23: **end if**

as described above. Finally, all network parameters are updated on line 17-23. Of course for CD-k, this process is repeated k steps before updating parameters.

5.3 Experimental Design

We used the MNIST dataset for our experiments due to its wide use in evaluating RBMs and deep learning algorithms for classification accuracy. The MNIST dataset is described in Section 4.4.

Rather than using the pre-defined test set of 10,000 images, we repeatedly split the training dataset for our cross-validation experiments. Unless stated otherwise, for all experiments, we trained models for 20 iterations. Moreover, when we compare methods in terms of the significance of results, we compare them using a paired t-test with 99% confidence intervals.

5.4 Results

Table 5.1 shows the results of our Partitioned-RBM experiments with 1500 hidden nodes. In the configuration column, Single RBM represents the traditional RBM and Partitioned-RBM represents a Partitioned RBM. The number of partitions in each training stage is defined in parentheses; (16-4-1) indicates that we trained the RBM first with 16 splits, then 4, and finally trained it as a single partition. Note that each successive Partitioned-RBM configuration starts with the output of the previous configuration, as described in Chapter 4. The Samples column gives the number of training instances, selected at random from the total training set, that were used to train the given RBM. As the number of partitions decreases, we decrease the training set size to match the time complexity of the full Partitioned-RBM training process to that of the Single RBM. Each RBM was run for 20 iterations, and the classification accuracy rates reported are the mean values from 10-fold cross-validation (not using MNIST's predefined split between training and test data). As shown, Partitioned-RBM significantly outperforms the Single RBM.

By design, the computational complexity of the Partitioned-RBM is significantly better than that of the Single RBM trained on the entire dataset; it is evident that less computation would have been necessary for the Partitioned-RBM to yield superior performance. Based on Equation 4.2 (repeated below for convenience) we could tune

Table 5.1: Classification Accuracy Rates

Configuration	**Samples** (10^3)	**Accuracy** (%)	**Chain Operations** (10^{10})
Single RBM	54	96.97	131.71
Partitioned-RBM-(16-4-1)	54-50-30	97.18	78.42

the number of samples used in each stage and/or the number of partitions, in order to adjust the runtime performance. Thus, we are seeking ways to obtain reasonable classification accuracy rates under bounded resources. Nevertheless, Partitioned-RBM significantly outperforms Single RBM as shown in Table 5.1 in terms of classification accuracy with significantly lower CPU requirements.

$$ChainOps \simeq O\left(I \cdot H \cdot V \cdot \sum_{\substack{n\in\{n_0,n_1,\ldots,1\}\\ s\in\{s_0,s_1,\ldots,\}}} \frac{s_i}{n_i^2}\right)$$

In addition to classification accuracy, we analyzed recall and precision of the algorithms using $F1$ scores (which is the harmonic mean of precision and recall). Table 5.2 shows $F1$ scores for all class labels. Partitioned-RBM results are comparable to Single RBM if not better. This indicates that Partitioned-RBM has robust accuracy even though we partition the whole network into atomic partitions.

Indeed, when Partitioned-RBM has a smaller number of stages, the runtime performance will improve. However, ideally, the runtime performance gain should not be at the cost of degradation in classification accuracies. In the following experiments, we ran Partitioned-RBM with fewer stages. Table 5.3 demonstrates that classification accuracy is still comparable but runtime is less. This is important, because training the model with many samples in the first stage appears to optimize the weights

Table 5.2: Classification F1 Scores

Labels	**PRBM (%)**	**Single RBM (%)**
0	98.27	98.49
1	98.00	98.13
2	97.01	96.99
3	96.15	96.63
4	97.31	97.27
5	96.67	97.34
6	98.32	98.09
7	97.09	96.94
8	95.51	96.12
9	95.17	95.75

Table 5.3: Partitioned-RBM Classification Accuracy

Configuration	**Samples** (10^3)	**Accuracy (%)**	**Chain Operations** (10^{10})
Partitioned-RBM-(16-4-1)	54-50-30	97.18	78.42
Partitioned-RBM-(16-1)	54-30	96.78	71.07

sufficiently; one does not have to use more samples when there are fewer splits to maintain a reasonable accuracy.

The purpose of the current study was to determine if RBM can be a viable learning technique under bounded computational resources. We can claim that increasing the number of partitions in the first stage is sufficient to optimize network weights to a degree that fewer samples or fewer training epochs are required in the last stage. In other words, the last stage with one split does not need to run on the entire dataset. Most of the computational effort is spent in the last stage when there is only one split, because the training needs to cover the whole weight matrix.

We ran a series of experiments to determine the effects of sample size in last the stage and compared the results with Single RBM. As seen in Table 5.4, keeping runtime approximately the same, Partitioned-RBM performs significantly better than

Table 5.4: Classification Accuracy Rates with samples

Configuration	**Samples** (10^3)	**Accuracy** (%)	**Chain Operations** (10^{10})
Single RBM	20	96.43	47.04
Single RBM	10	95.47	23.52
Single RBM	5	94.15	11.76
Partitioned-RBM-(16-4-1)	54-10-20	96.90	49.02
Partitioned-RBM-(16-4-1)	54-10-10	96.25	25.50
Partitioned-RBM-(16-4-1)	54-10-5	95.44	13.74

Single RBM for all experiments when the sample size decreases. This is not surprising, since Partitioned-RBM uses the full data set in the first stage. However, the result is important because the number of computations in the first stage is insignificant compared to the total number of operations. Thus, the following conclusions can be made: 1) If dimensions of the data are too high, increasing the number of partitions or splits will improve the runtime performance. 2) If the volume of data is too high, using more samples in early stages and fewer samples in later stages with fewer partitions will improve runtime performance.

Finally, to show how fast Partitioned-RBMs optimize weights, we ran experiments with different training epochs. As seen in Table 5.5, Partitioned-RBM performs significantly better than Single RBM when trained for fewer epochs (for all experiments). This again demonstrates that Partitioned-RBM can perform well under bounded computational resources. On the other hand, Single RBM must run many iterations in order to obtain reasonable accuracy. The evidence from this experiment suggests that if one cannot afford to train a regular RBM for many iterations, partitioning will allow it to run for many iterations and will yield competitive results.

Table 5.5: Classification Accuracy Rates with iterations

Configuration	**Samples** (10^3)	**iterations**	**Accuracy** (%)	**Chain Operations** (10^{10})
Single RBM	54	1	93.72	6.59
Single RBM	54	5	96.50	32.93
Single RBM	54	10	96.89	65.86
Partitioned-RBM-(16-4-1)	54-50-50	1	94.30	6.27
Partitioned-RBM-(16-4-1)	54-50-50	5	96.67	31.37
Partitioned-RBM-(16-4-1)	54-50-50	10	97.26	62.73

5.5 Conclusion

This study set out to improve the runtime performance of RBMs without significant cost to precision and recall rates. From the results of our experiments, we are led to the conclusion that the Partitioned-RBM performs as well as or better than a Single RBM with less CPU time. Table 5.1 demonstrates that the Partitioned-RBM has significantly better accuracy than Single RBM, with only about half the CPU time. This is important because Partitioned-RBM can run on very high dimension and high volume datasets. A single RBM cannot be run efficiently on high volume data, while Partitioned-RBM can use all samples in the first stage, with many partitions running in parallel. When weights are optimized in early stages with many samples, the final stage requires a smaller number of samples.

Under bounded computational resources, with Partitioned-RBM we can either increase the number of splits and train it on many data samples, or adjust sample size and number of iterations to obtain better runtime performance, as seen in Tables 5.3, 5.4, and 5.5. We demonstrated that a single RBM, in general, requires many iterations and many training samples. However, this is not practical when computational resources are bounded.

One might ask why we did not add class nodes in early stages. Our initial results indicated that such a scheme does not provide any advantage. It appears that when weights between hidden nodes and class nodes, **U**, are updated by all partitions, the weight matrix takes a long time to be optimized; one partition changes the effect of a previous partition. However, we plan to investigate each partition optimizing its own **U** matrix, and, we need to find a better mechanism to combine all **U** matrices when we move to the next stage in the training process.

CHAPTER 6

PARTITIONED DEEP BELIEF NETWORKS

To show how the performance can be improved while simultaneously decreasing total training time, a DBN composed of the Restricted Boltzmann Machines (RBMs) will be explored next. We present this by introducing the vector-partitioning described in Chapter 4. We then analyze the input data to see if we can identify the statistical properties that are being exploited by the Partitioned-RBM to achieve this performance. Our goal is to investigate the representation bias of the deep, vector-partitioning approaches in general. Examination of that bias is critical to understanding and improving our learning algorithms, as Tom Mitchell pointed out in his seminal paper [71], in which he also noted that a bias necessary for learning. Moreover, we analyze the role of spatial locality in Deep Belief Networks (DBN) and show that spatially local information becomes diffused as the network becomes deeper. We demonstrate that our method is capable of retaining spatially local information when training DBNs. Specifically, we find that spatially local features are completely lost in DBNs trained using the "standard" RBM method, but are largely preserved using our partitioned training method. In addition, reconstruction accuracy of the model is improved using our Partitioned-RBM training method.

6.1 Deep Belief Networks with Partitioned Restricted Boltzmann Machines

In the past few years, the area of exploration known as *Deep Learning* has demonstrated the ability of multilayer networks to achieve good performance on a range of difficult machine learning problems and has been gaining increasing prominence

and attention in the machine learning and neural network communities and rapid adoption in commercial products. While these techniques have achieved great success on a number of difficult classification problems, for example in computer vision, the role of representation bias has not been thoroughly explored. In other words, we do not know the underlying reasons *why* these techniques perform well on particular problems. A deeper understanding of how and why deep learning algorithms work will help us to decide which problems they are best applied to, and may also lead to improvement of existing techniques or extending them to in novel contexts.

We demonstrated in Chapters 4 and 5 that partitioned learning can be applied effectively to RBMs. Here, we apply that same thought to deep learning. As a first step to examine the role of representation bias, we use statistical models to examine how much spatially local structure exists in the MNIST dataset. We then present experimental results from training RBMs using partitioned data and demonstrate the advantages they have over non-partitioned RBMs. Through these results, we show how this performance advantage depends on spatially local structure by demonstrating the performance impact of randomly permuting the input data to destroy local structure. Overall, our results support the hypothesis that a representation bias relying on spatially local statistical information can improve performance if this bias is a good match for the data. We also suggest statistical tools for determining *a priori* whether a dataset has spatially local features that will make it a good match for this bias.

The question we want to answer is, "Do deep learning algorithms make use of spatially local structure in their input data to help them achieve good performance?" There has long been an intuition in the deep learning community that this hypothesis is likely to hold, based partly on everyday experience, and partly on the structure

of the human visual cortex. To our knowledge, however, there has been no previous attempt to test this hypothesis.

Deep networks have a built-in regularization effect that remains strong even when working with large amounts of data [34]. This gives them an advantage on data with noise or complexities resembling noise. In addition, for *partitioned* deep models like Convolutional Networks, exploiting spatially local information is important to performance [35].

Partitioned deep models work by partitioning nodes within layers of a network. As shown in Figure 4.5, this can be visualized as an RBM in which layers are not fully connected. Instead, the nodes of each layer are broken into subsets, and each subset of nodes is fully connected. As an example, in a classic Convolutional Networks, a data vector represents an input (e.g. an image) and is effectively split into several small overlapping regions (image patches).

In a typical DBN, a Restricted Boltzman Machine is at each layer and the network is trained layer-wise by non-linearly transforming the input while minimizing reconstruction error. Once all layers have been trained, the resultant network can then be used in different ways, including adding a new output layer and running a standard gradient descent algorithm to learn a supervised task such as classification. We use the same architecture and training process; however, instead of using a monolithic RBM, we use Partitioned-RBMs and carry out the partitioned training process described in Chapter 4 at each layer of the DBN.

Performance gains come from all training stages sharing the same weight matrix. As each RBM covers its own part of the globally shared weights and biases, this method enables data-independent parallelization of earlier stages.[1] The later stages,

[1]If we allow for overlap of partitions, parallelization becomes problematic. However, Fortier *et al.* suggest an approach that enables parallelization while exploiting overlap [72–74].

while allowing less parallelization, begin their training with weights that have been pre-trained by the earlier stages. This has several advantages. First, when RBMs have fewer nodes and weights to be updated, they can be trained more quickly. While the results of the disjoint training will not be perfect because some relationships will be missing, they can be allowed to run for many epochs and on large dataset. At the later stages, as the RBMs cover more links, the training requires fewer epochs than normal to converge because the weights are closer to their optimal values than would be the case with random initialization. This enables the overall Partitioned-RBM hierarchy to achieve the same or higher performance in a fixed time period than a single RBM trained all at once.

This type of partitioning method can have detrimental effects on performance. After all, any statistical information relating two features that are not contained in the same partition is completely hidden from the model. In practice, however, for most real-world problems, we have neither enough samples nor the computational capacity to generate a fully optimal statistical model of our data. Most of the models we are interested in yield exponential complexities, so we must rely on approximations to estimate them. The central issue in neural networks, going back to McCulloch and Pitts [75], is the intractability of finding the optimal set of connection weights. The history of the field has largely been a progressive improvement of gradient descent-based approximation algorithms, which have enabled more complex network architectures to be trained. Simplifying assumptions often allow more tractable approaches to problem solving, but assumptions made should be consistent with the original problem.

We suggest that deep learning algorithms, and in particular the ones that partition data vectors, are taking advantage of spatially local statistical structure for their performance. This requires not only that such structure exists, but that it be highly

relevant to the performance criterion being optimized. If this hypothesis is correct, it means we may be able to exploit this structure in other contexts as well.

We can now describe the statistical properties of random variables across the dataset. For individual features, we can compute statistical measures like mean and variance. For any given pair of features (i, j), we can compute statistical measures like correlation, covariance, mean-deltas, and so forth.

By applying a partitioning function π (not to be confused with the partition function defined for Boltzmann Distribution) in Equation 4.1 to every element of a dataset $\mathbf{D}$, we can generate a new dataset, which will be a set of the sets created by applying π to the $\mathbf{x}_i$. In some instances, we may be able to treat the partitioned sub-vectors uniformly, in which case we may want to combine them into a single set by taking the union of the subsets created by the partitioning.

$$\mathbf{D}_\pi = \{\pi(\mathbf{x}_0) \cup \ldots \cup \pi(\mathbf{x}_m)\}, \tag{6.1}$$

This will be appropriate for datasets where all features are interpreted the same way. However, this may not hold for data where features need to be interpreted differently. It also helps if the data is isotropic (i.e., changes are independent of direction) and spatially invariant (i.e., a given pattern is equally likely to occur anywhere in the data vector). Natural image data tends to fit these assumptions fairly well, as do some types of time-series data, geological and meteorological data (for which this type of analysis is called *geostatistics*), and location-based medical, social, or economic datasets (e.g. for the analysis of cancer clusters).

The main advantage of using the union in Equation 6.1 is that we get a larger number of samples, which allows for better estimation. As an example, for natural image data, using the union is generally safe, since we frequently want to create

spatially invariant models anyway. In a more structured dataset, such as the MNIST dataset analyzed in this dissertation, we do not expect spatial invariance in the data (because the images are always centered and surrounded by a white border, the location of the digit does not vary), so taking the union would create more samples. However, if samples are not from a uniform distribution, this will not help.

When partitioning, we will need to keep track of how random variables in the original dataset map to element(s) in the partitioned dataset. If we do so, we will then be in a position to describe which statistical quantities can be calculated and which cannot. So long as the partitioning function preserves locally adjacent blocks of the original vectors, it will be the case that we can still measure statistical properties of feature pairs that are "near" each other in the original vectors, but we will be unable to measure statistical properties of features that are "far apart" in the original vectors (here, we use Euclidean distance as the measure of how far apart two features are). In other words, spatially local statistical information is preserved, even while much of the non-local information is lost.

This emphasis on spatial locality means that we will draw from the field of spatial statistics. While some of the techniques used in geostatistics, for example, will not be relevant to all types of data, there are a number of principles and techniques that can be used in our analysis of the impact of partitioning.

6.2 Analysis of Spatial Features

To analyze the spatial behavior of different learning algorithms, we need tools to measure and describe spatial structure in data. For this, we look primarily to the field of spatial statistics. In this work, we apply two different methods for detecting spatial structure. The first is to measure how inter-feature variance and correlation

changes with spatial distance between features. This gives us a quantitative measure, but tells us only about pair-wise relationships on average. The second is a more holistic qualitative analysis that can be done by using dimensionality reduction to embed the data in a plane so it can be visualized. In this way, we can find what kind of clusters or structure exists in the data and compare the amount of structure present in different datasets.

For quantitative analysis, we use a tool from spatial statistics called a *variogram*, which lets us examine the relationship between spatial distance and statistical correlation. Note again that we use *spatial* in the sense of spatial statistics; the distances here are *between features*, not between datapoints.

The generic equation for a *variogram* is described in Section 2.5 as:

$$2\gamma(h) = var(Z(s+h) - Z(s)), h \in \mathbb{R}^d$$

where $\{Z(s) : s \in D \subset \mathbb{R}^d\}$ is a random process which produces n data samples $Z(s_1), Z(s_2), ..., Z(s_n)$ and h is separation (distance) vector. Generally, this function will be plotted and examined to observe the relationship between distance and difference. In geostatistics where variograms are used for predictive modeling, these assumptions are often closely matched by the underlying problems. Here, we use an empirical estimation of the variogram as a descriptive analytic tool. We acknowledge that the assumptions are violated by natural image data, so a "true" variogram is not well defined. Instead, we calculate an "average" empirical variogram. A "sample" in the context of image analysis is basically a pixel, so the location of the sample is merely the pixel location, and the value of the sample is the pixel value.

To generate the variogram plots, we compute the variance of each pair of features (computed across all images in the set). For each pair of features (i.e. pixels) (i, j),

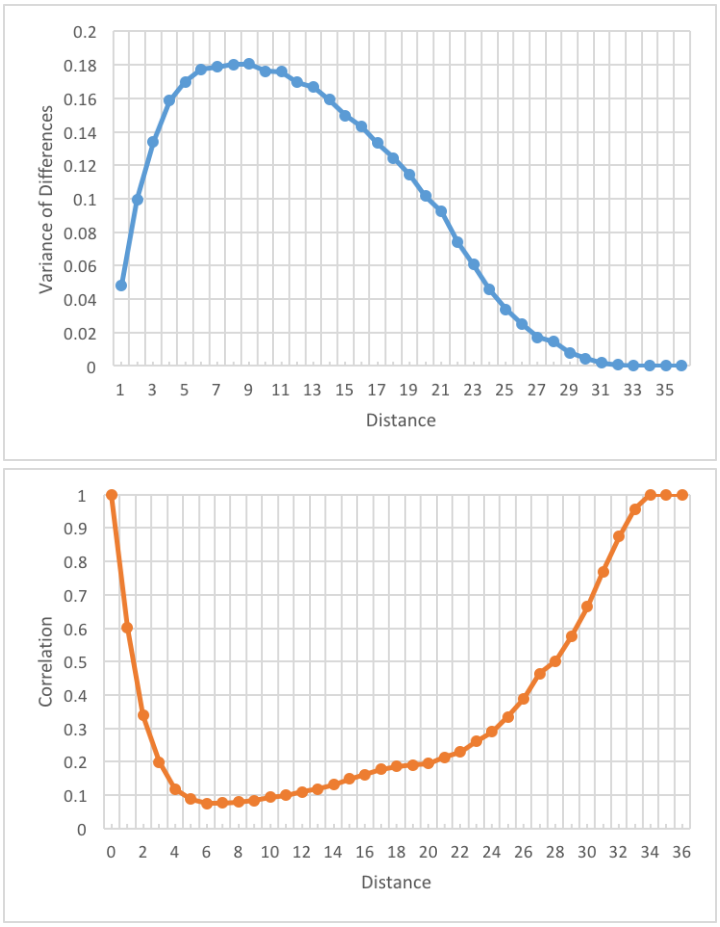

Figure 6.1: Variogram and mean-correlation plots for the MNIST.

we have n samples (one per image in the dataset); this can be thought of as two vectors of values, where the length of the vector is n. We take the difference between these vectors, and then compute the variance of the resulting vector, $var(X^i - X^j)$. This gives us one scalar term for each pair of features. At this point, to make the distance-based function static and isotropic, we average together all feature pairs with equal inter-feature distances. Figure 6.1 shows the variogram and mean-correlation of the original MNIST dataset; note that artifact at the far right side of the plots is caused by the white "border pixels" that are an artifact of MNIST.

In fact, we can make similar plots for any other pairwise statistical measure; for example, we have done something similar using correlation in place of variance-of-differences.

6.3 Experimental Setup

Here we again used the MNIST dataset for our experiments, due to its wide use in evaluating RBMs and deep learning algorithms. A description of the dataset is given in Section 4.4.

We measured the performance of the DBNs using reconstruction error, which is defined to be the mean difference between the original and reconstructed images. We used a binary reconstruction error with a fixed threshold value of 30 to map pixels in the range $[0 - 255]$ to a binary 1 or 0 for the original images. To get the reconstructed image from the DBN, we propagate the image all the way to the last hidden layer of Deep Belief Network, then reconstruct it by reverse propagation to the visible layer. The resulting vector is binarized and compared with the original vector to calculate a reconstruction error using following equation:

$$E(\mathbf{x}, \mathbf{x}') = \frac{1}{n} \sum_{i=1}^{n} I(x_i \neq x_i')$$

To examine whether spatially local features are being preserved, we constructed a 2-layer deep belief network, where each layer is composed of 784 hidden nodes. We calculated the variogram and mean-correlation plot for the output of hidden nodes at each layer.

To apply t-SNE to hidden nodes, we generated sample points by setting a selected hidden neuron to 1.0 and all other hidden nodes to 0, and then computing

corresponding input node activations. Thus, the weights between that hidden node to all visible nodes captures a "feature" (this can also be referred to as a filter, or template, depending on context).

6.4 Results

To examine what statistical information is being exploited by the Partitioned-RBMs, we performed a series of experiments on a randomly permuted version of the data set. Since permuting the data will destroy spatially local features, this allows us to asses how a learning model makes use of these features. To generate this new data set, a mapping was defined that assigned each element of an input vector to each element of the output vector with equal probability. The resultant mapping is 1-to-1 and onto, and is referred to as a random permutation. While the generation of the mapping is randomized, once a permutation has been generated its operation on input vectors is deterministic.

The permutation experiments were performed by generating a random partitioning of data, applying it to each vector in the original dataset to generate a permuted dataset, and then training the RBMs on this dataset. We can then compare the performance of the RBMs using raw and permuted data to see whether or not the RBMs make use of any statistical information that is disrupted by the permutation. See the last row of Figure 6.2 for example permuted images. The last row shows the randomly permuted images corresponding with the original images in the first row.

We also generated a variogram and a mean correlation plot for both the original dataset and the permuted dataset to determine the presence and strength of local statistical structure in the two versions of the dataset.

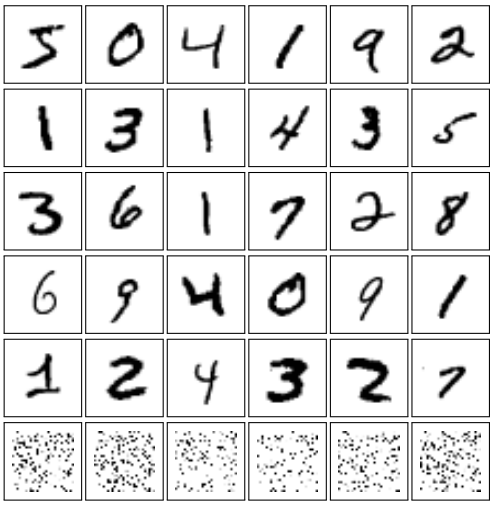

Figure 6.2: Sample images from the MNIST dataset.

Table 6.1 shows the results of our RBM experiments. In the configuration column, Single RBM indicates the RBM was trained on the raw data vectors (i.e. no partitioning); RBM-n indicates a Partitioned-RBM with n partitions. RBM-1 is equivalent to Single RBM in terms of its configuration, but the RBM-1 is trained on fewer samples. Note that each successive RBM-n configuration starts with the output of the previous configuration, as described in Chapter 4. The Samples column gives the number of training instances that were used to train the given RBM, selected at random from the total training set. As the number of partitions decreases, we decrease the training set size to match the time complexity of Single RBM. Each RBM was run for 15 iterations, and the error rates reported are the mean values from 10-fold cross-validation (not using MNIST's predefined split between training and test data).

For the original MNIST dataset, the Partitioned-RBM outperforms the Single RBM not only for RBM-1, but in all configurations except RBM-28. Additionally, when Single RBM is trained using the same reduced-size dataset as the final level

Table 6.1: Reconstruction Errors

Configuration	**Samples**	**Original data Error (%)**	**Permuted Data Error (%)**
Single RBM	60000	2.46	2.44
Single RBM	30000	2.55	2.55
RBM-28	60000	3.32	7.00
RBM-20	50000	2.20	6.42
RBM-15	40000	1.87	6.13
RBM-10	30000	1.64	5.00
RBM-5	25000	1.49	3.88
RBM-2	20000	1.44	2.89
RBM-1	30000	1.42	2.24

Table 6.2: Reconstruction Errors for 2-layer DBN

Configuration	Samples (10^3)	Error (%)
Single RBM	60	2.59
Partitioned-RBM-(16-4-1)	60-50-30	1.05

of the Partitioned-RBM, its performance decreases even further. By design, the computational complexity of the full stack of Partitioned-RBMs is comparable to that of the Single RBM trained on the entire dataset; however, it is evident that less computation would have been necessary for the Partitioned-RBM to yield superior performance.

For the Partitioned-RBM, reconstruction error on the permuted dataset is significantly worse (using a paired t-test with 99% confidence intervals) than the original dataset. Permutation has no statistically significant impact on the performance of the standard Single RBM, as we would expect.

Table 6.2 shows the results of training our DBN with two layers. The configuration column specifies the training method used. The number of partitions in each training stage is defined in parentheses: (16-4-1) indicates that we trained a Partitioned-RBM

first with 16 splits, then 4, and finally trained as a single partition. As before, when the number of partitions decreases, we decrease the training set size to match the time complexity of the full Partitioned-RBM training process to that of the Single RBM. Each RBM was run for 15 iterations, and the error rates reported are the mean values from 10-fold cross-validation (not using MNIST's predefined split between training and test data).

Partitioned-RBM significantly outperforms the Single RBM ($p > 99.99\%$ using a paired t-test). By design, the computational complexity of the full stack of Partitioned-RBMs is comparable to or faster than that of the Single RBM trained on the entire dataset; however, it is evident that less computation would have been necessary for the Partitioned-RBM to yield superior performance.

We generated variogram and mean correlation plots as described in Section 6.2. Figure 6.3 shows the variogram plots for subsets of the data corresponding to digits 0, 5 and 9 (from top to bottom). The first column shows variograms of the raw input vectors for each subset, the second column shows results of the Single RBM, and the third shows results of the Partitioned-RBM. The $y-axis$ represents the mean variance of differences, and the $x-axis$ represents Euclidean pixel distance between points. Labels of the form $N-P$ indicate data for hidden layer N of a Deep Belief Network based on Partitioned-RBMs with P partitions. For all digits, Partitioned-RBM produces an "arch" pattern consistent with the original digit plot. In comparison, the hidden layers of the traditional RBM do not preserve the relationship between distance and difference. Variograms for other digits can be found in Appendix A.

Similar to variogram, Figure 6.4 shows the mean correlation plots for subsets of the data corresponding to digits 0, 5 and 9. As with variograms, the first column depicts digits, the second column shows results of the Single RBM, and the third

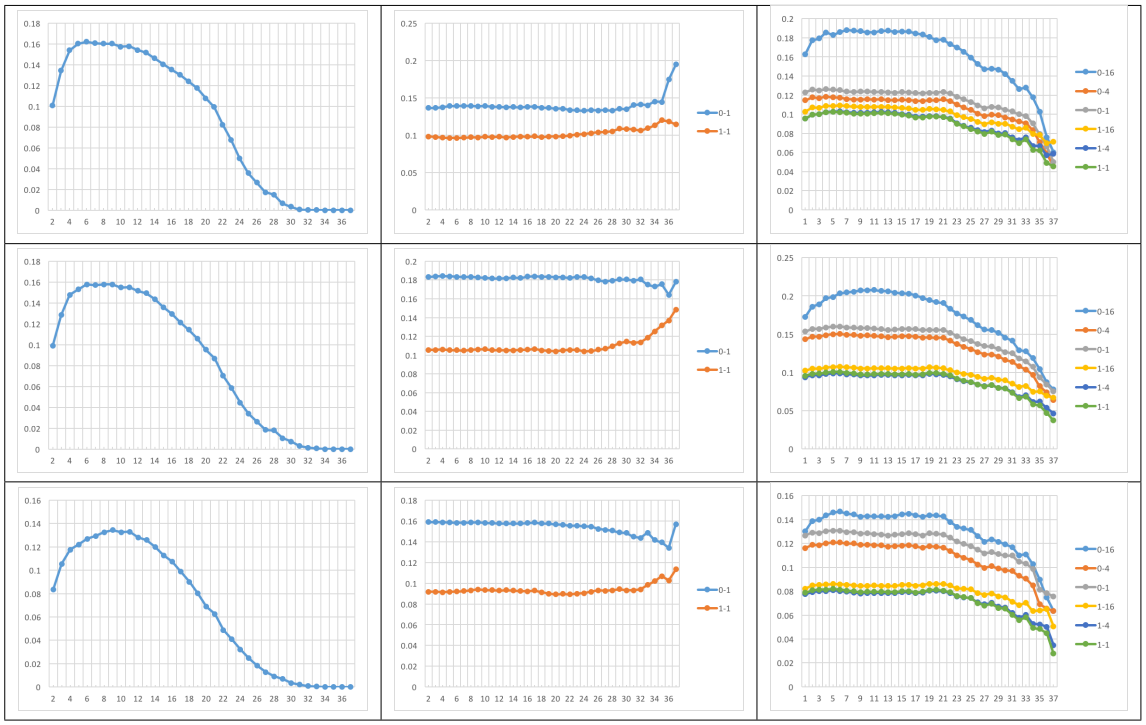

Figure 6.3: Variograms: labels 0, 5 and 9.

column shows results of the Partitioned-RBM. These are consistent with the variogram results: The Single RBM does not show any relationship between distance and mean correlation, while the raw data and the Partitioned-RBM output both show correlation that changes with distance. Mean correlations for other digits can be found in Appendix B.

We also used t-SNE (as described in Sec. 2.5.3) to visualize the activations at the hidden nodes. For this experiment, we constructed a 3-layer Deep Belief Network where each layer has 784 nodes. Results are shown in Figure 6.5. The first row shows the results for the Partitioned-RBM and the second row for a Single RBM. Columns corresponds to network layers 1–3. The scatter plot of activations shows that the

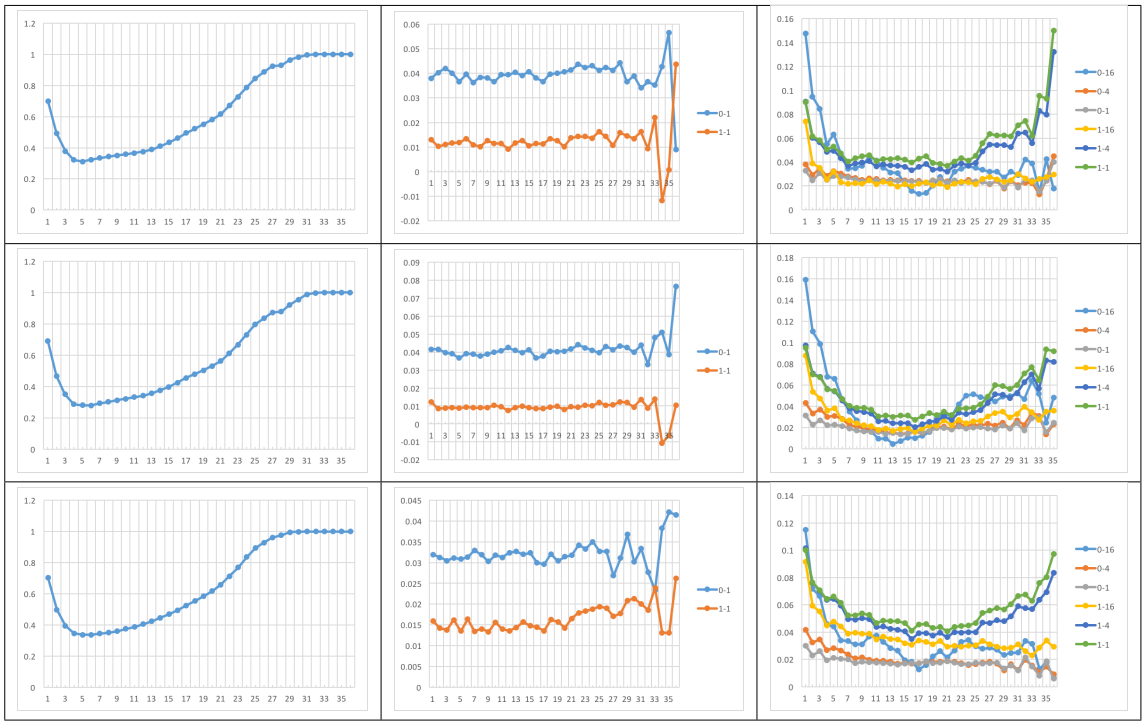

Figure 6.4: Correlations: labels 0, 5 and 9.

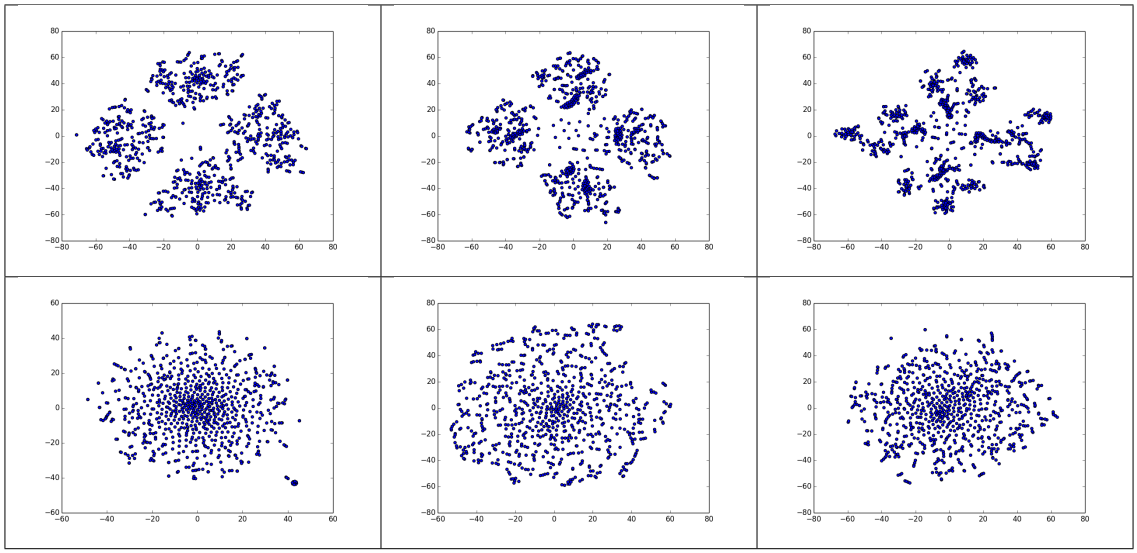

Figure 6.5: Hidden node activations: 15 iterations

Partitioned-RBM has some natural clusters, whereas the Single RBM output closely approximates a zero-mean Gaussian.

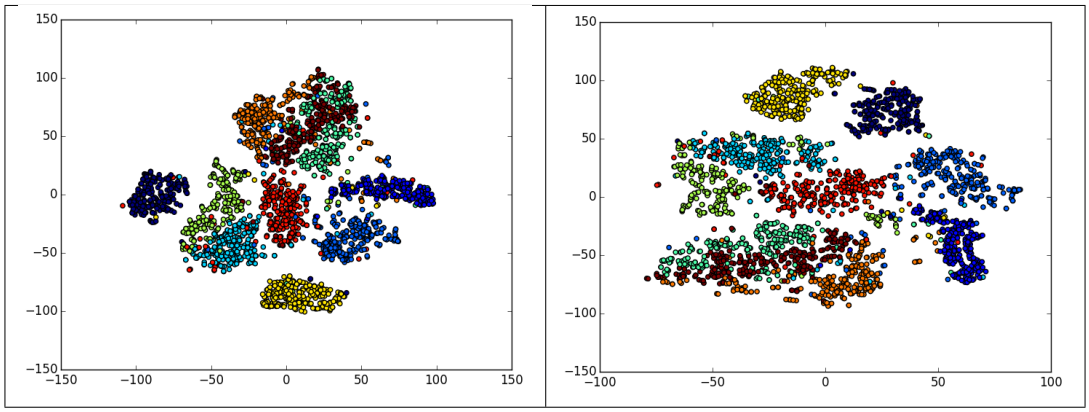

Figure 6.6: MNIST t-SNE mappings

To ensure that the t-SNE method is correctly accounting for possible re-ordering of features, we applied t-SNE to both permuted and non-permuted MNIST data. Figure 6.6 shows results of these experiments. The left figure is for the original data and right figure corresponds to permuted data. The permuted data generates a t-SNE plot with qualitatively similar structure to that generated from the original data; importantly, this resembles the output generated from the Partitioned-RBM, but it does not resemble the Gaussian-like output generated from the traditional RBM.

To explore how diffusion progresses across layers in the Partitioned-RBM, we paused the training between stages (i.e. just before the number of partitions was decreased). As the number of partitions changed, we plotted the t-SNE mapping for the first hidden layer of the DBN (first RBM). Figure 6.7 shows that structure continues to be present, though some consolidation does take place as partitions are joined.

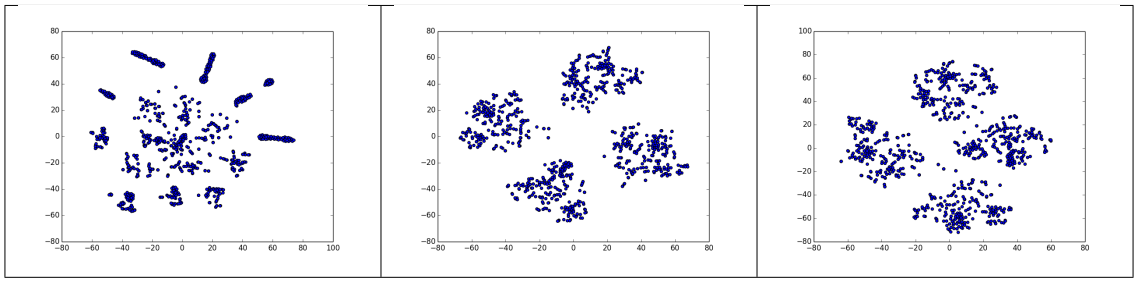

Figure 6.7: Hidden node activations: Partitions

6.5 Discussion

The plots for the original data exhibit some interesting structure. The first is that adjacent features have high correlation, and the variance of the inter-pair differences is low. As the feature-pairs get farther apart, the degree of correlation drops off rapidly. By a distance of 5 pixels, there remains on average little statistical relationship between feature pairs. This is likely related to the average line-width of the hand-written digits, which is generally 2-3 pixels. The fact that correlation improves again as distances increase may seem counterintuitive; however, this is an artifact of the construction of the MNIST dataset. Recall that the MNIST images all have a centered digit surrounded by a white border. Since background pixels have the same value in *all* images, correlation scales with the likelihood that both members of a pair are background. The greater the distance between a pair of features, the more likely that both features will be a part of the background; in fact, beyond a distance of 30 (note that maximum distance is $28 \times \sqrt{2} \approx 40$) both pixels are guaranteed to be background pixels, meaning they are guaranteed to always have the same value. Note that most correlation measures are actually undefined when correspondence is perfect; for the purposes of Figure 6.1, we have set these values to 1.

From the results of our experiments using the permuted dataset, we believe that the Partitioned-RBM is making use of statistical information that is spatially localized, where the Single RBM is not. The permutation results in no loss of information for the Single RBM. It simply re-orders the elements of the vectors. For this reason, any pair-wise correlation between a given pair of features will be unaltered by the permutation. The unchanged behavior of the Single RBM is, therefore, exactly what we expected.

Things are different for the Partitioned-RBM, however, since the location of the two features in a given pair will be altered. This means that two features that would have been assigned to the same partition in the original dataset might *not* be assigned to the same partition in the permuted dataset. Since each piece of a Partitioned-RBM only has access to features in its partition, this means that whatever statistical information was contained in the correlation between this pair of features is no longer available to the Partitioned-RBM.

In fact, Partitioned-RBM will always be cut off from a great many of the pair-wise feature correlations; the difference between the original and permuted datasets is simply in *which* correlations are lost. The fact that the Partitioned-RBM performs significantly worse on the permuted dataset implies that not all correlations are of equal value. In particular, it means that correlations between pairs of features that are spatially close in the original data are more important to the success of the algorithm than correlations between arbitrary pairs (which will, on average, be significantly farther apart in the original image).

Thus, the results lead us readily to the conclusion that the Partitioned-RBM is making use of spatially local statistical information in the MNIST dataset to achieve its performance. Work described [35] that partitioned deep learning algorithms rely on such local information.

We have begun to explore one of the potential representation biases that deep learning techniques leverage to achieve their performance. Our experimental results suggest that partitioned-data techniques are able to make use of spatially local information, and we have in the variogram and the mean-correlation plot some crude tools for analyzing how much spatially local structure exists in a dataset. While these results are promising, they offer only a first jumping off point for the work that could be done in the area of understanding and exploiting the biases that underpin deep learning.

In partitioned learning models, the partitioning can be thought of as a simplifying assumption that reduces both the total number of parameters and the number of inter-parameter dependencies, thus simplifying the learning process. If the data conform to this assumption, this should provide an advantage. We have tested the validity of this assumption by training partitioned models on both "normal" images and "scrambled" images (in which spatially a local structure was intentionally destroyed by permutation, but no statistical information was lost if the full vectors were considered). As expected, if the data badly violates the assumption of spatially local patterns, performance of partitioning techniques is severely degraded, but performance on non-scrambled images is increased by using partitioning [35].

One problem with these results is that they do not cover all deep learning methods; DBNs, for example, do not normally take a partitioned approach, so there may be different principles at play in their success. We mainly focused on the question of whether DBNs are in fact making use of spatially local statistical information, and if not whether we can modify the training procedure to incorporate this spatial locality prior and improve the performance of the network (without modifying the overall architecture or operation of the final DBN model). From the results of our experiments using spatial statistics and t-SNE, we conclude that the Partitioned-

RBM in a Deep Belief Network is making use of spatially local information, where the Single RBM-based DBN is not. The variograms (Fig. 6.3) demonstrate that the Partitioned-RBM output has broadly similar spatial statistics as the original dataset. While the plots are not identical, similar overall trends are present. Partitioned-RBM training preserves these statistical patterns even in higher layers of the network. The same plots for Single RBM training show that spatial locality is lost in the first hidden layer.

Figure 6.6 shows what happens when the original data is scrambled beforehand, by generating a random permutation, and then applying it to each input vector. Despite the disruption of spatial organization of features, the transformation is lossless, and structure obtained in the t-SNE projection is similar to that for the original data. This suggests that if the Single RBM had preserved any spatial features, we should see similar structure in the t-SNE projection (even if the spatial organization of those features was not preserved). As the t-SNE results show, there is no structure in the t-SNE projection after the first layer of the Single RBM; the projected distribution closely approximates a Gaussian (i.e., it is indistinguishable from noise). Thus, we conclude that the traditional RBMs do not retain spatially local statistical information in any recoverable form. As a result, any deep network trained using standard RBMs will lose all spatial information in the first hidden layer. On the other hand, the Partitioned-RBM training technique preserves spatially local information, meaning a deep network trained using this method can make use of spatial patterns in all layers of the network.

This result, combined with the performance edge the Partitioned-RBM has in practice, reinforces the hypothesis that the MNIST data has relevant spatially local structure, and that like other partitioned deep methods, the Partitioned-RBM achieves its performance due to an implicit model bias that assumes (and exploits) the

presence of spatially local features. DBNs trained with the standard RBM method lose spatially local features, and are therefore at a disadvantage because they are attempting to solve a harder problem. Without the constraint imposed by the assumption of local structure, the standard RBM training algorithm is left with a much larger hypothesis space to search.

CHAPTER 7

TIME SERIES CLASSIFICATION VIA PARTITIONED NETWORKS

Since time series data are typically very high dimensional, the use of RBMs in time series tasks is not common. But, in recent years, there have been a few attempts to use RBMs in high dimensional data such as time series and motion data. The following sections summarizes these studies. In the rest of this chapter, we describe Temporal Partitioned Restricted Boltzmann Machines (TPRBM), using partitioned-based training. We apply our partitioned model and Dynamic Time Warping (DTW) to several time series datasets for a sequence classification task.

7.1 Time Series Classification

We begin with a definition of time series data type.

Definition 7.1.1. *(Time Series)* $T = t_1, \ldots, t_n$ *is an ordered set of* n *real-valued variables.*

Depending on classification task, some times we are interested in the classifying the whole time series and sometimes a subsequence of the dataset. However, often the whole time series is not informative. For instance, four hours recording of a patient's heartbeat may not tell us if the hearbeat is abnormal or not. But, a subsequence of dataset may contain an abnormal pattern.

Definition 7.1.2. *(Subsequence) Given a time series* T *of length* n*, a subsequence* $T_s = t_s, \ldots, t_s + w$ *where* $w < n$ *is the length of subsection.*

In addition to DTW scoring method described in Section 2.5.4, *Euclidean Distance* is one of the most common measure for clasification.

Definition 7.1.3. *(Euclidean Distance) Given two time series T and S with both of length n, Euclidean distance is the square root of the sum of the squared differences between each pair of time values:*

$$d(T,S) = \sqrt{\sum_{n=1}^{n}(t_i - s_i)^2}$$

Time series *prediction* is a process of finding the value of t_i for given previous $t_1, \ldots, t_{j-1}$ values. Time series *classification* on the other hand, involves finding a categorical label for a giving time series. Classification is a specifically useful tool for indexing and querying a database of time series.

Definition 7.1.4. *(Time Series Classification) Given a set of unlabeled time series, the task of time series classification is assign a label from one of the predefined classes.*

A considerable amount of literature has been published on time series prediction and classification. In fact, time series prediction has been studied in statistics over many decades. One of the most successful models, Autoregressive Moving Average (ARMA), was developed by Peter Whittle in 1951 [76] and popularized by George E. P. Box and Gwilym Jenkins in 1971 [77]. ARMA and its extension, Autoregressive Integrated Moving Average (ARIMA), are still very popular time series prediction models today. It has only been over the last couple of decades that machine learning has been used for time series prediction tasks using methods such as Neural Networks and Support Vector Machines.

On the other hand, the need for time series classification mainly has arisen when people need to store/index large volumes of time series data and query that. For

example, querying a gene sequence database for given sequence pattern requires classification. Dynamic Time Warping (DTW), discussed in Chapter 2, is one of the most important tools for time series classification.

7.2 Temporal Restricted Boltzmann Machines

The Conditional Restricted Boltzmann Machine (CRBM) is a non-linear generative model designed to model human motion where real-valued visible variables represent joint angles and hidden/latent variables represents motion [78]. The model is the same as a regular RBM; however, the hidden and visible layers are both conditioned on visible variables from the last few time-steps.

As shown in Figure 7.1a, the hidden layer and visible layer both have direct connections from the visible layer in previous time steps. Given data at n previous steps, hidden layers are independent. With a minor change to the energy function, the Contrastive Divergence algorithm is used for training CRBMs. The only change required is to use direct connections from previous layers to update hidden and visible biases. For a regular RBM, the energy function is the following:

$$E(\mathbf{x}, \mathbf{h}) = -\mathbf{h^T W x} - \mathbf{b^T x} - \mathbf{c^T h},$$

whereas the CRBMs, the energy function becomes:

$$E(\mathbf{x}, \mathbf{u}, \mathbf{h}) = -\mathbf{h^T W x} - \mathbf{b^T x} - \mathbf{c^T h} - \mathbf{u^T W x} - \mathbf{u^T W h}$$

where $\mathbf{u}$ is an input vector that represents a visible layer from the previous time step. So, the only change is including components with the $\mathbf{u}$ term.

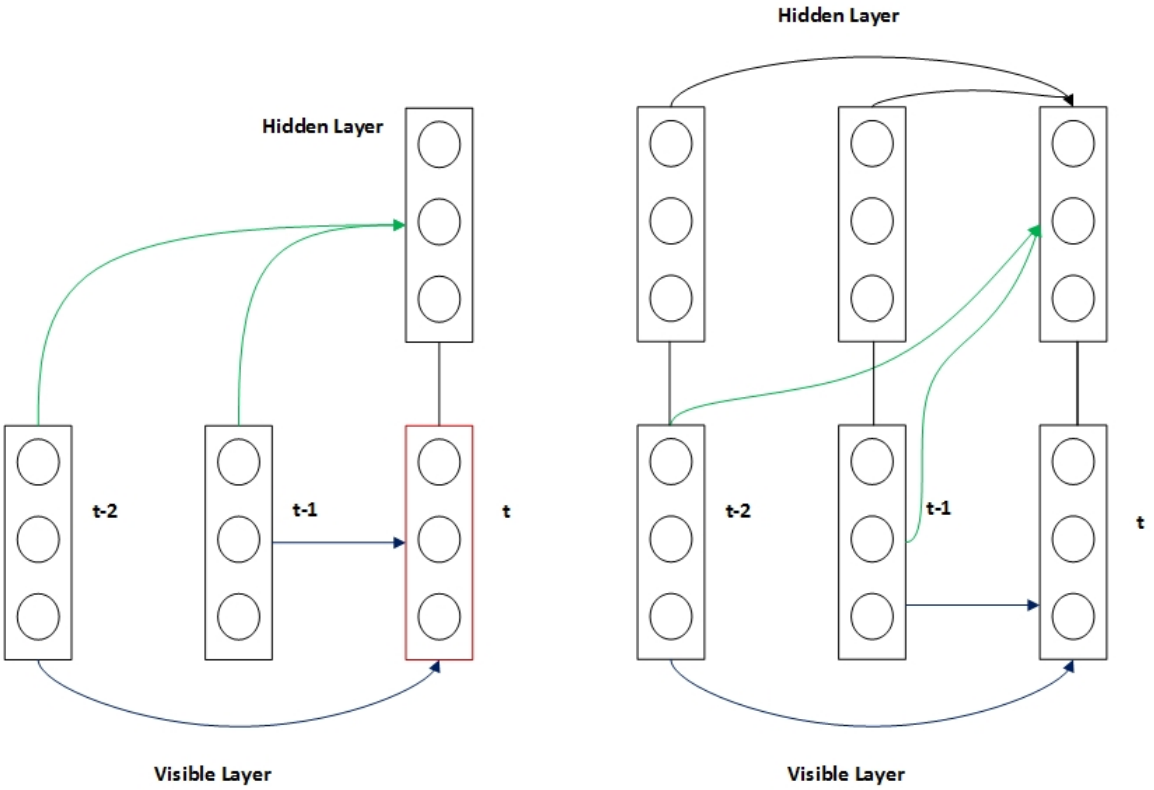

(a) Conditional Restricted Boltzmann Machine

(b) Temporal Restricted Boltzmann Machine

After the full training of CRBM, the last model parameters capture the representation of motion. Thus, the CRBM is the first successful temporal RBM model applied to human motion and video textures.

Along similar lines, Sutskever *et al.* came up with the Temporal Restricted Boltzmann Machine (TRBM) [79] to represent sequential data that can be learned one hidden layer at a time. Similar to CRBM, TRBM also conditions on the previous states as shown in Figure 7.1b. It should be noted that in a TRBM, the hidden layer is not only conditioned on previous visible layers but also on previous hidden layers. Thus, the model resembles a dynamic Bayesian network [80].

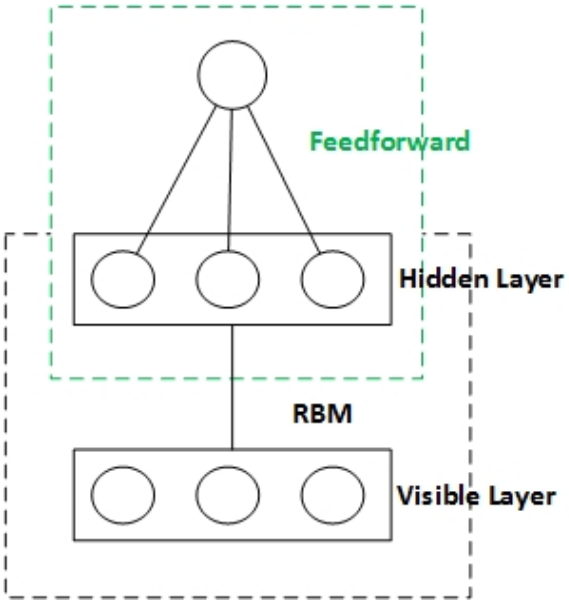

Figure 7.2: RBM with Feedforward

The resulting sequence model is defined as a product of regular RBMs, where each RBM is conditioned on previous RBMs and trained independently using Contrastive Divergence. These models are also applied successfully to video sequences and evolution of objects.

Häusler *et al.* extended the TRBM with only hidden-to-hidden layer connections [81]. Similar to CRBMs, RBMs are stacked side by side. The connections between them (between hidden layers) are trained using Autoencoders. Thus, the model is called "Temporal Autoencoding Restricted Boltzmann Machines (TARBM)." The model has also been successfully applied to time series classification tasks.

Hrasko *et al.* took a hybrid approach when applying RBMs to time series predictions [82]. As show in Figure 7.2, the output of an RBM is fed to a Feedforward Neural network for prediction.

7.3 Partitioned Restricted Boltzmann Machines

Here, we show that Partitioned-RBM is a natural model for learning time series classification for the following reasons. 1) Each partition can learn local features or trends efficiently since sub-RBMs are small. 2) As we combine partitions, at the later stages of the learning, the model can learn longer trends and features. 3) Time series have very high dimensions; thus, by partitioning the data as well as the model, Partitioned-RBM will significantly improve the computational performance.

TPRBM is basically the same model as Partitioned-RBM described in Chapter 5. However, instead of using quadtree partitioning, here we use a naïve partitioning. The whole time series is divided into k sub-vectors without overlap. The remainder of the training is the same. For example, Figure 7.3 represents a time series of length 132 and four partitions. Each RBM works on one section of the time series.

The idea here is that each individual RBM will capture local trends/features within the window. Thus, distant features will not be represented. However, in later stages, when we have fewer splits, distant features will also be captured. We demonstrated in Chapter 6 that regular RBMs do not preserve spatially local features. We assert that regular RBMs will not preserve temporal local trends and features either. Moreover, as demonstrated by Schulz *et al.*, a monolithic RBM will not capture local features as most of its detectors will have uniform weights after the training is done [56].

Training time complexities of regular RBMs and Partitioned-RBMs are given in Equations 4.1 and 4.2, which are repeated here for convenience. The time complexity of regular RBM is $O(I \cdot S \cdot H \cdot V)$ where I, S, H, and V are number of iterations, number of samples, number of hidden nodes, and number of visible nodes respectively.

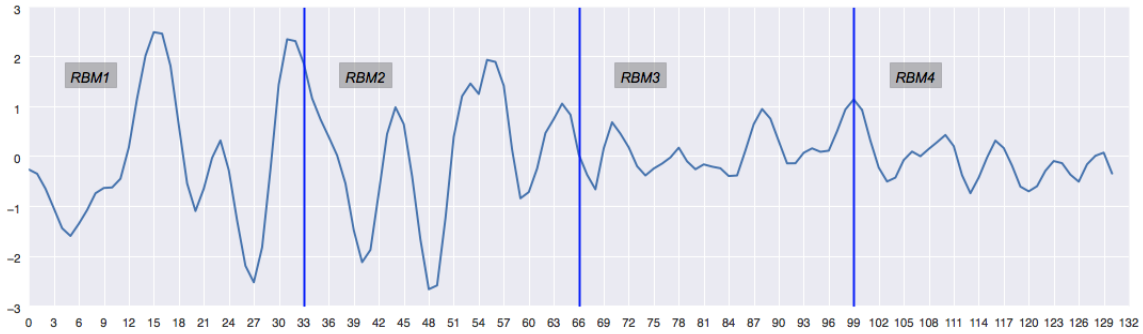

Figure 7.3: Partitioned Time Series

The time complexity for Partitioned-RBM is

$$O\left(I \cdot H \cdot V \cdot \sum_{\substack{n \in \{n_0, n_1, \ldots, 1\} \\ s \in \{s_0, s_1, \ldots,\}}} \frac{s_i}{n_i^2}\right)$$

where n_i represents the number of splits in stage i, and s_i represents the number of samples used in stage i for training. If we keep I, H, and V constant, we can vary the number of samples used in each stage and/or the number of partitions to improve runtime performance of Partitioned-RBMs significantly. For instance, for a very high dimensional dataset, we can increase the number of partitions to reduce the number of computations over each set of partitions. For large datasets, we can use more samples in earlier stages where the training is fast, but fewer training samples in later stages as training slows. This flexibility enables tuning of Partitioned-RBM performance to suit the particular dataset being studied.

7.4 Experimental Setup

We selected five time series from the UCR Time Series Classification Archive [63]. Each dataset has series of different lengths, numbers of classes, and numbers of

Table 7.1: Partitioned-RBM configuration

Data Series	**Size**	**Labels**	**Samples**	**Partitions**	**Hidden nodes**
FaceAll	131	14	2250	50-20-5-1	1000
RefrigerationDevices	720	3	750	50-20-5-1	1000
ECG5000	140	5	5000	50-20-5-1	1000
ElectricDevices	96	7	16637	20-5-1	1000
ShapesAll	512	60	1200	50-20-5-1	1000

samples. The UCR time series are split into test and training sets. Generally, the training set is a lot smaller than the test set because prior studies mostly used the k-Nearest-Neighbor algorithm for classification (k-NN). k-Nearest-Neighbor Classifiers is a lazy learner [83]; the model is constructed during query or classification time. In query time, however, using a large training set is inefficient. Thus, we did not use the pre-defined test and training batches. Instead, we combined both to create a full dataset so that we could use 10-fold cross-validation. Moreover, we binarized data using the following naïve method: anything less than or equal to 0 was set 0 and anything greater than 0 was set to 1.

The time series datasets that we used are shown in Table 7.1. The size column indicates the time series length, and the partitions column indicates the number of partitions used to train Partitioned-RBM. $50-20-5-1$ means, we initially trained the model with 50 partitions followed by 20 partitions in the second stage, and 5 partitions in third. In the final stage, we trained the model as a full RBM. It should be noted, however, that we selected samples in each stage such that the time complexity of Partitioned-RBM is comparable to or better than that of Single RBM.

Table 7.2: Time Series Classification Accuracy

Data Series	**Accuracy Single**	**Accuracy TPRBM**	**Accuracy 1-NN DTW**
FaceAll	76.22 ± 0.038	90.00 ± 0.020	96.98 ± 0.016
RefrigerationDevices	46.27 ± 0.057	53.60 ± 0.052	57.87 ± 0.046
ECG5000	89.88 ± 0.032	91.62 ± 0.020	92.96 ± 0.011
ElectricDevices	39.33 ± 0.051	53.99 ± 0.031	67.19 ± 0.021
ShapesAll	59.08 ± 0.028	59.17 ± 0.029	79.42 ± 0.033

7.5 Results

The average classification accuracies and standard deviation of folds are shown in Table 7.2. Here, $1-NNDTW$ is 1-Nearest-Neighbor classifier using DTW distance measure. Partitioned-RBM significantly outperforms regular RBM on all datasets except *ShapesAll* using a paired t-test with 99% confidence intervals. This demonstrates that using more examples improves model accuracy of Partitioned-RBM with the same or better computation performance. We also compared our method to DTW, but DTW outperformed all RBMs on these datasets. We believe the reason for this is that these data do not have a sufficient number of dimensions to fully exploit temporal features.

We also decided to study how our algorithm behaves when the same pattern in repeated in a time series. For this, we created a modified version of the *FaceAll* dataset by repeating each time series three times. For example, abC is modified as $abCabCabC$. As shown in Table 7.3, although Partitioned-RBM still outperforms Single RBM, DTW is still superior in terms of classification accuracy.

In previous experiments, the test and training datasets had equal lengths. Thus, alignment is done on the whole sequence. To show how subsequence classification will

Table 7.3: Classification Accuracy with Repeated Patterns of FaceAll

Model	**Accuracy**
Single RBM	77.82 ± 0.027
Partitioned-RBM	80.04 ± 0.028
1-NN DTW	96.84 ± 0.018

Table 7.4: Subsequence Classification Accuracy with Repeated Patterns of FaceAll

Model	**Accuracy**
Single RBM	81.78 ± 0.029
Partitioned-RBM	90.06 ± 0.026
1-NN DTW	14.04 ± 0.024

work, we created training data with repeated patterns as described above. However, when we created the test dataset, we did not repeat the sequence. In other words, the test set contains the original pattern as a subsequence of the training time series. Thus, when we do classification, we are comparing a short test sequence with long repeated sequences. However, for both Single RBM and Partitioned-RBM, we appended zeros to test sequences for classification because number of visible nodes in RBM are equal to the length of training data. Table 7.4 demonstrates that Partitioned-RBM outperforms both DTW and Single RBM. In fact, the results of DTW are close to random guessing. Thus, DTW does not work well when test and template time series have different lengths.

7.6 Conclusion

Lazy learning algorithms that require query-time computation are not efficient because time series data often has high dimensions. For example, an algorithm using DTW score and k-NN during query has the following drawbacks. 1) If the database that we run the query against is fairly large, the response time of the algorithm is

very slow. 2) Because of the first drawback, one has to select a subset of the dataset for runtime query; however, this kind of knowledge engineering is expensive. We selected samples in each stage such that the time complexity of Partitioned-RBM is comparable to or better than that of Single RBM. Thus, we demonstrated that Partitioned-RBM can effectively be applied to time series datasets without these drawbacks.

CHAPTER 8

SUMMARY AND CONCLUSIONS

In this dissertation, we presented a partitioned learning approach and applied it to Restricted Boltzmann Machines. Specifically, we demonstrated the effectiveness of this method in the context of both standalone RBMs and DBNs. In this chapter, we conclude with a summary of our contributions and directions for future work.

8.1 Summary of Contributions

8.1.1 Partitioned Learning

This study set out to develop a generic learning algorithm that not only partitions the input vector, but also the model parameters. Thus, we developed a novel meta-algorithm that converts a monolithic model into submodels where each submodel is trained on a corresponding partition of the input vector. However, learning proceeds in multiple stages where the model and the input vector are split into fewer partitions in each successive stage. In other words, as the stages proceed, smaller partitions are combined into larger partitions. This dissertation has shown that this partitioned approach results in better feature representation.

8.1.2 Computational Efficiency

As we demonstrated in Chapter 4, training Partitioned-RBMs is faster than training non-partitioned versions. In addition, we demonstrated that Partitioned-RBMs have the same or better feature representation power as a monolithic RBM,

Partitioned-RBMs yield two major improvements: 1) a faster algorithm for learning with high dimensional data; and 2) a novel algorithm for training RBMs under resource-bounded conditions. When there are limited computational resources, the algorithm can terminate early with a good generative performance.

8.1.3 Efficient Classification

We demonstrated in Chapter 4 that Partitioned-RBM can be used efficiently as a discriminative model. We demonstrated that Partitioned-RBM has the same or better classification accuracy as regular RBMs. However, it requires less computation.

8.1.4 Preserving Spatially Local Features

As shown in Chapter 6, Partitioned-RBM can be used effectively as part of Deep Belief Networks. We further demonstrated that Partitioned-RBM preserves spatially local features while regular RBM-based DBN does not.

8.1.5 Sparsity

A sparse RBM is a model that, when trained, has most of the weights close to zero and only a few either highly positive or highly negative. In a sparse RBM, only a few neurons (hidden nodes) will be active at any given time. This enables the network to learn sparse representations. Researchers often limit the number of neurons that are active for a given input by explicitly adding a sparsity factor in the training process so that most of the weights between visible and hidden nodes are close to zero. Partitioned-RBMs possess natural sparsity because each Partitioned-RBM is trained on a reduced region of the dataset.

8.1.6 Time Series Classification

In Chapter 7, we demonstrated that Partitioned-RBMs are effective in a time series classification task. The partitioned training model fits well with time series datasets because such datasets have very high dimensions. Both regular RBMs and DTW-based k-Nearest Neighbor algorithms cannot perform well when the dimensionality is very high. Moreover, since DTW requires query time model construction, knowledge engineering is needed to select a subset of the whole data, making this method impractical.

8.2 Publications

This study resulted in several published papers and more papers to be submitted for publication. The related publications are:

- H. Tosun and J. W. Sheppard, Training restricted Boltzmann machines with overlapping partitions, in Proceedings of the European Conference on Machine Learning-Principles and Practice of Knowledge Discovery in Databases (ECML-PKDD). Springer, 2014, vol. 8726, pp. 195-208.

- B. Mitchell, H. Tosun, and J. Sheppard, Deep learning using partitioned data vectors, in Proceedings of the IEEE International Joint Conference on Neural Networks (IJCNN), 2015, pp. 1–8.

- H. Tosun, B. Mitchell, and J. Sheppard, Assessing diffusion of spatial features in deep belief networks, to appear in IEEE International Joint Conference on Neural Networks (IJCNN), 2016.

- H. Tosun and J. Sheppard, Fast classification under bounded computational resources using partitioned-rbms, to appear in IEEE International Joint Conference on Neural Networks (IJCNN), 2016.

- H. Tosun and J. Sheppard, Fast time series classification using Partitioned Restricted Boltzmann Machines, conference or journal to be identified.

8.3 Future Work

Our approach opens the door to many potential applications. Since training is done on partitioned small RBMs, we believe the method will learn multi-mode data, that is data from multiple sources, more accurately. Other directions for future work include carrying out additional experiments to demonstrate that this training method can be applied to domains with a high volume of features.

Our algorithm also has similarities to transfer learning. Since in each stage we learn some weights and those weights are used as a base configuration for the next stage, it is analogous to feature representation transfer [84]. One interesting direction for future work would be to investigate whether other methods of transfer learning can be used during training.

In Chapter 5 we demonstrated that Partitioned-RBM performs significantly better than single RBM under bounded computational resources. To see our method perform even better, we need to run it on a dataset with extremely high volume and high dimensions. We speculate that a single RBM cannot be trained optimally unless it runs many iterations, which will take days to train. On the other hand, Partitioned-RBM can run many iterations in the first stage with all data samples efficiently. We

are planning to use this scheme to run classification tasks on many datasets with high dimensions and high volume.

Moreover, better runtime performance also enables us to create an ensemble of Partitioned-RBMs. Therefore, we plan to run experiments using ensembles. We hypothesize that an ensemble of Partitioned-RBMs will result in even better classification accuracy.

The results of our classification study also suggest that Partitioned-RBM will provide even better runtime improvement when used as a component of a DBN. As we stack up more layers of RBMs, the runtime performance becomes more relevant. Our preliminary experiments indicate that Partitioned-RBM has comparable classification accuracy rates with Single RBM when used in DBNs. Contrary to expectation, the results were not significantly better. Additionally, we found that a DBN does not increase accuracy rates drastically as compared to a regular RBM. It is possible this is because of the relative simplicity of the MNIST data set. Hence, we plan to 1) explore methods to improve classification accuracy of Partitioned-RBM when used as a component of a DBN, 2) investigate why a DBN does not drastically improve accuracy rates, and 3) investigate alternative data sets.

As we demonstrated with DBNs, Partitioned-RBM preserves statistical spatial features in all layers of the network, while regular RBMs diffuse all spatially local features. We plan to carry out further experiments to determine whether preserving statistically local features will result in higher classification accuracy.

Traditional DBNs achieve remarkable performance when applied to classification, image recognition and many other applications. We have begun to explore applications where we can apply partitioned-data techniques, and we are in the process of comparing a partitioned-data DBN to a traditional DBN in terms of classification performance (as opposed to the reconstruction task examined here). This is impor-

tant in two ways: 1) we would like to determine whether preserving spatially local structure in higher layers of the network can improve classification accuracy, and 2) we would like to explore further how and why deep learning works, by analyzing how traditional DBNs achieve their performance even without exploiting any spatially local information.

When applied to time series classification, we demonstrated that Partitioned-RBM outperforms regular RBMs. However, the time series in the datasets we have chosen have relatively short lengths. Applying query-based algorithms to time series with very long lengths will become impractical. However, with Partitioned-RBM, we can increase the number of partitions and therefore, thereby increase the computation performance. As a result, we should be able to obtain even better classification accuracies.

Finally, we also plan to develop with a better Partitioned-RBM subset classification of time series. So far, we have implemented a fairly naïve method by setting all missing values to 0. A reasonable approach in this direction will be to have each partition to return a classification score. In other word, each sub RBM will have its own classification nodes. Some kind of majority-voting mechanism needs to be applied to obtain final classification score.

REFERENCES CITED

[1] Tijmen Tieleman. Training restricted boltzmann machines using approximations to the likelihood gradient. *Proceedings of the 25th International Conference on Machine Learning*, pages 1064–1071. ACM, 2008.

[2] Ooh! ahh! google images presents a nicer way to surf the visual web [online]. Available at `http://googleblog.blogspot.com/2010/07/ooh-ahh-google-images-presents-nicer.html`, Accessed 2014-08-09.

[3] Bruno A Olshausen, i in. Emergence of simple-cell receptive field properties by learning a sparse code for natural images. *Nature*, 381:607–609, 1996.

[4] Yoshua Bengio, Aaron Courville, Pascal Vincent. Representation learning: A review and new perspectives. *IEEE Transactions on Pattern Analysis and Machine Intelligence*, 35:1798–1828, 2013.

[5] Hasari Tosun, John W. Sheppard. Training restricted boltzmann machines with overlapping partitions. *Machine Learning and Knowledge Discovery in Databases,ECML PKDD*, Volume 8726 series *Lecture Notes in Computer Science*, pages 195–208. Springer, 2014.

[6] Don S Lemons. *A student's guide to entropy*. Cambridge University Press, 2013.

[7] P. Smolensky. Information processing in dynamical systems: Foundations of harmony theory. David E. Rumelhart, James L. McClelland, editors, *Parallel Distributed Processing: Explorations in the Microstructure of Cognition, Vol. 1*, pages 194–281. MIT Press, Cambridge, MA, USA, 1986.

[8] David H Ackley, Geoffrey E Hinton, Terrence J Sejnowski. A learning algorithm for boltzmann machines. *Cognitive Science*, 9:147–169, 1985.

[9] Geoffrey E Hinton. Training products of experts by minimizing contrastive divergence. *Neural computation*, 14:1771–1800, 2002.

[10] Yoshua Bengio. Learning deep architectures for ai. *Foundations and Trends in Machine Learning*, 2:1–127, 2009.

[11] Geoffrey E Hinton, Ruslan R Salakhutdinov. Reducing the dimensionality of data with neural networks. *Science*, 313:504–507, 2006.

[12] Noel A. C. Cressie. *Statistics for Spatial Data*. Wiley-Interscience, 1993.

[13] Alan E Gelfand, Peter Diggle, Peter Guttorp, Montserrat Fuentes. *Handbook of spatial statistics*. CRC press, 2010.

[14] Michael de Smith, Michael F. Goodchild, Paul A Longley. *Geospatial Analysis*. The Winchelsea Press, 2015.

[15] Laurens Van der Maaten, Geoffrey Hinton. Visualizing data using t-sne. *Journal of Machine Learning Research*, 9:2579–2605, 2008.

[16] T Cox, M Cox. Multidimensional scaling. *Chapman&Hall, London, UK*, 1994.

[17] Lawrence K Saul, Sam T Roweis. An introduction to locally linear embedding. *Available at: http://www. cs. toronto. edu/˜roweis/lle/publications.html*, 2000.

[18] Hiroaki Sakoe, Seibi Chiba. Dynamic programming algorithm optimization for spoken word recognition. *Acoustics, Speech and Signal Processing, IEEE Transactions on*, 26:43–49, 1978.

[19] Max Welling, Yee W Teh. Bayesian learning via stochastic gradient langevin dynamics. *Proceedings of the International Conference on Machine Learning*, pages 681–688, 2011.

[20] Sungjin Ahn, Anoop Korattikara, Max Welling. Bayesian posterior sampling via stochastic gradient fisher scoring. *Proceedings of the International Conference on Machine Learning*, pages 1591–1598, 2012.

[21] Lucien Le Cam. *Asymptotic methods in statistical decision theory*. Springer Science & Business Media, 2012.

[22] Yoshua Bengio, Pascal Lamblin, Dan Popovici, Hugo Larochelle. Greedy layer-wise training of deep networks. *Advances in Neural Information Processing Systems*, 19:153–160, 2007.

[23] Geoffrey Hinton, Ruslan Salakhutdinov. Discovering binary codes for documents by learning deep generative models. *Topics in Cognitive Science*, 3:74–91, 2011.

[24] George E Dahl, Ryan P Adams, Hugo Larochelle. Training restricted boltzmann machines on word observations. *Proceedings of the 29th International Conference on Machine Learning*, pages 679–686. ACM, 2012.

[25] Hugo Larochelle, Yoshua Bengio. Classification using discriminative restricted boltzmann machines. *Proceedings of the 25th International Conference on Machine Learning*, pages 536–543. ACM, 2008.

[26] Jérôme Louradour, Hugo Larochelle. Classification of sets using restricted boltzmann machines. *Uncertainty in Artificial Intelligence*, pages 463–470. AUAI, 2011.

[27] Ruslan Salakhutdinov, Andriy Mnih, Geoffrey Hinton. Restricted boltzmann machines for collaborative filtering. *Proceedings of the 24th International Conference on Machine Learning*, pages 791–798. ACM, 2007.

[28] Daphne Koller, Nir Friedman. *Probabilistic Graphical Models: Principles and Techniques*. MIT press, 2009.

[29] Philemon Brakel, Sander Dieleman, Benjamin Schrauwen. Training restricted boltzmann machines with multi-tempering: Harnessing parallelization. *Artificial Neural Networks and Machine Learning–ICANN 2012*, pages 92–99. Springer, 2012.

[30] Guido Montúfar, Jason Morton. Discrete restricted boltzmann machines. *The Journal of Machine Learning Research*, 16:653–672, 2015.

[31] Benjamin M. Marlin, Nando de Freitas. Asymptotic efficiency of deterministic estimators for discrete energy-based models: Ratio matching and pseudolikelihood. *CoRR*, abs/1202.3746, 2012.

[32] Benjamin M Marlin, Kevin Swersky, Bo Chen, Nando D Freitas. Inductive principles for restricted boltzmann machine learning. *International Conference on Artificial Intelligence and Statistics*, pages 509–516, 2010.

[33] Tanya Schmah, Geoffrey E Hinton, Steven L Small, Stephen Strother, Richard S Zemel. Generative versus discriminative training of rbms for classification of fmri images. *Advances in Neural Information Processing Systems*, pages 1409–1416, 2008.

[34] D. Erhan, Y. Bengio, A. Courville, P. Manzagol, P. Vincent. Why does unsupervised pre-training help deep learning? *Journal of Machine Learning Research*, 11:625–660, 2010.

[35] B. Mitchell, J. Sheppard. Deep structure learning: Beyond connectionist approaches. *International Conference on Machine Learning and Applications (ICMLA) '12*, pages 162–167, 2012.

[36] Y. Bengio, P. Simard, P. Frasconi. Learning long-term dependencies with gradient descent is difficult. *IEEE Transactions on Neural Networks*, 5:157–166, March 1994.

[37] K. Fukushima. Neocognitron: A self-organizing neural network model for a mechanism of pattern recognition unaffected by shift in position. *Biological Cybernetics*, 36:193–202, 1980.

[38] G. E. Hinton, S. Osindero, Y. W. Teh. A fast learning algortihm for deep belief nets. *Neural Computation*, 18:1527–1554, 2006.

[39] MarcAurelio Ranzato, Christopher Poultney, Sumit Chopra, Yann L Cun. Efficient learning of sparse representations with an energy-based model. *Advances in neural information processing systems*, pages 1137–1144, 2006.

[40] Honglak Lee, Chaitanya Ekanadham, Andrew Y Ng. Sparse deep belief net model for visual area v2. *Advances in Neural Information Processing Systems*, pages 873–880, 2008.

[41] Dong Yu, Michael L Seltzer, Jinyu Li, Jui-Ting Huang, Frank Seide. Feature learning in deep neural networks-studies on speech recognition tasks. *International Conference on Learning Representations (ICLR)*, 2013.

[42] Geoffrey E Hinton, Simon Osindero, Yee-Whye Teh. A fast learning algorithm for deep belief nets. *Neural Computation*, 18:1527–1554, 2006.

[43] Ruslan Salakhutdinov, Geoffrey E Hinton. Deep boltzmann machines. *International Conference on Artificial Intelligence and Statistics*, pages 448–455, 2009.

[44] Hugo Larochelle, Yoshua Bengio, Jérôme Louradour, Pascal Lamblin. Exploring strategies for training deep neural networks. *The Journal of Machine Learning Research*, 10:1–40, 2009.

[45] Pascal Vincent, Hugo Larochelle, Yoshua Bengio, Pierre-Antoine Manzagol. Extracting and composing robust features with denoising autoencoders. *Proceedings of the 25th International Conference on Machine Learning*, pages 1096–1103. ACM, 2008.

[46] Junyuan Xie, Linli Xu, Enhong Chen. Image denoising and inpainting with deep neural networks. *Advances in Neural Information Processing Systems*, pages 341–349, 2012.

[47] Y. LeCun, L. Bottou, Y. Bengio, P. Haffner. Gradient-based learning applied to document recognition. *Proceedings of the IEEE*, 86:2278–2324, 1998.

[48] Y. LeCun, F. Huang, L. Bottou. Learning methods for generic object recognition with invariance to pose and lighting. *Proceedings of Computer Vision and Pattern Recognition (CVPR), '04*, 2:97–104, 2004.

[49] Honglak Lee, Roger Grosse, Rajesh Ranganath, Andrew Y Ng. Convolutional deep belief networks for scalable unsupervised learning of hierarchical representations. *Proceedings of the 26th Annual International Conference on Machine Learning*, pages 609–616. ACM, 2009.

[50] Geoffrey E Hinton, Nitish Srivastava, Alex Krizhevsky, Ilya Sutskever, Ruslan R Salakhutdinov. Improving neural networks by preventing co-adaptation of feature detectors. *arXiv preprint arXiv:1207.0580*, 2012.

[51] George E Dahl, Tara N Sainath, Geoffrey E Hinton. Improving deep neural networks for lvcsr using rectified linear units and dropout. *IEEE International Conference on Acoustics, Speech and Signal Processing (ICASSP)*, pages 8609–8613, 2013.

[52] Nitish Srivastava, Geoffrey Hinton, Alex Krizhevsky, Ilya Sutskever, Ruslan Salakhutdinov. Dropout: A simple way to prevent neural networks from overfitting. *The Journal of Machine Learning Research*, 15:1929–1958, 2014.

[53] S. Behnke, R. Rojas. Neural abstraction pyramid: a hierarchical image understanding architecture. *Proceedings of International Joint Conference on Neural Networks (IJCNN) '98*, 2:820–825, 1998.

[54] D. George, B. Jaros. The HTM Learning Algorithm. *Numenta, Inc.* `www.numenta.com`, March 2007, March 2007.

[55] Jeffrey Dean, Greg Corrado, i in. Large scale distributed deep networks. *Advances in Neural Information Processing Systems*, pages 1232–1240, 2012.

[56] Hannes Schulz, Andreas Müller, Sven Behnke. Exploiting local structure in boltzmann machines. *Neurocomputing*, 74:1411–1417, 2011.

[57] Shane Strasser, John Sheppard, Nathan Fortier. Factored evolutionary algorithms. *Submitted to IEEE Transactions on Evolutionary Computation*, 2016.

[58] David Sankoff, Joseph B Kruskal. Time warps, string edits, and macromolecules: the theory and practice of sequence comparison. *Addison-Wesley*, 1, 1983.

[59] Donald J Berndt, James Clifford. Using dynamic time warping to find patterns in time series. *KDD workshop*, Volume 10, pages 359–370. Seattle, WA, 1994.

[60] Eamonn Keogh, Chotirat Ann Ratanamahatana. Exact indexing of dynamic time warping. *Knowledge and Information Systems*, 7:358–386, 2005.

[61] Hui Ding, Goce Trajcevski, Peter Scheuermann, Xiaoyue Wang, Eamonn Keogh. Querying and mining of time series data: experimental comparison of representations and distance measures. *Proceedings of the VLDB Endowment*, 1:1542–1552, 2008.

[62] Xiaoyue Wang, Abdullah Mueen, Hui Ding, Goce Trajcevski, Peter Scheuermann, Eamonn Keogh. Experimental comparison of representation methods and distance measures for time series data. *Data Mining and Knowledge Discovery*, 26:275–309, 2013.

[63] Yanping Chen, Eamonn Keogh, Bing Hu, Nurjahan Begum, Anthony Bagnall, Abdullah Mueen, Gustavo Batista. The ucr time series classification archive, July 2015. `www.cs.ucr.edu/~eamonn/time_series_data/`.

[64] Bing Hu, Yanping Chen, Eamonn J Keogh. Time series classification under more realistic assumptions. *International Conference on Data Mining (SDM*, pages 578–586. SIAM, 2013.

[65] Thanawin Rakthanmanon, Bilson Campana, Abdullah Mueen, Gustavo Batista, Brandon Westover, Qiang Zhu, Jesin Zakaria, Eamonn Keogh. Addressing big data time series: Mining trillions of time series subsequences under dynamic time warping. *ACM Transactions on Knowledge Discovery from Data (TKDD)*, 7:10–31, 2013.

[66] Ben Mitchell, Hasari Tosun, John Sheppard. Deep learning using partitioned data vectors. *International Joint Conference on Neural Networks (IJCNN)*, pages 1–8, 2015.

[67] Raphael A. Finkel, Jon Louis Bentley. Quad trees a data structure for retrieval on composite keys. *Acta Informatica*, 4:1–9, 1974.

[68] Y. LeCun, Corinna Cortes, Christopher J.C. Burges. The MNIST database of handwritten digits [online]. Available at `http://yann.lecun.com/exdb/mnist/`, Accessed 2014-01-15.

[69] Hasari Tosun, Ben Mitchell, John Sheppard. Assessing diffusion of spatial features in deep belief networks. *IEEE International Joint Conference on Neural Networks (IJCNN)*, 2016.

[70] Hugo Larochelle, Michael Mandel, Razvan Pascanu, Yoshua Bengio. Learning algorithms for the classification restricted boltzmann machine. *The Journal of Machine Learning Research*, 13:643–669, 2012.

[71] T. Mitchell. The need for biases in learning generalizations. *Technical Report CBM-TR-117*, 1980.

[72] Nathan Fortier, John W Sheppard, Karthik Ganesan Pillai. DOSI: Training artificial neural networks using overlapping swarm intelligence with local credit assignment. *Joint 6th International Conference on Soft Computing and Intelligent Systems (SCIS) and 13th International Symposium on Advanced Intelligent Systems (ISIS)*, pages 1420–1425. IEEE, 2012.

[73] N. Fortier, J. Sheppard, S. Strasser. Abductive inference in bayesian networks using overlapping swarm intelligence. *Soft Computing*, pages 1–21, May 2014.

[74] N Fortier, J Sheppard, S Strasser. Learning bayesian classifiers using overlapping swarm intelligence. *Proceedings of the IEEE Swarm Intelligence Symposium*, pages 205–212, December 2014.

[75] W. McCulloch, W. Pitts. A logical calculus of the ideas immanent in nervous activity. *Bulletin of Mathematical Biophysics*, 5:115–133, 1943.

[76] Peter Whitle. *Hypothesis testing in time series analysis*, Volume 4. Almqvist & Wiksells, 1951.

[77] GM Jenkins, GC Reinsel. *Time series analysis: forecasting and control*. Holden-Day, 1976.

[78] Graham W Taylor, Geoffrey E Hinton, Sam T Roweis. Modeling human motion using binary latent variables. *Advances in Neural Information Processing Systems*, pages 1345–1352, 2006.

[79] Ilya Sutskever, Geoffrey E Hinton. Learning multilevel distributed representations for high-dimensional sequences. *International Conference on Artificial Intelligence and Statistics*, pages 548–555, 2007.

[80] Paul Dagum, Adam Galper, Eric Horvitz. Dynamic network models for forecasting. *Proceedings of the Eighth International Conference on Uncertainty in Artificial Intelligence (UAI)*, pages 41–48. Morgan Kaufmann Publishers Inc., 1992.

[81] Chris Häusler, Alex Susemihl. Temporal autoencoding restricted boltzmann machine. *arXiv preprint arXiv:1210.8353*, 2012.

[82] Rafael Hrasko, André GC Pacheco, Renato A Krohling. Time series prediction using restricted boltzmann machines and backpropagation. *Procedia Computer Science*, 55:990–999, 2015.

[83] Jiawei Han, Micheline Kamber, Jian Pei. *Data mining: concepts and techniques*. Elsevier, 2011.

[84] Sinno Jialin Pan, Qiang Yang. A survey on transfer learning. *IEEE Transactions on Knowledge and Data Engineering*, 22:1345–1359, 2010.

APPENDICES

APPENDIX A

VARIANCES

Here we include variogram plots for all MNIST labels. The first row shows variograms of the raw input vectors, the second row shows results of the Single RBM, and the third shows results of the Partitioned-RBM. The $y-axis$ represents the mean variance of differences, and the $x-axis$ represents Euclidean pixel distance between points. Labels of the form $N-P$ indicate data for hidden layer N of a Deep Belief Network based on Partitioned-RBMs with P partitions.

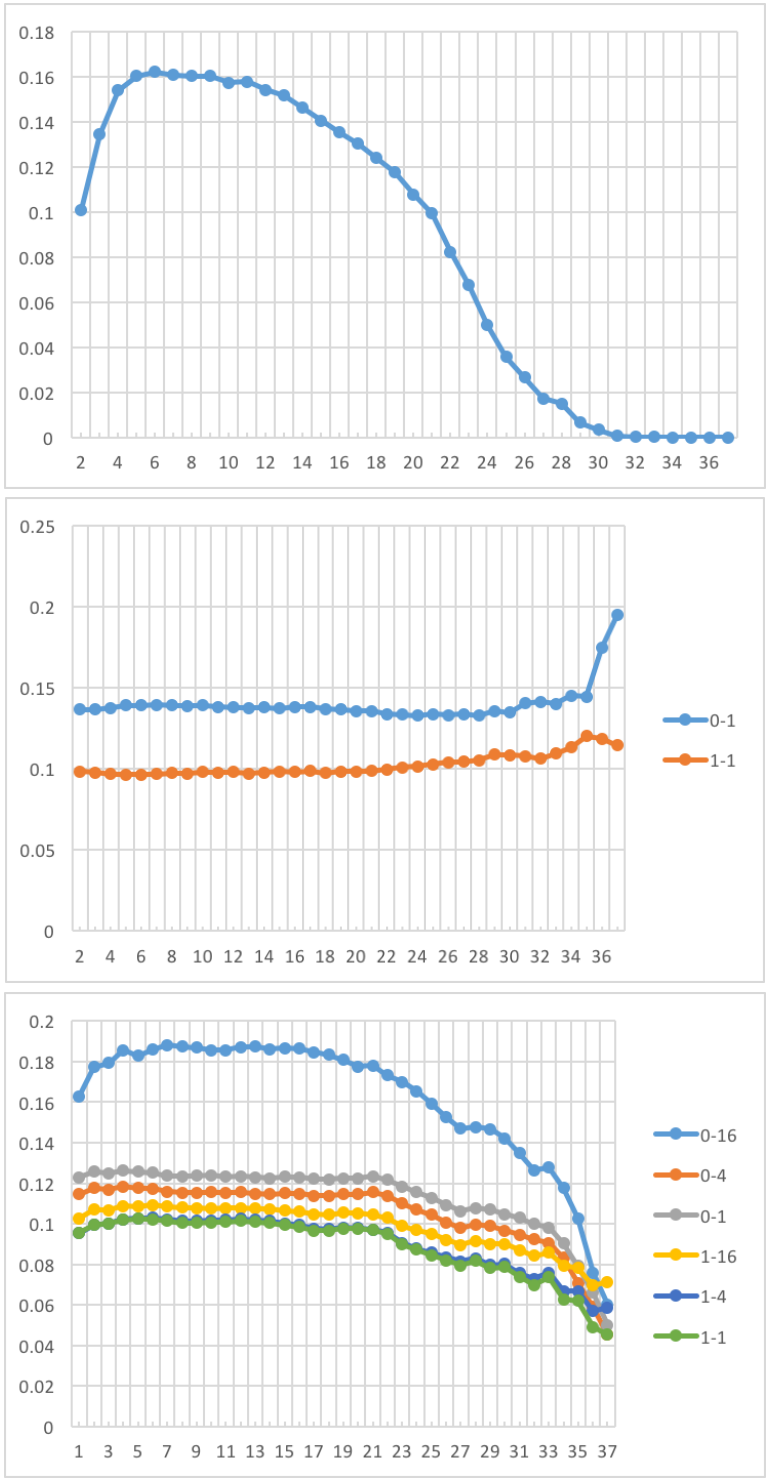

Figure A.1: Variogram: Label 0

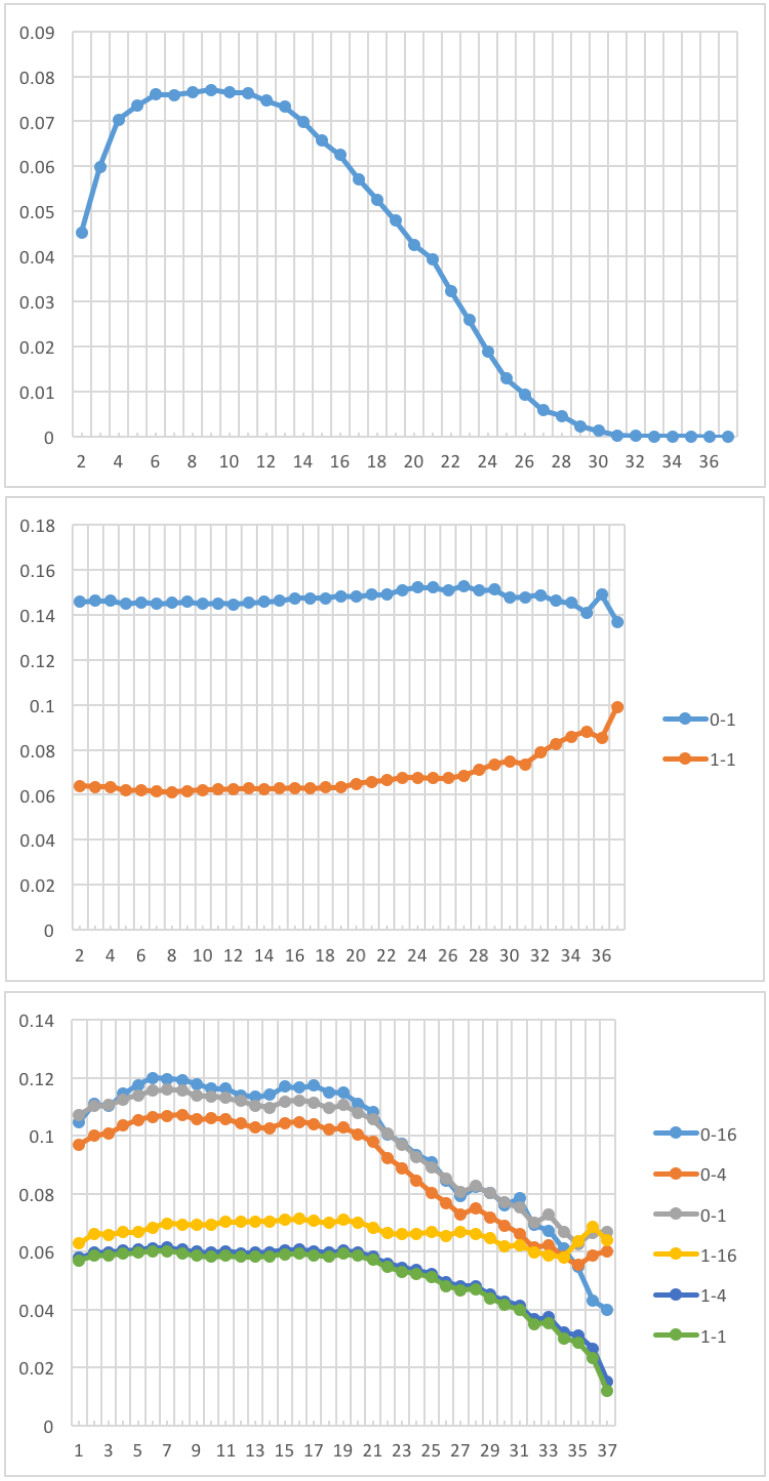

Figure A.2: Variogram: Label 1

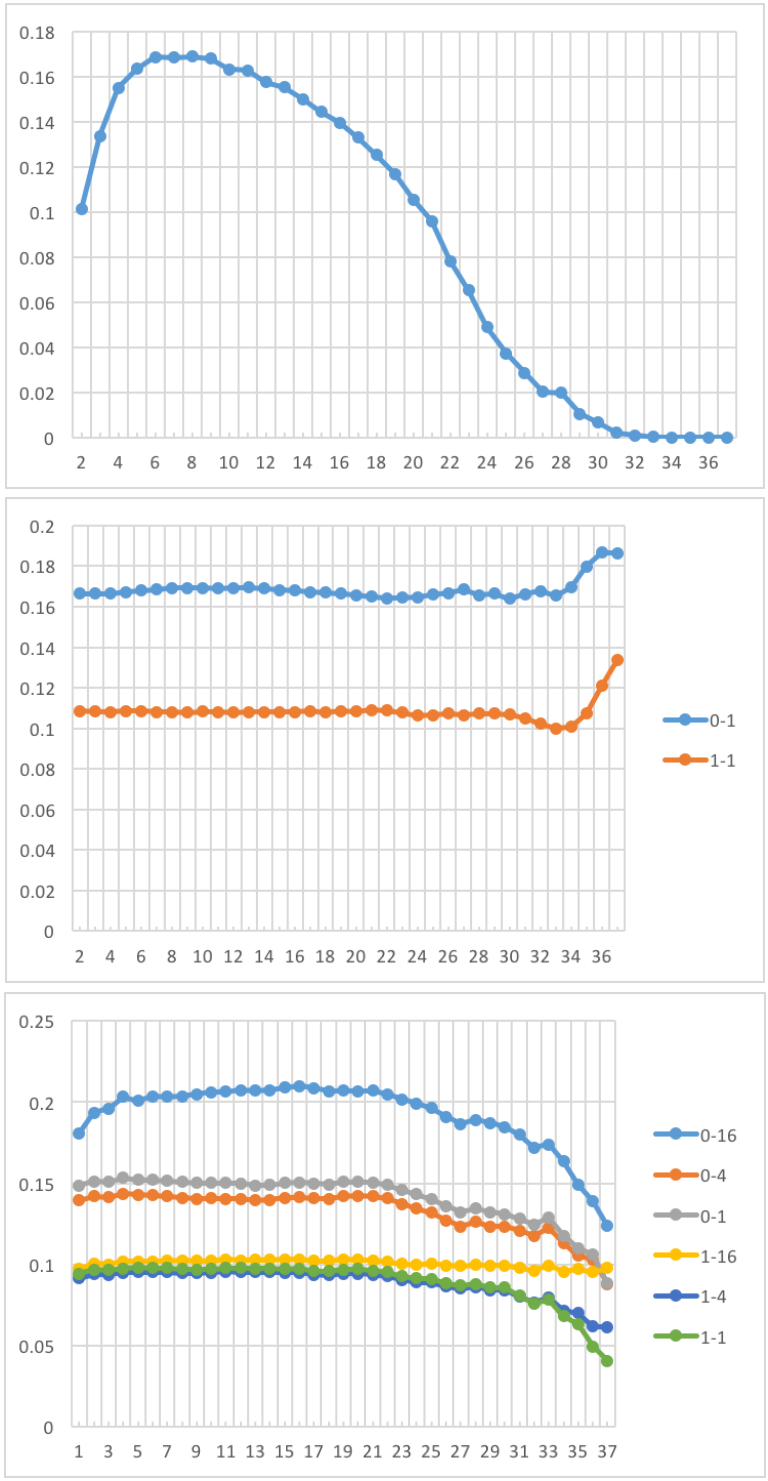

Figure A.3: Variogram: Label 2

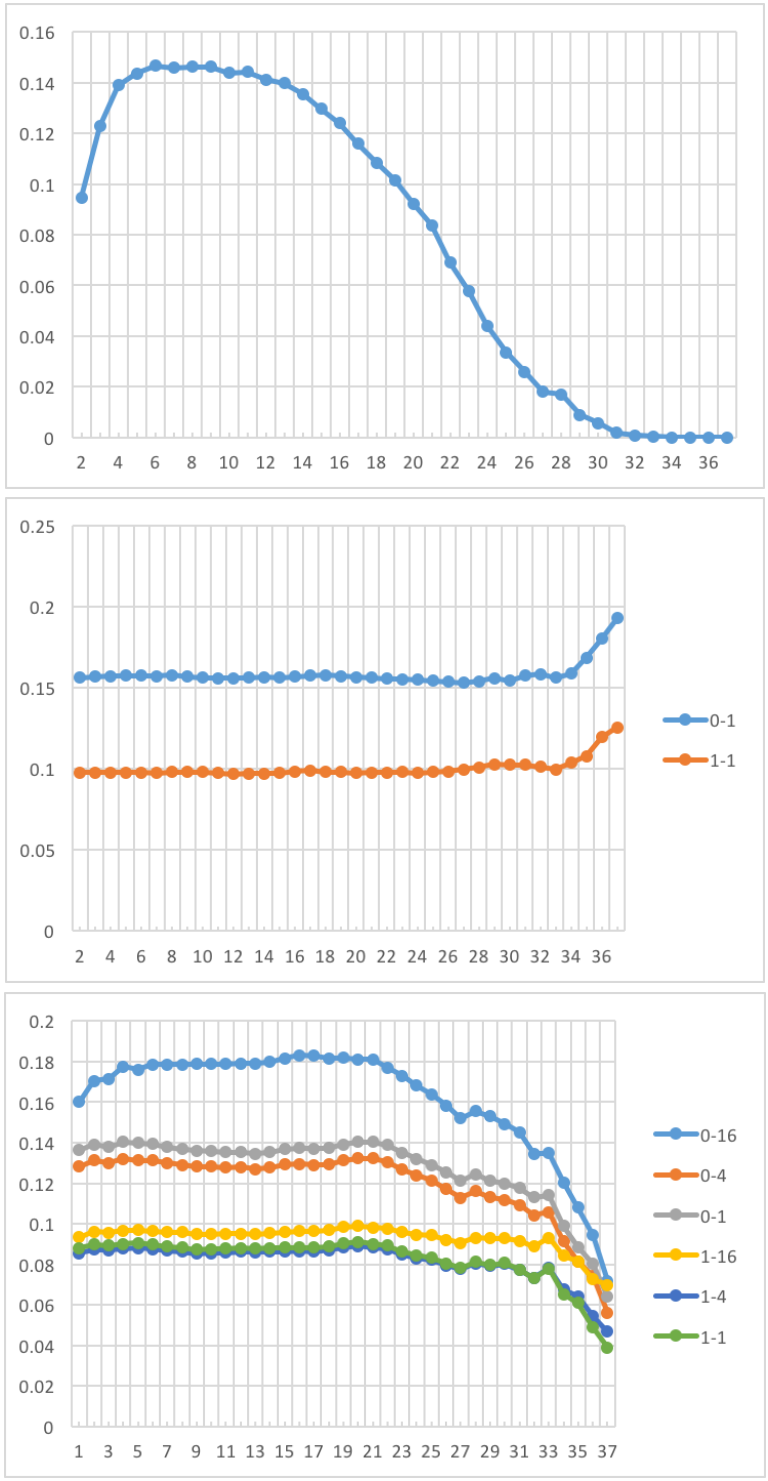

Figure A.4: Variogram: Label 3

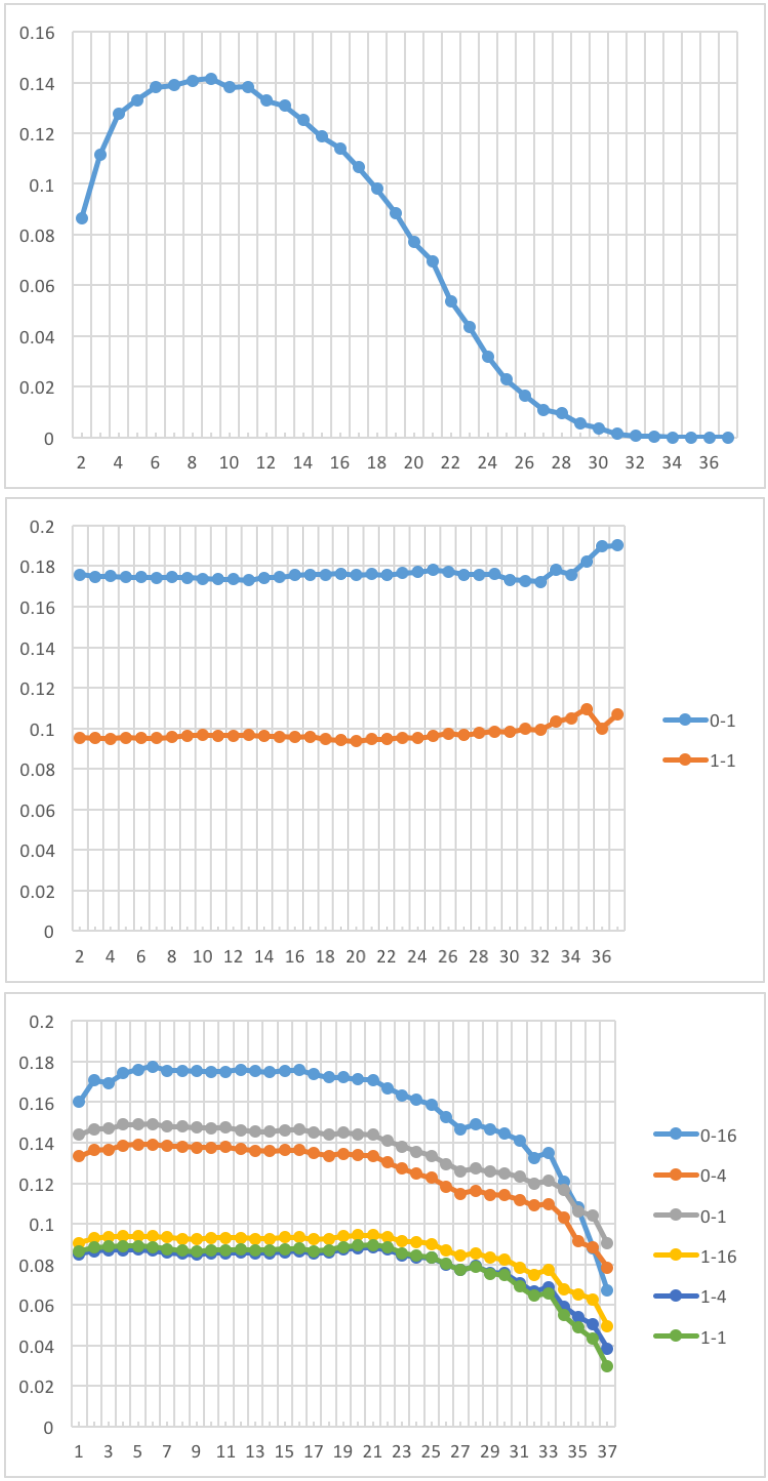

Figure A.5: Variogram: Label 4

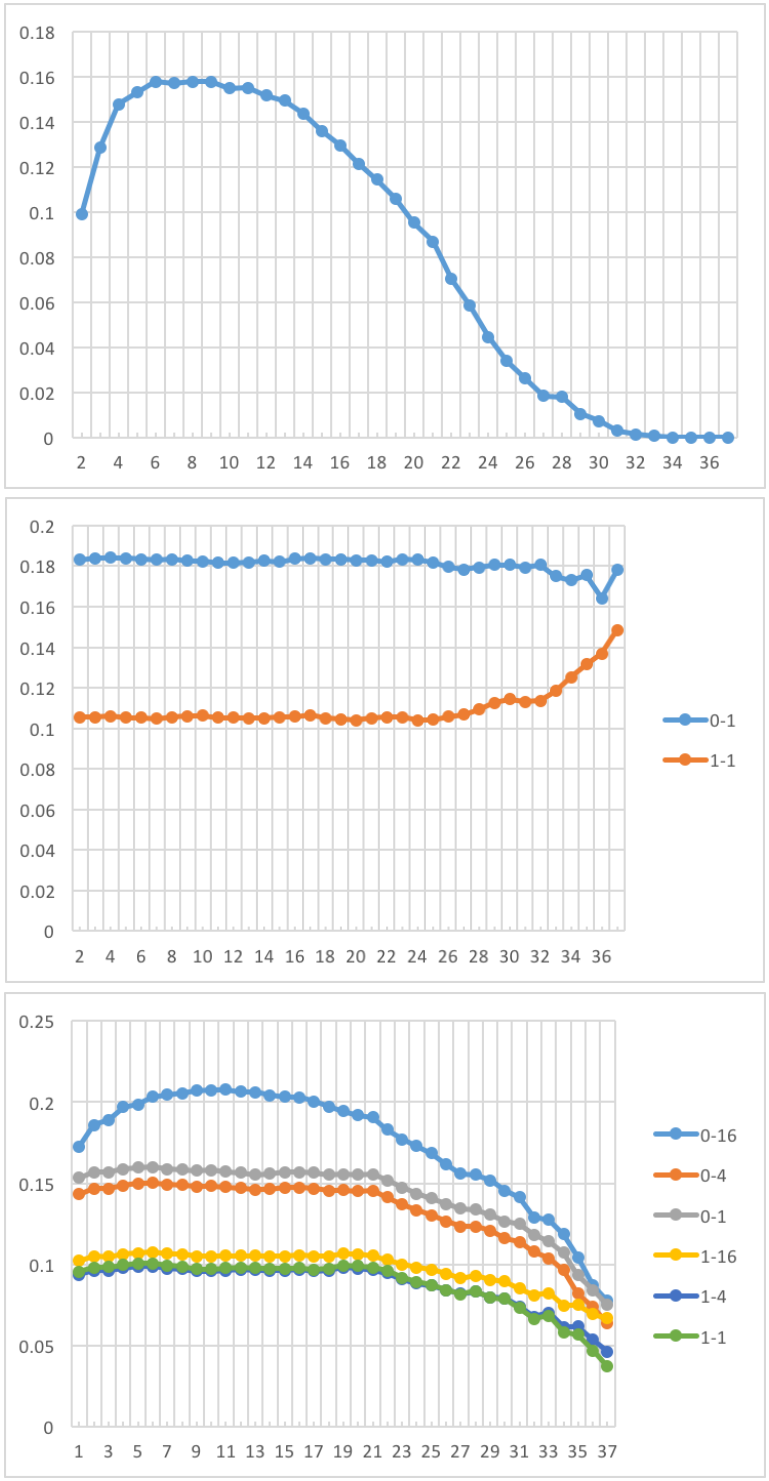

Figure A.6: Variogram: Label 5

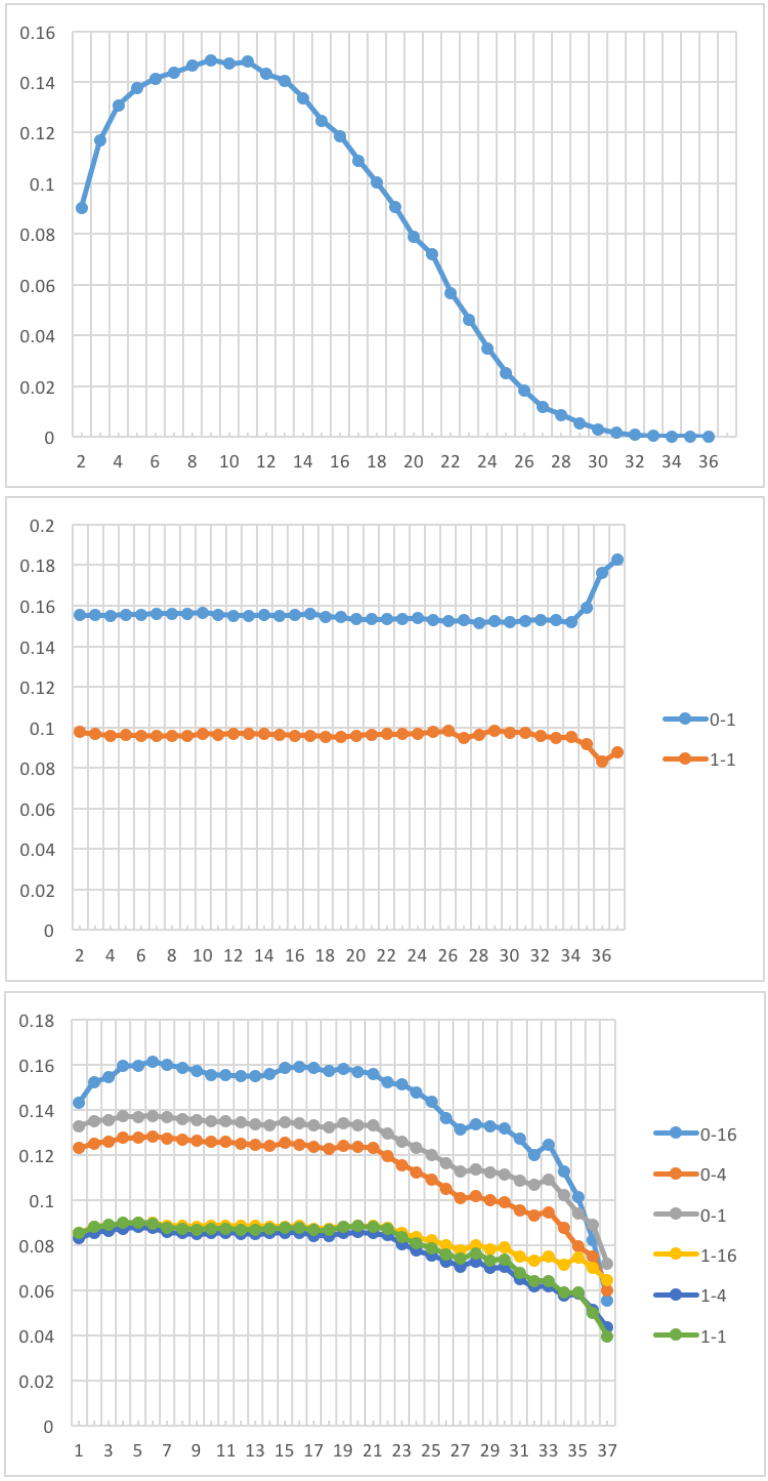

Figure A.7: Variogram: Label 6

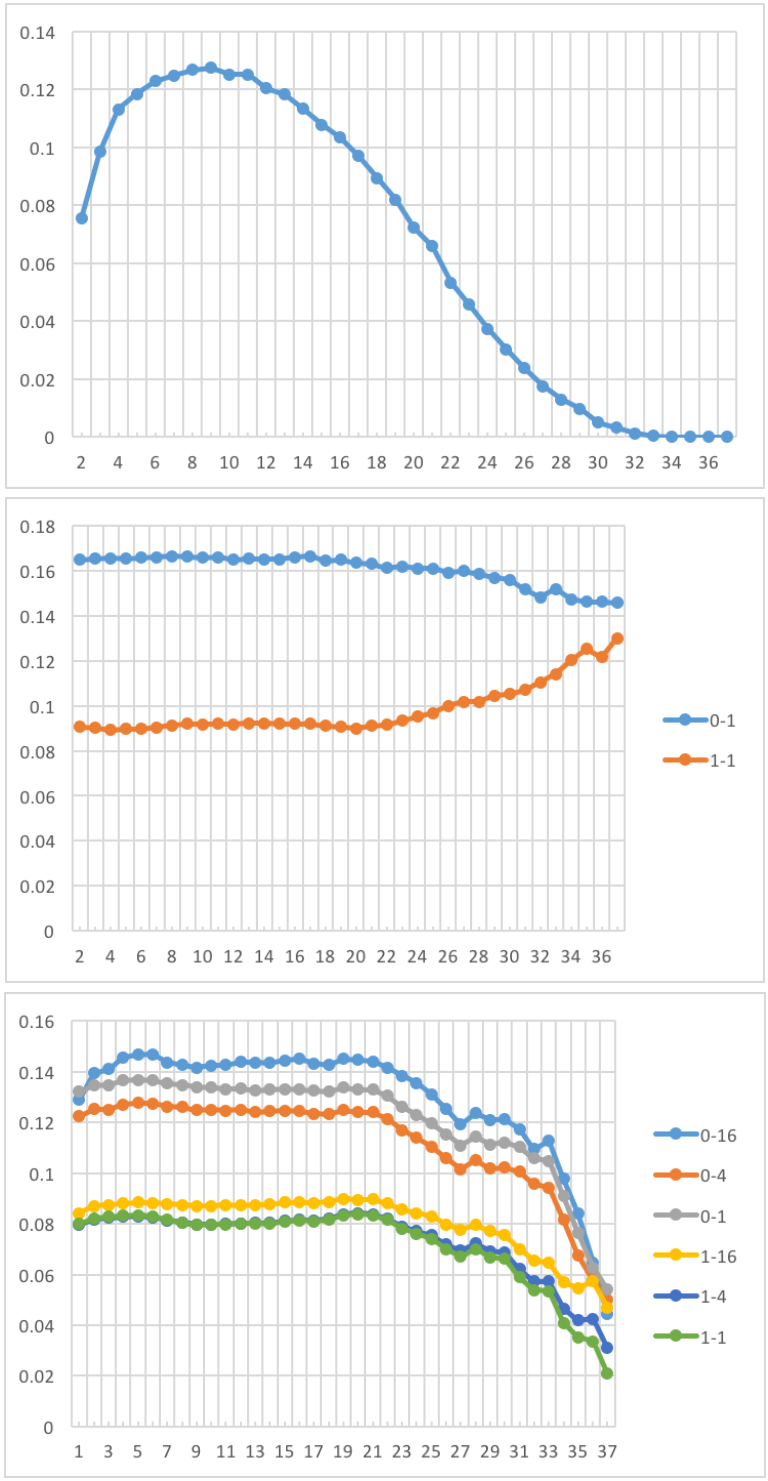

Figure A.8: Variogram: Label 7

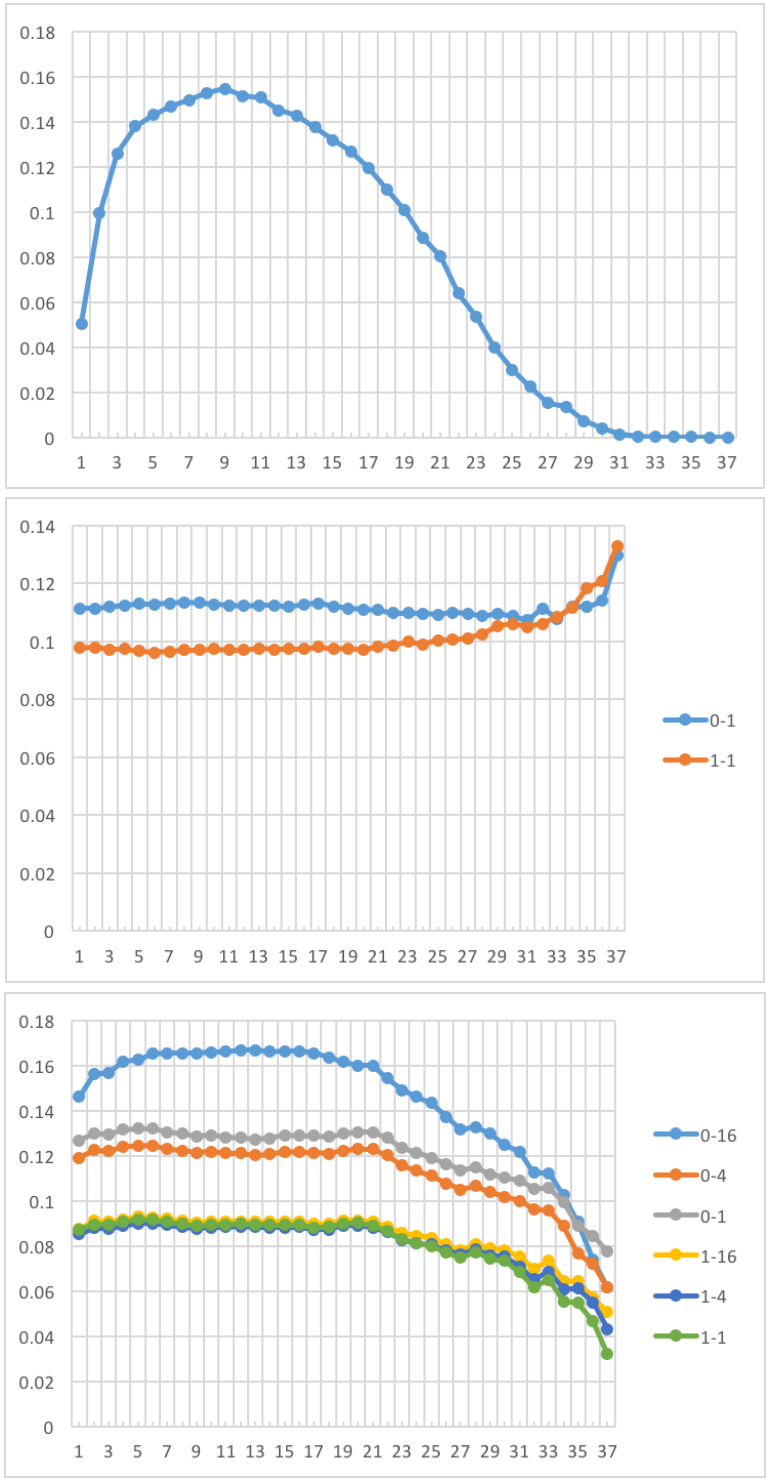

Figure A.9: Variogram: Label 8

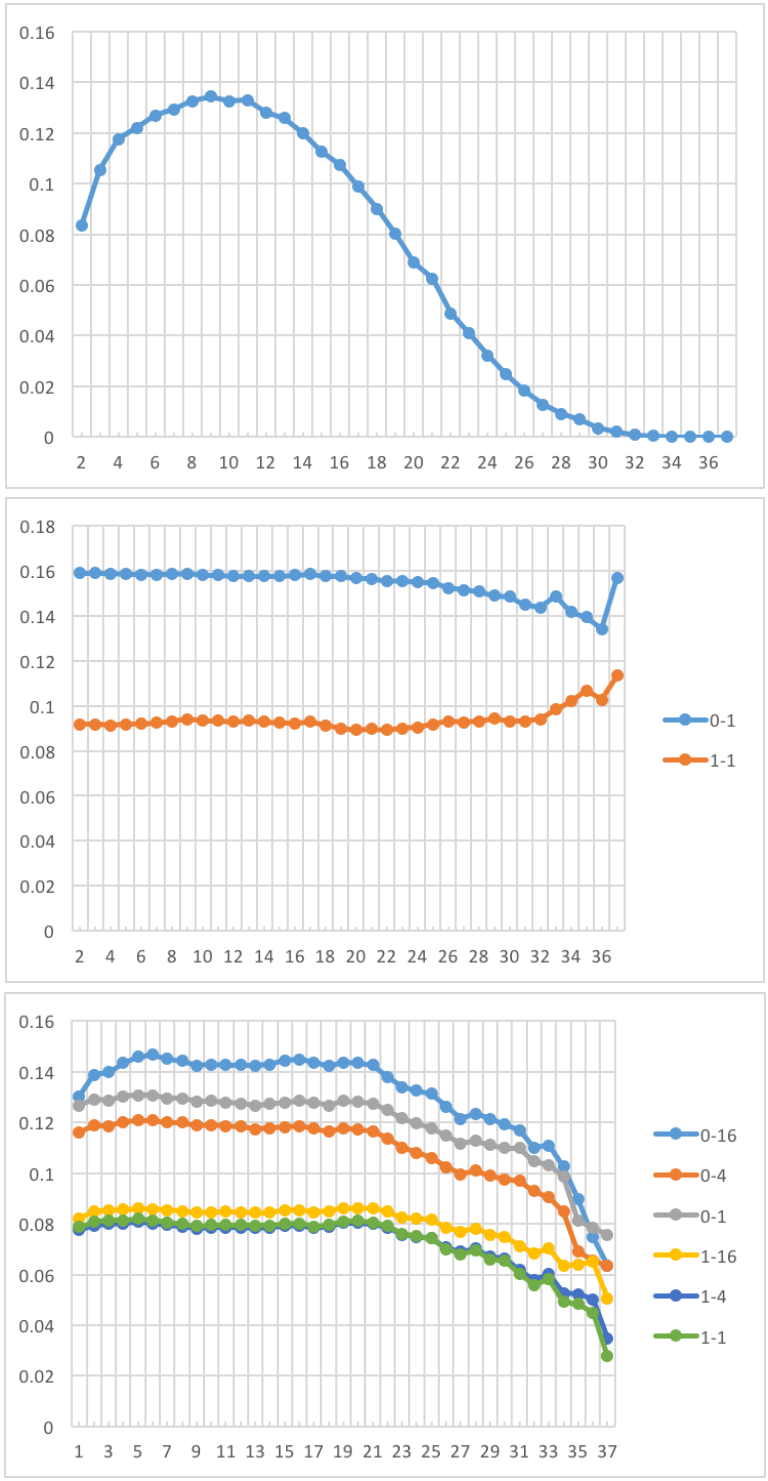

Figure A.10: Variogram: Label 9

APPENDIX B

CORRELATIONS

Here we include mean-correlation plots for all MNIST labels. The first row shows correlations of the raw input vectors, the second row shows results of the Single RBM, and the third shows results of the Partitioned-RBM. The $y-axis$ represents the mean correlations, and the $x-axis$ represents Euclidean pixel distance between points. Labels of the form $N-P$ indicate data for hidden layer N of a Deep Belief Network based on Partitioned-RBMs with P partitions.

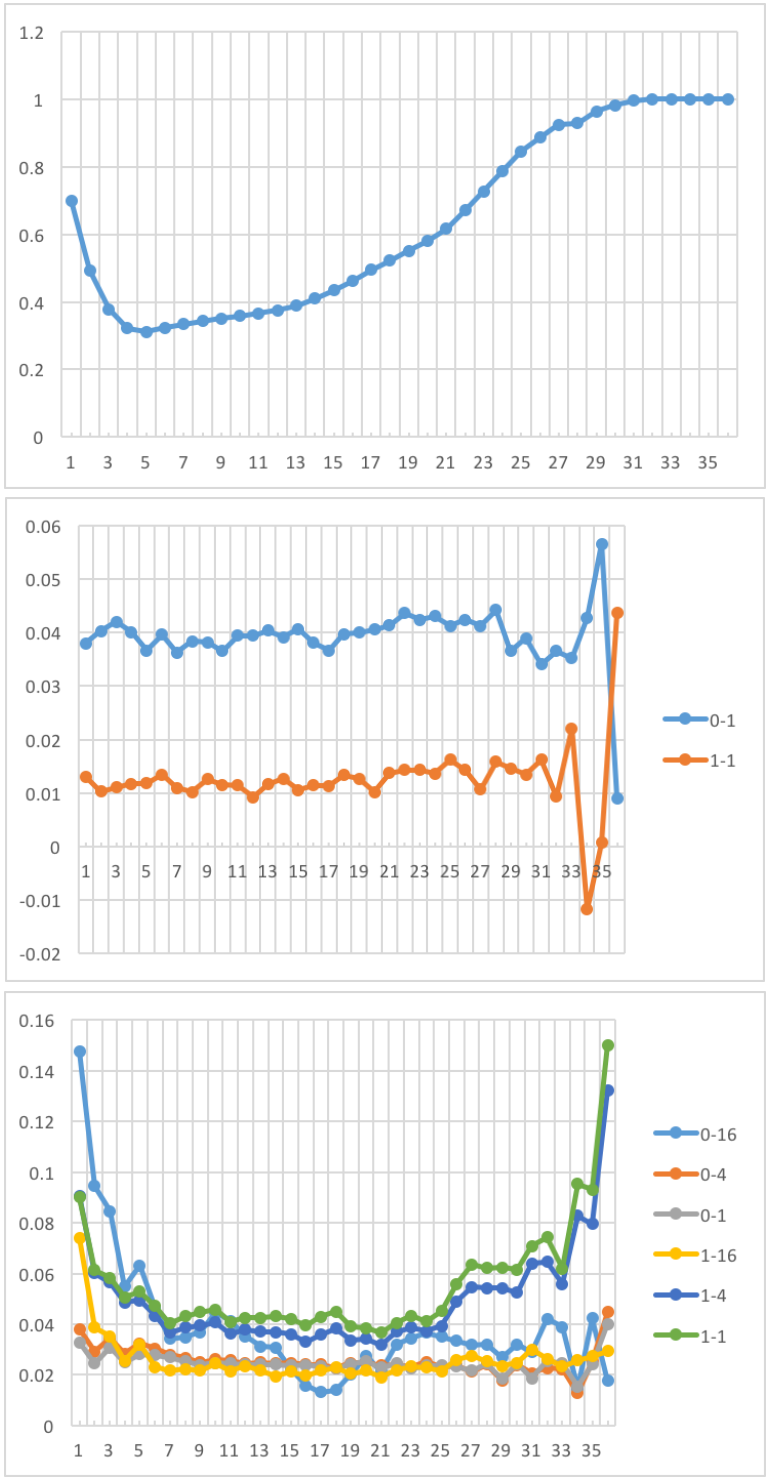

Figure B.1: Mean Correlation: Label 0

Figure B.2: Mean Correlation: Label 1

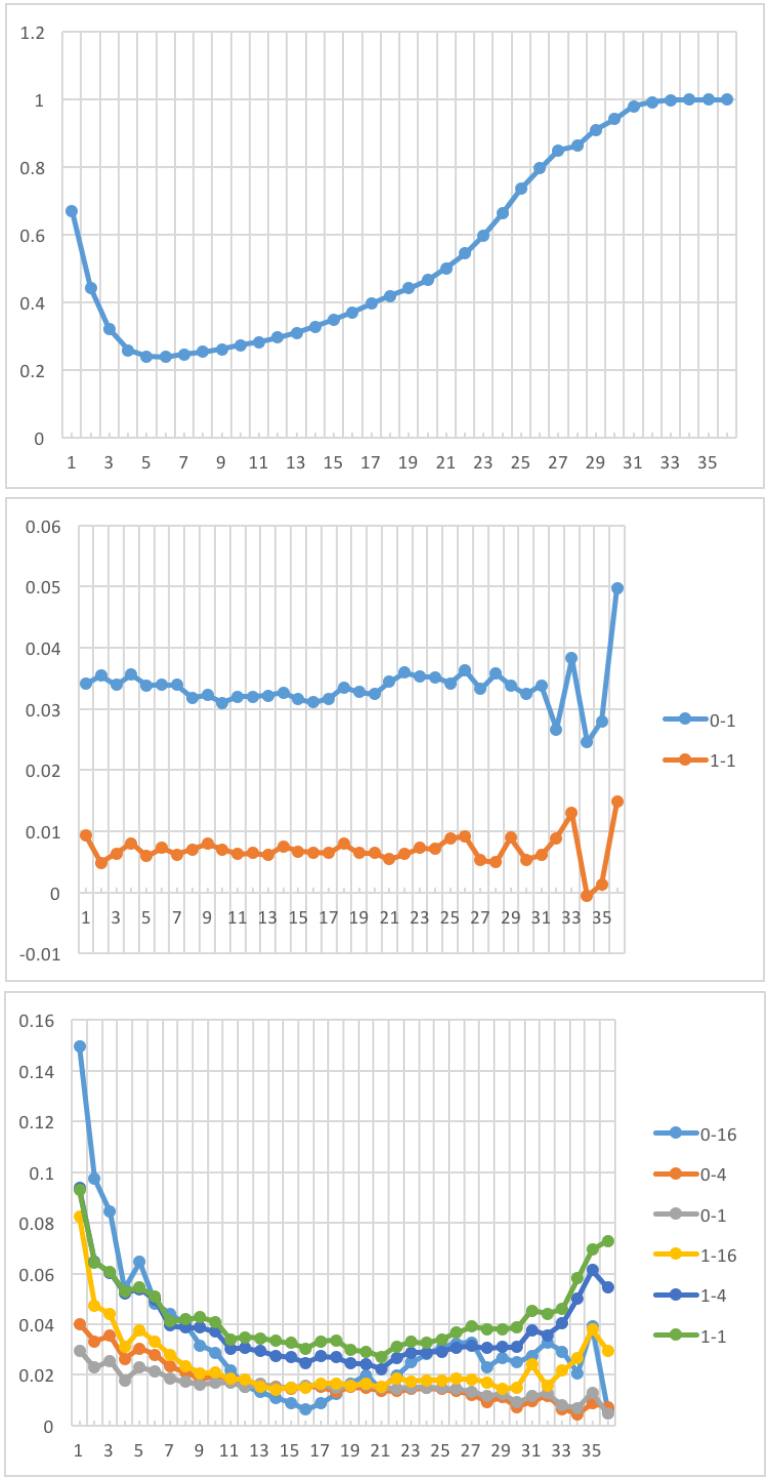

Figure B.3: Mean Correlation: Label 2

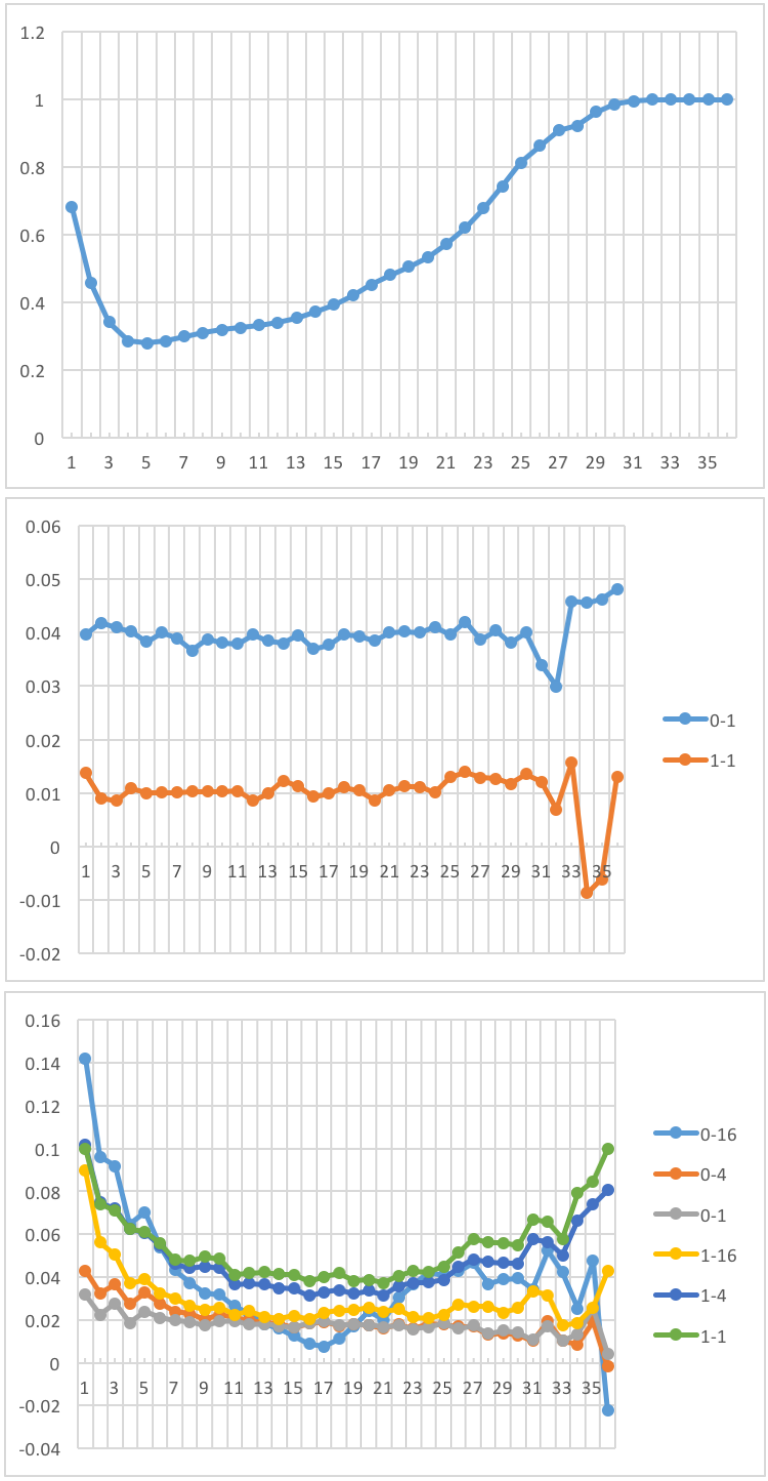

Figure B.4: Mean Correlation: Label 3

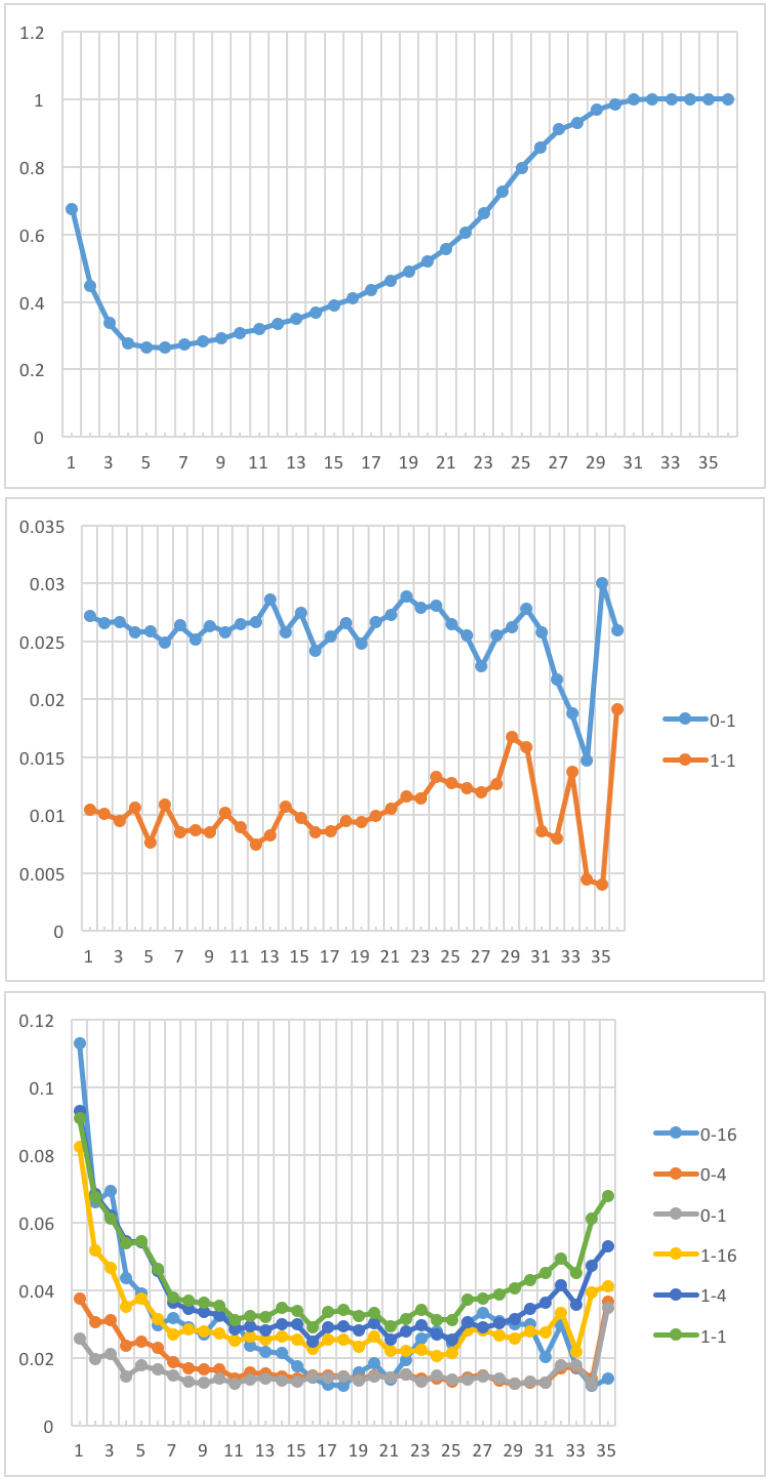

Figure B.5: Mean Correlation: Label 4

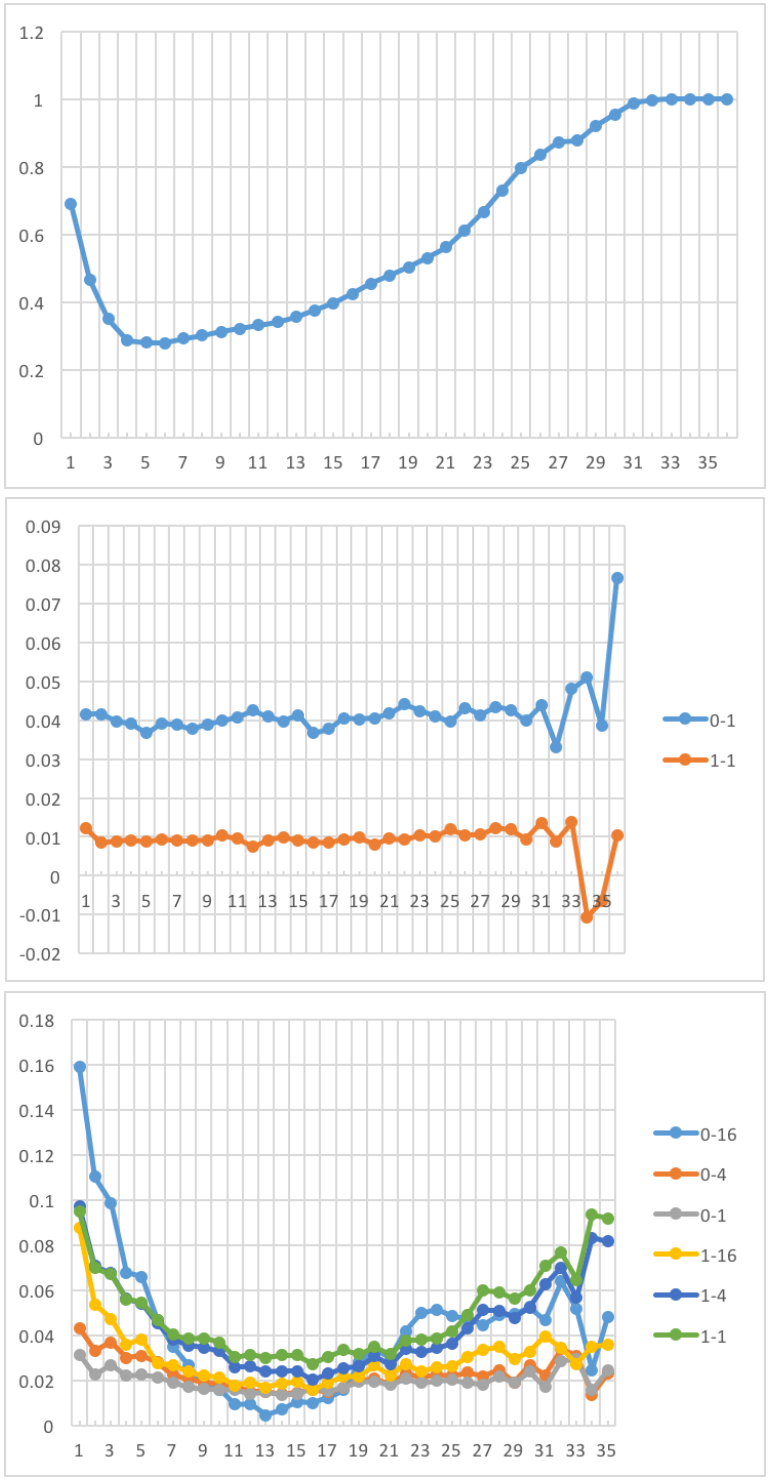

Figure B.6: Mean Correlation: Label 5

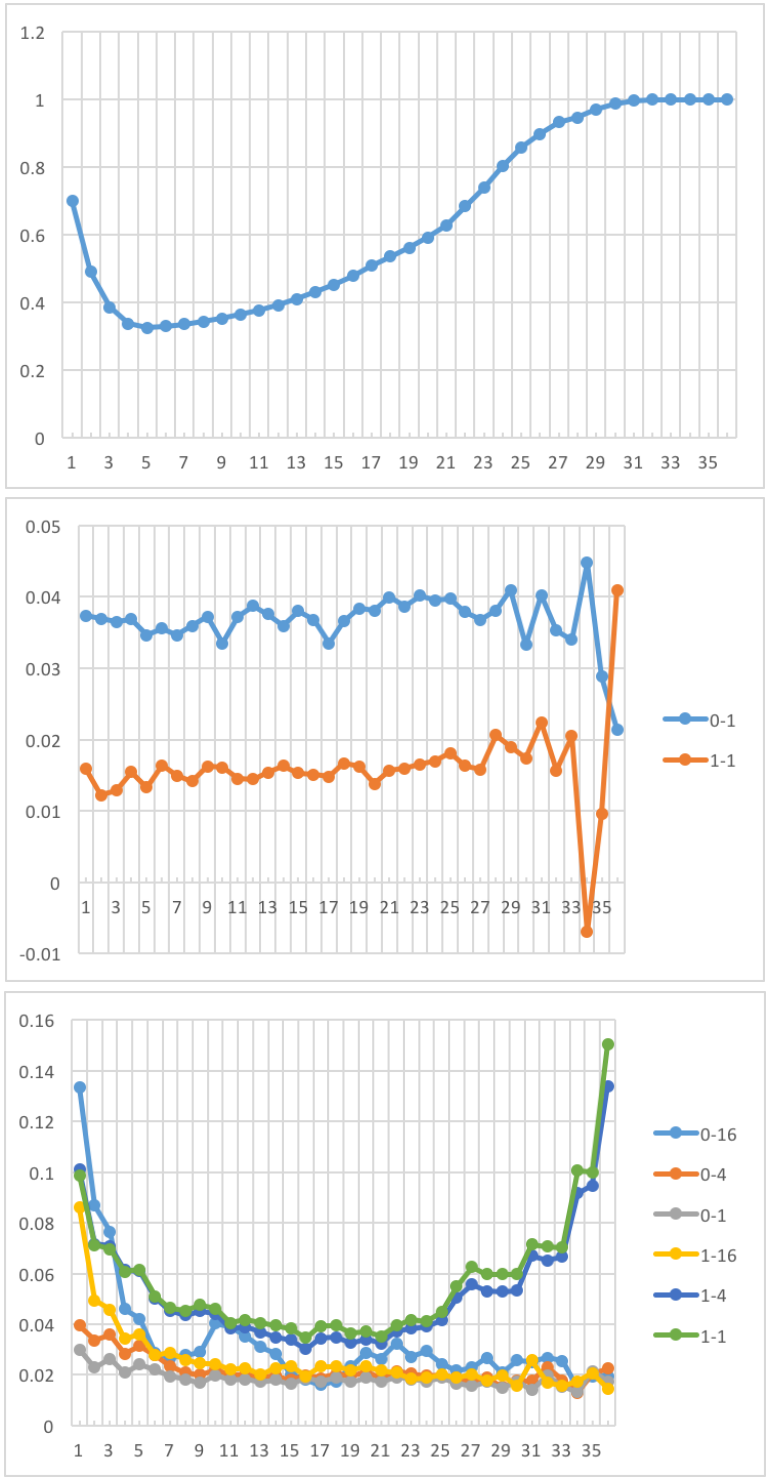

Figure B.7: Mean Correlation: Label 6

Figure B.8: Mean Correlation: Label 7

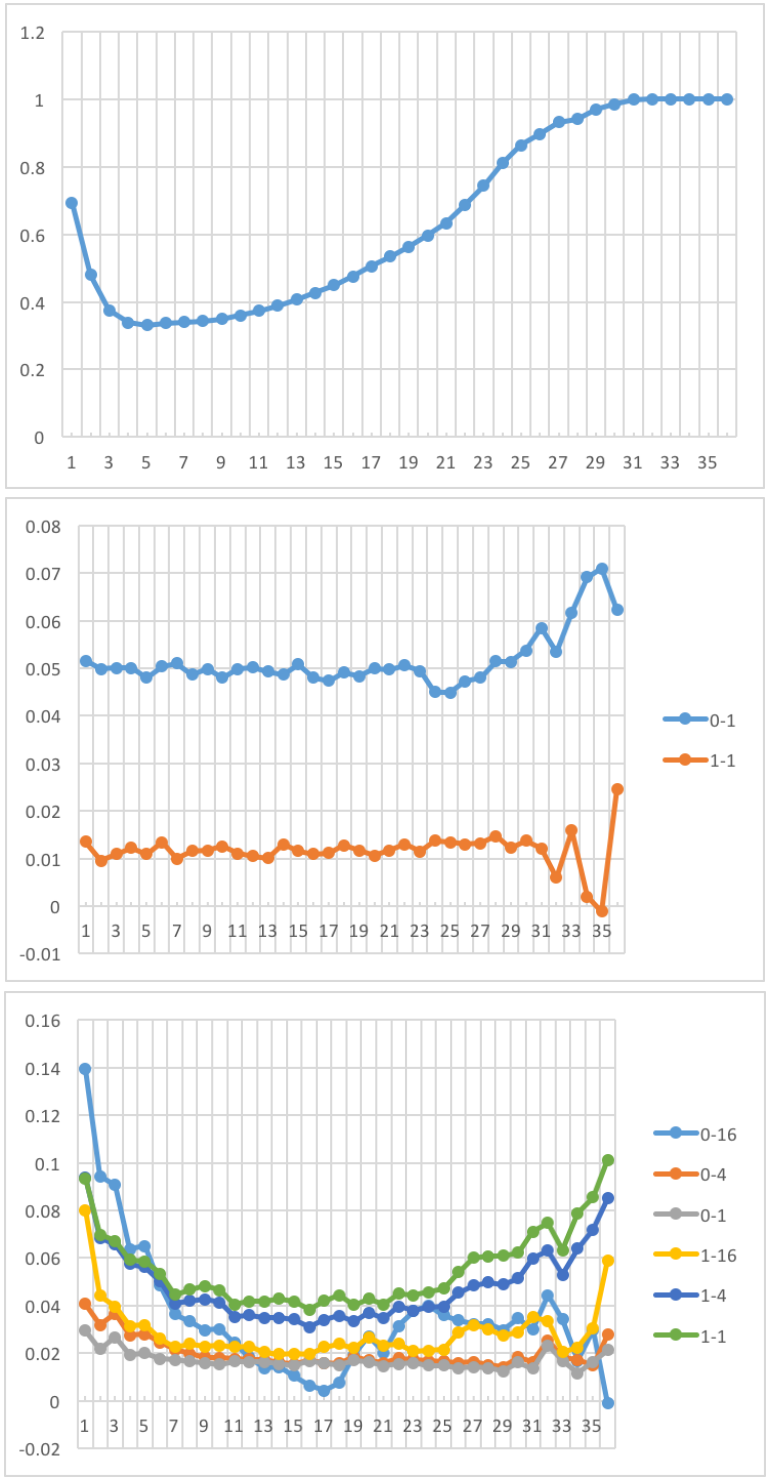

Figure B.9: Mean Correlation: Label 8

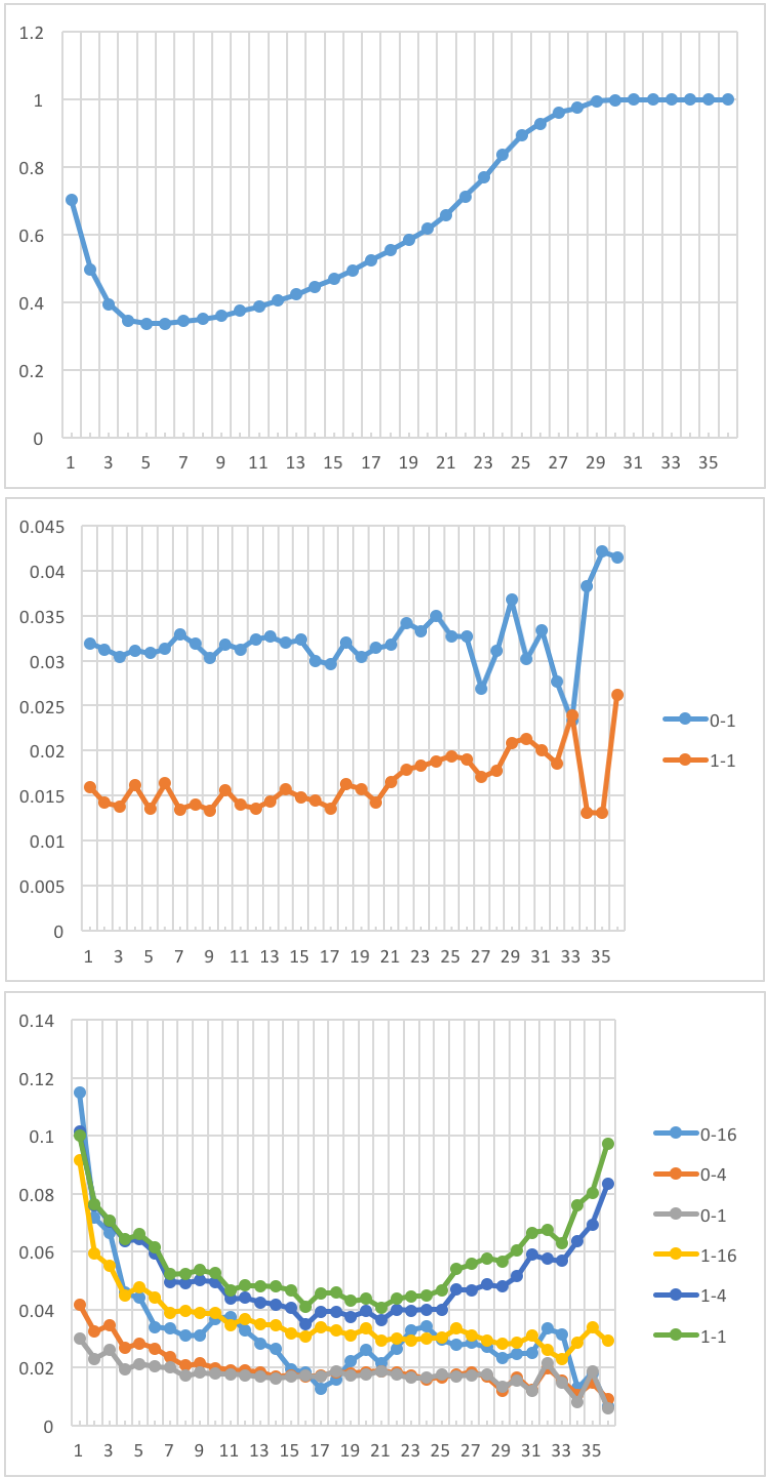

Figure B.10: Mean Correlation: Label 9